



Grant Agreement No. 228296

# **SFERA**

Solar Facilities for the European Research Area

**SEVENTH FRAMEWORK PROGRAMME**

Capacities Specific Programme

Research Infrastructures

Integrating Activity - Combination of Collaborative  
Project and Coordination and Support Action

## **R12.4 Guidelines for Testing of CSP components**

Due date of deliverable: Month 24

Actual submission date: Month 52

Organisation name of lead contractor for this deliverable: DLR

## Contents

1. Introduction.....	5
2. General Recommendations for Testing.....	6
2.1. Good testing practice .....	6
2.1.1. Methodological Aspects .....	6
2.2. Uncertainty analysis .....	7
2.2.1. Uncertainty versus Error .....	8
2.2.2. Accuracy versus precision .....	8
2.2.3. Uncertainty budget of measurands and derived quantities .....	9
2.2.4. Parameter uncertainty .....	11
PART 1 Concentrating Solar Power Technologies and Specific Testing Requirements.....	13
3. Parabolic Trough.....	14
3.1. Component Performance Evaluation.....	14
3.1.1. Indoor tests for facets .....	14
3.1.2. Solar reflectance.....	14
3.1.3. Shape accuracy .....	15
3.1.4. Indoor tests for Heat Collecting Elements (HCE).....	17
3.2. System/Module Performance Evaluation .....	18
3.2.1. Geometric Precision and Optics .....	19
3.2.2. Tracking accuracy and stability of the drive system.....	20
3.2.3. Mechanical testing aspects: Accuracy and stiffness of the structure .....	20
3.2.4. Measurement of thermal, optical and total performance/efficiencies of the solar collector system .....	21
3.3. Heat Transfer Fluid .....	22
4. Tower.....	25
4.1. Component Performance Evaluation.....	26
4.1.1. Heliostats.....	26
4.1.2. Receiver .....	29
4.2. System Performance evaluation .....	29
4.3. Chemical test .....	31
4.4. Performance of Solar Receivers .....	31
4.5. Heliostat Field Control for Solar Chemical Processes.....	32

5.	Dish.....	36
5.1.	System Performance evaluation .....	36
5.2.	Component Performance Evaluation.....	36
5.2.1.	Measurement of environmental conditions .....	36
5.2.2.	Mirror Reflectance.....	37
5.2.3.	Optical quality of dish concentrators .....	37
5.2.4.	Intercept Factor .....	37
5.2.5.	Engine efficiency.....	38
6.	Furnace (CNRS).....	40
6.1.	Presentation .....	40
6.2.	Applications.....	40
6.3.	Testing .....	41
Part 2 Measurement Methods.....		43
7.	Solar Resource and meteorological Data Measurement .....	44
7.1.	Irradiance.....	44
7.2.	Other meteorological parameters.....	49
7.2.1.	Air Temperature and Relative Humidity.....	49
7.2.2.	Atmospheric Pressure .....	50
7.2.3.	Wind Speed and Wind Direction .....	51
8.	Temperature Measurement.....	55
8.1.	Optical Temperature Measurement .....	55
8.1.1.	Instruments .....	55
8.1.2.	Solar blind pyrometry.....	56
8.2.	Temperature Measurement with contact probes.....	59
9.	Mass flow measurement.....	62
10.	Optical Properties.....	68
10.1.	Reflectance .....	68
10.2.	Reflectance, absorptance and emittance of the absorber coating.....	70
11.	Heat Flux Measurement.....	73
11.1.	Direct method using radiometers .....	73
11.2.	Flux density measurement: indirect measurement method .....	78
11.3.	Calculated method: raytracing.....	81
12.	Calorimetry.....	85

13. Shape Measurement .....	93
13.1. 3D shape measurement using a laser-scanner .....	95
13.2. Estimation of slope deviations of CSP reflectors using deflectometric methods .....	97
13.3. Geometric analysis of solar concentrators with close range photogrammetry .....	99
13.4. 3D shape analysis by reverse analysis: VISprofile .....	102
14. Canting and alignment of CSP concentrators.....	105
14.1. General procedure .....	105
14.2. Check of the mutual optical alignment of receiver and concentrator in the field by reverse analysis (VISfield).....	106
15. Mechanical testing procedures .....	110
15.1. Drive backlash ultimate strength .....	110
15.2. Tracking and Torsion of Parabolic Trough Collector Drives .....	110
15.3. Concentrator structure tests .....	111
16. Performance Measurement .....	113
1.1. Thermal Performance Tests for Collector Modules .....	113
16.1. Measurement of the receiver heat loss vs. temperature .....	117
17. Heat Transfer Fluid Properties and their Measurement.....	120
1.1. Thermal Oil .....	120
17.1. Molten Salts.....	123
18. Measurement of Electric Power.....	126
19. Measurement of the solar-to-fuel efficiency of solar receivers.....	128

## 1. Introduction

Concentrating Solar Power (CSP) technologies convert solar irradiance into useful heat by means of concentration using parabolic trough and linear fresnel collectors, solar power towers and dishes. In accordance with their functioning principle and the solar resource used, these technologies have particular operation and testing requirements in terms of geometrical precision and tracking, high temperatures and particularities of heat transfer fluids. In order to meet the demands of research and development investigating CSP systems, various measurement and evaluation methods have been developed at the key European research centers for concentrating solar technologies. Most of them deal with measuring in a scientific environment, where available field measurement techniques are also referred to for on-site diagnostic.

The aim of this guideline is to give an overview of key measurement and evaluation quantities, typical issues and best practice test methods as well as achieve agreement on specific procedures for the respective technologies. For more detailed information on particular measurement methods the reader is redirected to selected concise literature sources.

Following a chapter containing general test recommendations this guideline is divided into two main parts:

**PART 1** describes different technologies (Parabolic Trough, Tower, Dish and Furnace) available for conversion of solar irradiance to heat/electricity by means of concentration. The focus is on the particular testing needs for the characterization of the components and system involved naming suitable measurement methods and typical test procedures.

**PART 2** covers the most relevant measurement methods in greater detail. Their measurement principle, sensors/ equipment requirements, calibration issues, expected accuracies and recommendations are included.

According to the differing research focus of the SFERA project partners in the field of CSP technologies this guideline includes contributions from:

- the German Aerospace Center DLR e.V.: Institute of Solar Research
- the French National Center of Scientific Research (CNRS): laboratory PROMES (UPR8521)
- the Spanish research centre, Centro de Investigaciones Energéticas, Medioambientales y Tecnológicas (CIEMAT)
- The Italian National Agency for New Technologies, Energy and Sustainable Economic Development (ENEA)

The main authors and their affiliations are

Stefan Wilbert	
Wolfgang Reinalter	DLR (Germany)
Nicole Janotte	
Emmanuel Guillot	CNRS laboratory PROMES (France)
Jesús Fernández Reche	CIEMAT (Spain)
Marco Montecchi	ENEA (Italy)

## 2. General Recommendations for Testing

### 2.1. Good testing practice

Along with a common definition of key measurement quantities and methods, any attempt to improve comparability of test results originating from different CSP test facilities requires adequate quality assurance measures and the application of good scientific practice by the individual institutions. Though extremely important, such general measures are not within the scope of this guideline but entrusted to the individual quality management of the institutions. Only the most relevant aspects with respect to testing shall be mentioned in the following.

#### **Test documentation**

The long-term usefulness of test data and results can only be assured by a full documentation and preservation of the information for later reference. This can serve later comparison or review of procedures in retrospective. Such documentation should include sketches and photographs of the test set-up, test protocols and observations, full (raw) data records, sensor IDs/ positions/ calibration information, test protocols, data evaluation, results and potential reports.

#### **Sensor calibration and traceability**

The use of sensors calibrated on a regular basis is the basic prerequisite for generating valid test data. Established calibration procedures should be documented and calibrations traceable to national or internal standards.

#### **Publication of test results**

The usefulness of documented/ published test results is mainly determined by the information they contain. To improve comparability all the final report should fully inform the reader about:

- component under testing (type, manufacturer, serial number, etc.)
- instruments used
- relevant test boundary and operation conditions
- results and uncertainty

#### *2.1.1. Methodological Aspects*

##### **Steady-state conditions**

All thermal tests described in this guideline require (quasi) steady operating conditions for evaluation to the accuracy and precision defined. Consequently, flow rates, temperatures, ambient conditions etc. may only vary within tight limits. Allowable variations cannot be defined in general for all tests but depend on the individual method and the test accuracy aimed at. Instead, they have to be determined from sensitivity analysis and test experience.

##### **Durability of components**

In order to pay back their high investment cost, CSP plants are to reliably generate heat and electricity over their calculated lifetime. As this period can reach 25 to 30 years, the durability of the components is an important issue. In this context, the plant operating conditions of high temperatures and concentrated irradiation as well as the harsh ambient conditions of the desert areas present a challenge to component manufacturers and design engineers.

Defining detailed procedures for durability testing by accelerated aging of CSP materials or components and testing for specific aging effects is beyond the scope of this guideline. Thus, only the general approach and most common procedures are described briefly:

- The durability of reflector materials is tested by accelerated aging in climatic chambers or mechanical abrasion and subsequent re-evaluation of reflectance characteristics. For accelerated aging purposes the materials are exposed to high intensity UV light, high humidity and/or salt spray. In the course of the aging process, the specimens are periodically measured in order to monitoring their degradation.
- For facets, reflectance and shape accuracy parameters are investigated in durability tests.
- Parabolic trough receivers to be investigated for aging effects are exposed to temperatures considerably above the nominal operating temperature for hundreds of hours and expansion bellows are subjected to thousands of typical axial movements (at operating temperature). In the course of the potential aging process, the specimens are periodically evaluated in terms of their specific heat loss.

In order to relate the results obtained in accelerated ageing tests to normal ageing processes, a suitable function modelling degradation versus the acceleration parameter should be established; Arrhenius's law is the typical example for such a function for thermal ageing.

The proposed component tests in this guideline are designed in such a way, that no aging should occur during testing of current standard commercial components. For new materials or components this assumption needs to be verified prior to testing. Otherwise, the significance and reproducibility of test results can be affected should relevant aging processes occur during testing.

## 2.2. Uncertainty analysis

Including an uncertainty analysis with any test or measurement result is good scientific practice and essential for judging the quality of results obtained. There are various motivations for uncertainty analysis.

Most importantly, the uncertainty of a result determines its significance. A measurement reading or result as such is essentially a random guess of the measurand. It does not contain any information on how likely the value is to represent the actual measurand until the width of the associated uncertainty band is determined. Consequently, reliable values of uncertainty are absolutely necessary for the assessment and valid comparison of test results

Furthermore, carrying out a full uncertainty analysis requires a thorough knowledge of a measurement process. If this knowledge already exists, the uncertainty analysis is a mere review of the measurement process and data acquisition. Thus, it constitutes a good opportunity to detect and eliminate possible errors or inconsistencies. Should the knowledge be incomplete, the uncertainty analysis is likely to reveal existing gaps, so that they can be filled in. In any case uncertainty analysis is a means of reviewing a measurement as well as a good awareness of the measurement process itself.

Results of more complex tests are typically derived from various measurands with a certain functional relationship linking the actual measurands and the desired measurement quantity. In this context it is instructive to determine the contributions of individual measurands to the overall uncertainty in order to identify the most relevant influences. With the help of such sensitivity data, the overall uncertainty can be reduced most effectively.

### ***2.2.1. Uncertainty versus Error***

The uncertainty of a measurement is defined as a parameter, associated with the result of a measurement, that characterizes the dispersion of the values that could reasonably be attributed to the measurand. In other words, an interval about a measured value that is likely to encompass the true value with a certain probability.

In the past measurement uncertainty was considered in terms of “errors”. The concept of error implies that there is a true value relative to which the magnitude of errors can be quantified. In practice however, such true values will never be known. The concept of uncertainty refers to the measured value and is preferred today. Mathematically, the two concepts are very similar. The term error rather tends to be associated with actual errors, like misinterpretation of readings, wrong wiring or confusion of signals. Such errors are virtually impossible to detect and correct once a test has been completed and therefore, extra effort should be spent to prevent them.

The general rules for expressing and evaluating measurement uncertainty are set in the “Guide to the Expression of Uncertainty in Measurement “(GUM).

### ***2.2.2. Accuracy versus precision***

In order to qualify the uncertainty of data collected the terms or accuracy and precision are to be distinguished. The accuracy of a measurement system refers to the degree of closeness of the measurements of a quantity to the actual, true or reference value. Thus, how far a measurement might potentially be off the target. In terms of probability or frequency distributions of measured data this translates as an offset of the mean value of the distribution with respect to the reference value (Figure 1).

The precision of a measurement system in contrast, describes the degree to which repeated measurements under unchanged conditions show the same results. This is also referred to as reproducibility (between-run precision, variability on different occasions) or repeatability (with-in run precision, variability on an occasion) which is expressed as variance or standard deviation of a probability density characteristic. The lower the variance, the higher the precision of the measurement is.

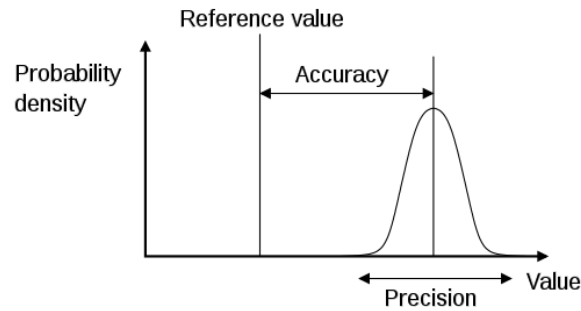


Figure 1: Illustration of precision and accuracy in measurement

The fact that precision and accuracy are independent characteristics of a measurement is illustrated in Figure 2 using the examples of targets with the reference value at the center.

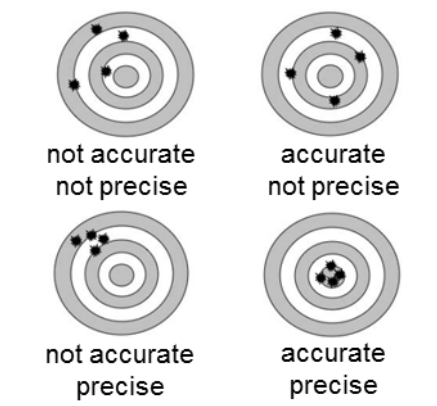


Figure 2: Illustration of independence of accuracy and precision for an exemplary measurement

At the same time as clarifying the meaning of accuracy and precision, Figure 2 indicates the challenge in distinguishing them from measurement data: while precision can be deduced from the data and its reproducibility itself, an assessment of accuracy requires the knowledge of the actual target value which is hardly available. In practice the accuracy of measurements can only be assessed by comparison to reference instruments of higher accuracy.

### 2.2.3. Uncertainty budget of measurands and derived quantities

Regardless of their classification according to accuracy or precision GUM distinguishes two types of uncertainty effects.

#### Type A

Type A encompasses all uncertainty effects that become manifest as variation of the measured values such as signal noise or general reproducibility. These are evaluated by means of statistical analysis of  $n$  repeated measurements  $x_k$ . The standard uncertainty contribution of a Type A quantity is calculated as the experimental standard deviation of the mean according to

$$u(x) = \sqrt{\frac{s(x)^2}{n}} = \sqrt{\frac{1}{n(n-1)} \cdot \sum_{k=1}^n (x_k - \bar{x})^2}$$

### *Type B*

Type B uncertainty effects encompass all uncertainty effects that are not purely statistical, thus all additional knowledge of the measurement process. This includes various sources of information such as the instruments themselves (characterized by their calibration certificates, manufacturer's specifications), any available experience from previous measurement series as well as any additional experience or knowledge like results of instrument characterization

In order to be able to include this information in the calculation of the resulting measurement uncertainty, the individual uncertainty effects need to be modeled. Depending on the kind of information different modeling approaches can be applied:

- For uncertainty specified as multiples of standard deviations normal distributions are suitable. This mainly applies to previously evaluated uncertainties for example resulting from instrument calibration.
- In other cases limiting (maximum) values of uncertainty might be specified for which rectangular distribution are most suitable.

Selecting the correct modeling approach and assumptions requires experience and is decisive for type B results.

### *Combined standard uncertainty*

Similarly to the formerly used propagation of error, there is a propagation of uncertainty that is more commonly called determination of combined uncertainty. As indicated by the name, the combined uncertainty encompasses all uncertainty contributions so that their resulting effect on the target value of a measurement can be quantified. The combination of uncertainty effects can be calculated on several levels of an uncertainty analysis:

- One particular measurand (like temperature or flow rate) can be influenced by several uncertainty effects (for example one Type A and one Type B) so that the calculation of combined uncertainty makes sense on this level.
- Or the target value of a measurement (like useful heat or thermal efficiency as in the case of performance testing) is calculated from several measurands which also necessitates an evaluation of combined standard uncertainty.

And in case of later parameter identification, the separation of precision and accuracy effects yielding two combined uncertainties can be very relevant.

In any of the mentioned cases a functional relationship linking the individual uncertainty effects and the target value is required.

$$y = f(x_1, x_2, x_3, \dots, x_N)$$

With the help of this functional relationship, and the standard uncertainties of the contributing measurands, the combined standard uncertainty of the target value is calculated according to:

$$u(y) = \sqrt{\sum_{i=1}^N \left[ \frac{\partial y}{\partial x_i} \right]^2 \cdot u(x_i)^2 + 2 \sum_{i=1}^{N-1} \sum_{j=i+1}^N \frac{\partial f}{\partial x_i} \cdot \frac{\partial f}{\partial x_j} \cdot u(x_i, x_j)}$$

Combined uncertainty thus is a function of sensitivities and individual standard uncertainties as well as correlation of measurands or uncertainty effects. This formula is valid for correlated and uncorrelated input quantities as the contribution of the second summand is negligible for the latter.

In the context of uncertainty evaluation “standard” always refers to a coverage of 1sigma or  $k = 1$ . A normal distribution of the resulting uncertainty is assumed so that a this value corresponds to covering 68.2% of all possible outcomes. If larger fractions are to be covered, a coverage factor of  $k > 2$  must be chosen and stated. The typical value are  $k = 2$ , covering about 95 % of all possible outcomes, and  $k = 3$  for 99 %.

$$U(y) = k \cdot u(y)$$

#### 2.2.4. Parameter uncertainty

Measurement/test results are typically used to identify characteristic parameters of a tested component or model. In combination with an adequate model, these then serve for computational simulation of the behavior of the system under various boundary conditions.

Typical parameter identification methods are least square fitting and optimization. At the same time as yielding the values of best fit parameters, these standard fitting methods can be used to derive their uncertainties. In doing so, particular care is required however, as the evaluation of parameter uncertainty included is typically based on the assumption of independence of measurements points. This assumption is generally violated when a single test set-up and/or set of instruments/sensors is used for all measurement points. In case of predominant uncertainty contributions due to accuracy effects (compared to precision), the measurements are potentially subject to an offset random in value but identical (systematic) for all points.

By assuming independent data points, standard identification methods however, only account for the effect of random data variation (precision) and thus tend to underestimate parameter uncertainty in particular for large series of low accuracy. The sensitivity of identification results to data shifts (due to accuracy effects) is to be tested in a separated step of the analysis and the two results to be combined.

Due to calibration procedures, characteristics of individual instruments and high repeatability uncertainty budgets are typically dominated by accuracy rather than precision effects. Thus, the above considerations are vital for correctly concluding on the uncertainty of the identified parameters.

#### Literature

*International Organization for Standardization (2008): Evaluation of measurement data -Guide to the Expression of Uncertainty in Measurement (GUM), Geneva (Switzerland).*



*V.A. Press, S.A. Teukolsky, W. P. Vetterling, B.P. Flannery (1992): Numerical Recipes – The Art of Scientific Computing, Cambridge University Press, Cambridge (England), Second Edition.*

# PART 1

## Concentrating Solar Power Technologies and Specific Testing Requirements

---

### 3. Parabolic Trough

Parabolic trough collectors consist of cylindrically shaped reflectors with parabolic curvature (trough), tubular receivers and a support structure with a drive and controls to track the path of the sun. Solar radiation incident in parallel to the longitudinal symmetry plane (optical axis) is reflected on the surface and concentrated into the focal line of the collector. The concentrated radiation is intercepted by receivers, converting it to heat and transmitting it to the heat transfer fluid. In order to enable continuous operation by keeping the direction of the optical axis of the concentrator aligned with the direction of the sun throughout the day, the collectors are tracked about their longitudinal axis. The concentration ratio of the parabolic trough design determines the maximum allowable directional deviation of irradiance to be focused (acceptance angle).

#### 3.1. Component Performance Evaluation

The technology specific components of a parabolic trough collector system are its two-dimensional parabolic shaped facets (reflector), the linear trough receivers and the rotation and expansion performing assemblies (ball joints, flex hoses, etc.). Laboratory or indoor tests designed to investigate and evaluate the characteristics of these components under well-defined conditions ensure the reproducibility and comparability of the results obtained and their meaningfulness for field application. The smallest units of parabolic trough collectors consisting of a concentrator and receiver with the corresponding structures – the so called modules – are often too large for laboratory testing and are thus studied in workshop halls or outdoors.

##### 3.1.1. *Indoor tests for facets*

Facet testing is one of the most important issues because the final effectiveness of the solar collector strongly depends on the facet properties, i.e. *solar reflectance* and *shape* compliance with the ideal parabolic profile.

##### 3.1.2. *Solar reflectance*

Reflectance describes the efficiency of a material in redirecting incoming radiation distinguishing between specular and hemispherical reflectance according to the predominant direction of the reflected light. In concentrating solar power applications specular reflectance is of particular relevance as mirrors are generally used for concentration by multiple reflections.

Various reflector materials are used in parabolic trough and other CSP technologies as reflectors: front or back silver-coated glass mirrors, aluminium sheets or polymer film. The different materials differ in reflectance characteristics such as wavelength or angular dependence of reflection, beam spread and resistance to mechanical wearing. Accordingly, a number of different test procedures are typically required for their full characterisation. Recently, SolarPACES Task III released an official reflectance guideline that can be referred to for further information and recommendations.

#### *Typical Test Procedures*

Typically, the reflectance properties of a facet (or any other kind of CSP reflector) are characterised by measurement of:

- Hemispherical specular reflectance (see Measurement Methods Reflectance) and subsequent weighting with the solar spectrum to determine effective reflectance for solar radiation
- Near-specular reflectance, comprising specular reflectance and diffuse reflectance within a certain acceptance angle. The acceptance angle depends on the requirements of the specific CSP application and measurements for several acceptance angles in the range of interest should be carried out.

A more detailed description of the measurement method for reflectance is included in chapter°10.1.

### 3.1.3. Shape accuracy

The distribution around the focal line of the solar radiation reflected by the facet depends on the shape-compliance with the ideal parabola. In a given point of the facet surface, the shape-compliance is represented by the difference of the measured height ( $z$ ) and slopes ( $\partial z/\partial x$  and  $\partial z/\partial y$ ) from the ideal values. Generally, the effects of slope-deviation (SD) are more relevant because they cause twice the deviation in direction of reflected rays (see Figure 4), whilst height-deviation (HD) results as rays displacement which increases for points far away from the parabola vertex (see Figure 3).

In case of small height deviations, slope deviation can be calculated under the assumption that the surface was ideally shaped. Shape/height deviation is then obtained by integrating the data. However, if the geometry of the reflecting surface is not exactly known or large height deviations are expected, slope deviation should be calculated in an iterative process using the integrated data as new starting values. The more accurate procedure should also be adopted during the R&D activities of the optimization of facet shape-compliance when facets are shaped by a mold.

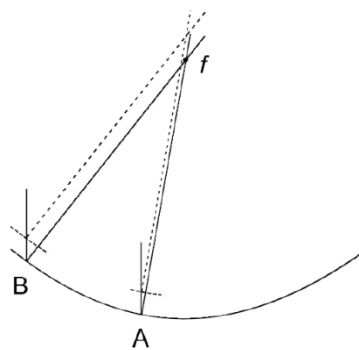


*Figure 3: The further the point is from the vertex, the more important larger HD becomes affecting FD and should thus be considered in addition to SD*

Concerning the final purpose, i.e. concentration of solar radiation, both HD and SC cause ray-displacement from the focal line. The extent of that displacement is called focus deviation (FD), and is the distance between two straight lines: the reflected ray and the focus line. FD is computed by means of raytracing considering both the Sun centre and the point of the Sun circumference for which the deviation is maximum as shown in Figure 3. These values are referred to as FD and MFD respectively. The latter also accounts for the spreading of the reflected beam along its way towards the focus.

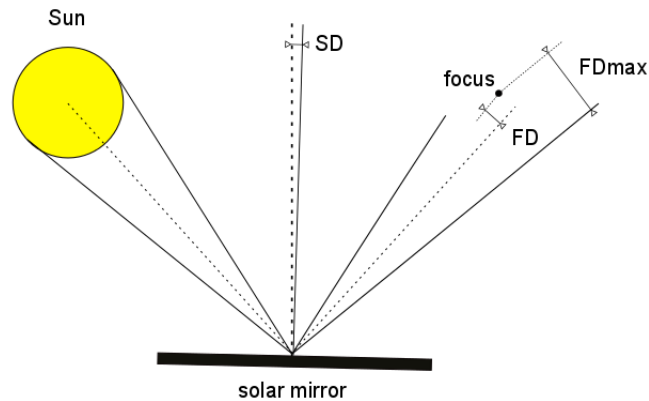


*Figure 4: Displacement of the reflected beam from the focus caused by slope deviation (SD). The distance from the focus of the axis of the conical bundle of reflected rays, and of the farther ray are called FD and FDmax, respectively*

Another important parameter that summarizes the concentration effectiveness is the intercept factor (IF), the ratio of solar radiation reflected towards the receiver and geometrically captured by it. Like MFD, the intercept factor is evaluated by raytracing, assuming a suitable model for the Sun. In the simplest one the Sun is modelled by a uniform circular source, with a diameter corresponding to 9.4 mrad viewed from the Earth.

The parameters SD and HD characterize the shape accuracy in the strict sense. FD and MFD and IF describe the facet effectiveness in concentrating solar radiation and depend on the angle between the incoming radiation and the parabola axis.

More recently, SolarPACES TASK III published the guideline draft “Measurement and Assessment of Mirror Shape for Concentrating Solar Collectors”. This document states only the main points. For more detailed information, see the guideline draft document.

Generally, facets are not perfectly rigid and their shape depends on the way they are mounted and oriented in the gravity field. Wind may also have an important effect. Currently, there are no standardized measurement or evaluation procedures to assess these effects. They can be summarized in terms of:

- **Stiffness:** ability to maintain a constant shape accuracy under gravity and wind solicitude. The gravity effect can be evaluated by comparing the results achieved for different choices of the tracking angle. The wind effects can be simulated by applying suitable forces to a set of points determined by FEM analysis.
- **Stability:** ability to maintain a constant “shape accuracy” and the “nominal intercept factor” along ageing and thermal expansion.

### *Typical Test Procedures*

Typically, the shape of parabolic trough concentrators is assessed by optical measurement methods such as reverse analysis, laser scanning or photogrammetry as described in chapter 13. These can be

carried out under varying boundary conditions or repeated in the course of an aging process in order to investigate the effect of boundary conditions or aging on the shape accuracy.

### *Literature*

*Parameters and Method to evaluate the Solar Reflectance Properties of Reflector Materials for Concentrating Solar Power Technology, SolarPACES Official Reflectance Guideline, version 2.5, June 2013. [http://www.solarpaces.org/Tasks/Task3/reflectance\\_guideline.htm](http://www.solarpaces.org/Tasks/Task3/reflectance_guideline.htm)*

*Draft of SolarPACES Guideline Measurement and Assessment of Mirror Shape for Concentrating Solar Collectors Version 02, June 2013*

#### *3.1.4. Indoor tests for Heat Collecting Elements (HCE)*

Parabolic trough linear receivers also known as Heat Collecting Elements (HCE) are trough specific components converting incoming concentrated irradiance into useful heat of the heat transfer fluid. They are designed with an optimum ratio of absorption for solar irradiance to thermal loss at elevated operating temperatures. For utility size parabolic trough receivers this is typically achieved by using a spectral selective coating on the absorber tube and evacuating the annulus between the absorber tube and the glass envelope.

#### *Heat transfer mechanisms*

A number of heat transfer processes of all typical mechanisms affect the performance of HCEs for parabolic troughs:

- **Forced convection** between the inner surface of the absorber/steel pipe and the heat transfer fluid
- **Radiation** between the outer surface of the steel pipe and the inner surface of the glass envelope
- **Conduction-convection** between steel/absorber tube and glass envelope if the level of vacuum decreases over time, due to the presence of gas in the annular cavity (for reasons of leakage, degassing of materials, or diffusion of ions through the steel)
- **Radiation** between the outer surface of the glass envelope and environment
- **Natural or forced convection** (depending on the speed of the wind), between the outer surface of glass envelope and ambient

The heat exchange coefficient for natural or forced convection between external surface of the glass and environment (as a function of average temperature of outer surface of glass and ambient air) can be evaluated by literature correlations between the Nusselt number and the Grashof or Reynolds numbers.

#### *Typical Test Procedures*

Selective coatings of parabolic trough receivers and anti-reflective coatings of their glass envelopes are typically characterized in terms of surface properties such as **reflectance**, **absorptance** and

**emittance** as described in chapter 10.2. In addition to these optical material properties parabolic trough receivers can be characterized in terms of or overall component properties such as:

- the **optical efficiency** of an HCE commonly determined in sun simulator test benches quantifying the total absorbed power at near ambient temperature by means of calorimetry and evaluated by comparing the measured heat gain to that of a particular well-characterised reference receiver,
- the specific **heat loss** of an HCE as a function of temperature typically determined in the laboratory by heating the receivers on the inside and measuring the temperature (distribution) and electrical power at steady-state conditions for a number of operating points as described in chapter Fehler! Verweisquelle konnte nicht gefunden werden.,
- the **thermal efficiency** of the HCE usually determined in outdoor tests as described in chapter 1.1.

The **maximum operating temperature of the absorber coating** can be determined in ageing tests, by heating the steel tube for a long time (at least one week) and to verifying the variation of the thermal efficiency or specific heat loss of the coating with time. The maximum operating temperature of the coating can be defined as the maximum temperature at which there is no appreciable changing of the emissivity with time.

### *Literature*

*Tairan Fu, Peng Tan, Chuanhe Pang (2012): A steady-state measurement system for total hemispherical emissivity Measurement, Science and Technology Volume 23.*

*Cheng Shu Xia, Ge Xin Shi, Yao Cheng Cai, Gao Ju Wen, Zhang Yong Zhong (1993): Research on the validity of the steady-state calorimeter for measuring the total hemispherical emissivity of solids, Measurement, Science and Technology Volume 4.*

*J. Pernpeintner, B. Schiricke, E. Lüpfer, N. Lichtenthäler, M. Anger P. Ant, J. Weinhausen (2011): Thermal and optical characterization of parabolic trough receivers at DLR's QUARZ Center - Recent advances. SolarPACES 2011, 20.-23. Sept. 2011, Granada, Spain.*

## **3.2. System/Module Performance Evaluation**

Each collector module consists of an orientable mechanical structure supporting the parabolic-trough reflector and the receiver tube, positioned in the focal line. Being the smallest full unit of a parabolic trough collector a module can serve for characterization of a new type of collector provided a suitable tracking unit or drive.

Individual module/collector designs can be distinguished in terms of the following descriptive characteristics that need to be collected for the module investigated and included in the final measurement report:

- **Typology:** torque-box and wings / torque-tube and wings / etc.
- **Technology:** main characteristics of the adopted manufacturing technology.

- **Dimension:** physical and nominal-area intercepting solar-radiation.
- **Tracking system:** info on the motorized system.

The aim of module testing is to assess the geometrical precision achieved by the design and assembly process and to investigate to which extent it is maintained under typical conditions (load, torsion). Furthermore, in thermal tests the overall module performance is investigated under defined boundary conditions yielding information on optical efficiency, thermal efficiency and heat loss.

### *3.2.1. Geometric Precision and Optics*

The capacity of a parabolic trough collector design to concentrate incoming solar radiation onto its receiver - thus the quality of the design and manufacturing - is characterized by its intercept factor. The contributions of the support structure and receiver positioning can be evaluated and optimized individually or the entire system is investigated as such.

#### *Typical test procedures*

Suitable qualification methods exist for the different components of parabolic trough collectors. In the following, measurement methods to determine the geometric accuracy of the collector structure with and without mirrors are presented briefly (see also chapters 13.3 and 13.1 on photogrammetry and deflectometry), while the main focus is on approaches to determine the ability of relevant components to maintain their geometric accuracy under operating loads:

- The deviation of the **support structure** and/or mirror mounting points from the ideal shape or positions may be determined by means of photogrammetry [4]. The resulting deviations between actual and ideal coordinates of measurement points can be derived and compared to tolerances.
- A parabolic-trough may be bent due to gravity, making proper **receiver alignment** more difficult. Therefore, the best practice is not align the receiver as a straight line, but following the torque tube/box bending: this makes the intercept factor more conservative over the Sun tracking. Another approach is to determine the characteristic bending curve from the photogrammetric data and to correct the data accordingly. That way, the reference for the receiver alignment is again the (straight) focal line. A simple approach to derive lateral deviations of the receiver from the focal line is to measure the distance of the glass envelope tube to both outer mirror edges. This method delivers reliable results as long as the mirror edge serves as a good reference.
- The module effectiveness is strongly related to the mutual **optical alignment** of parabolic-trough and receiver. Different approaches to evaluate this alignment (and the resulting intercept factors) from the image of the receiver in the concentrator have been developed (TOPCAT [1], TARMES [2, 3] and VISfield [5]) and are described in chapter 14. Other than the actual value of the intercept factor (ratio of solar radiation reflected towards the receiver and geometrically captured by it), these approaches yield spatially resolved information on the slope deviation (shape compliance) of the concentrator geometry. On this basis, problematic areas can be identified and geometries optimized. These approaches have in common that they are applied to the complete parabolic trough, so resulting shape

deviations include both shape deviations of the structure as well as shape deviations from the mirror.

### ***3.2.2. Tracking accuracy and stability of the drive system***

A tracking system is designed to maintain the optical axis of the parabola parallel to the incoming solar irradiance during operation.

#### ***Typical Test Procedures***

The qualification procedures for the drive system are based on a series of tests aiming at verifying the system's ability to operate in tracking ensuring the required levels of precision, to withstand the design loads and to maintain these characteristics over time (durability). They encompass tests for

- existing **backlashes** that characterize the drive system,
- **tracking and cycling tests under load** determining the accuracy of positioning under nominal load,
- **drive tests under high load** essential for safe positioning,
- **ultimate strength tests** indicating whether the drive system statistically withstands a load (torque) equal to the design limit.

The above tests methods are described in greater detail in chapter 15.

### ***3.2.3. Mechanical testing aspects: Accuracy and stiffness of the structure***

Commercially available parabolic trough systems are characterized by different technological solutions for the following relevant features of the mechanical structure:

- the two pivots allowing the module to track the Sun;
- the points where the facets are mounted;
- the points where the receiver tube units are mounted.

The reference frame illustrated in Figure 5 is oriented with the y-axis crossing the two pivots, the z-axis parallel to the parabola optical axis, and the x-axis as the parabola abscissa with origin in its vertex. The origin of the reference frame is set on the edge of the parabolic trough such that y-axis sense is that of the thermal fluid flow.

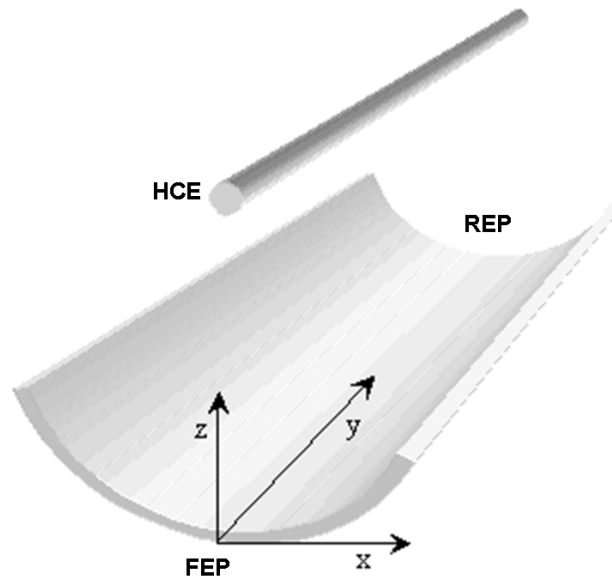


Figure 5: Reference coordinate system for parabolic trough collector modules (FEP= front end plate, REP= rear end plate)

The qualification procedures for the concentrator geometry and the receiver support systems are based on a series of tests aimed at assessing the capacity of the support systems to position both, the concentrator and the receiver, ensuring the required level of precision.

In the case of operating loads, it is necessary to limit the deformation of the supports within the specified values, to withstand the design loads and to maintain these characteristics over time (durability).

### *Typical Test Procedures*

There are **backlash, flexibility and strength/stiffness tests** aiming at verifying the deformability of the reflective surfaces and receiver supports when subjected to normal operating loads and their failure resistance when subjected to ultimate loads (e.g. storm).

#### *3.2.4. Measurement of thermal, optical and total performance/efficiencies of the solar collector system*

In contrast to component performance testing, the experimental determination of collector/module performance or efficiency aims at qualifying a parabolic trough as functional unit converting incident solar irradiation to useful heat. To this end, the performance of modules or collectors is commonly evaluated in terms of their useful power generation under particular operating conditions with respect to operating temperature level, angle of incidence of solar irradiation and irradiation.

The advantage of this approach lies in the possibility of evaluating a system/prototype “as built” and thus encompassing all relevant optical and thermal effects. Thus, it is often employed as an ultimate test in collector development and serving as a functional and operational check as well as for confirmation or proof of expected performance characteristics. The test results can be used in model validation and as a basis for performance predictions.

## Typical test procedures

Typical test procedures for the qualification of system performance typically encompass:

- **Efficiency testing** evaluating the ratio of useful power to effective solar power incident on the system in quasi steady-state operation. According to test conditions, different efficiency characteristics can be investigated:
  - **Peak optical efficiency** at near perpendicular incidence of solar irradiance on the collector aperture and mean fluid temperature near ambient temperature eliminating both angular dependent effects as well a thermal loss,
  - **Thermal efficiency** at normal incidence for a range of operating temperatures.
- The **Incident Angle Modifier (IAM)** as the ratio of optical efficiency at varying angles of incidence to peak optical efficiency for low fluid temperatures and a sufficiently broad spectrum of incidence angles.
- **Thermal losses** of the receiver and collector tubes as a function of temperature without irradiance.

These tests and their measurement quantities and requirements are described in greater detail in chapter 1.1.

## 3.3. Heat Transfer Fluid

Various heat transfer fluids for parabolic trough collectors have been proposed and employed. Currently, only two of them are commonly used in commercial power plants: thermal oils and molten salt mixtures (nitrates and nitrites). Among the others, water is currently being demonstrated in direct steam generation plants and CO<sub>2</sub> is still at an experimental stage. A definition of heat transfer fluids is given in DIN 51522.

### Thermal oils

Thermal oils are widely used in the majority of solar plants. Typical the eutectic mixture of biphenyl (BP) and diphenyl oxide (DPO) is applied except for some CSP plants coupled to organic Rankine processes. Silicon oil (dimethylpolysiloxane) is often used instead of the eutectic BP/DPO mixture in test facilities due to its low hazardness.

### Molten salt mixtures

The use of binary mixtures of sodium and potassium nitrates NaNO<sub>3</sub>-KNO<sub>3</sub> was deeply investigated in the eighties by the Sandia National Laboratories and other U.S. institutions. These materials are relatively cheap, have good chemical safety, and are not corrosive.

The range of operating temperature  $\Delta T$  for molten salt mixtures depends on two characteristic properties of the mixture:

- The freezing point: The freezing point is relatively high compared to organic heat transfer oils. For instance, diphenyl oxide oil freezing point is at about 12 °C, and the upper temperature limit is 393°C ( $\Delta T=281^\circ\text{C}$ ); while the eutectic of NaNO<sub>3</sub>-KNO<sub>3</sub> melts at 221°C and with a composition 0.6/0.4 (weight/weight) this point increased to 238°C. For multi-

component mixtures the freezing point is better defined by the “liquidus temperature”, which is the temperature at which solidification begins.

- The maximum operating temperature: The upper limit depends on the chemical stability of molten nitrates; it is evaluated to be around 600 °C, according to literature data. At those conditions, some chemical reactions became favored by the enhanced temperature and consequently the physical and chemical features of the system are changed. **Table 3** reports the existing chemical equilibriums (considering Na, the same situation can be described for K) in a NaNO<sub>3</sub>-KNO<sub>3</sub> mixture, which consist in: nitrates shift equilibrium (1, 2, 3); nitrates/nitrites interaction reaction with atmospheric gases such as oxygen (3) or decomposition reactions (4). Reaction (4) presents serious concerns, considering that insoluble products may form.

*Table 3: Nitrates/nitrites reaction pathways*

Reaction type	
$\text{NO}_3^- \leftrightarrow \text{NO}_2^- + 1/2\text{O}_2$	(1)
$\text{NaNO}_3 \rightarrow \text{NaNO}_2 + 1/2\text{O}_2$	(2)
$\text{NaNO}_2 + 1/2 \text{O}_2 \rightarrow \text{NaNO}_3$	(3)
$2\text{NaNO}_2 \rightarrow \text{Na}_2\text{O} + 3/2 \text{O}_2 + \text{N}_2$	(4)

In order to lower the freezing point, the addition of sodium nitrite NaNO<sub>2</sub> was first considered. In ternary mixtures NaNO<sub>3</sub>-KNO<sub>3</sub>-NaNO<sub>2</sub>, with respective concentrations of 7/53/40 (%w/w), the liquidus point is also lowered to 141°C. This mixture is frequently used in industrial applications, its maximum operation temperature in air is limited to 450°C.

Subsequently, the adding of calcium nitrate Ca(NO<sub>3</sub>)<sub>2</sub> and lithium nitrate LiNO<sub>3</sub> were considered. These ternary mixtures benefit from low melting points at 120 °C adding lithium, and 133 °C adding calcium. Concerning the stability, when lithium nitrate is used, the ternary mixture is stable up to 550 °C. This value is limited to around 450 °C when calcium nitrate is used. As a matter of fact, at higher temperature a solid phase was observed, which could probably be ascribed to the formation of insoluble CaO, according to the reaction ( $\text{Ca}(\text{NO}_3)_2 \rightarrow \text{CaO} + \text{N}_2 + 2\text{O}_2$ ); which can result in plugging of valves, pipes and heat transfer surfaces. Calcium nitrate addition to the molten salt can significantly reduce the liquidus temperature but it drastically increases the viscosity, especially near the melting point. Lithium nitrate addition shows only minor effects on the viscosity of the mixtures but is quite expensive compared to others nitrates.

Interesting results were discovered using quaternary nitrates mixtures, i.e Na-K-Li-Ca nitrates. In this case a value of the liquidus temperature of about 95 °C can be achieved, and the mixtures are stable up to 450 °C.

Table 4 summarizes the liquidus and maximum temperature of main mixtures proposed in literature.

Table 4: Liquidus and maximum temperature of binary-ternary-quaternary mixtures

NaNO <sub>3</sub> (% w/w)	KNO <sub>3</sub> (% w/w)	CaNO <sub>3</sub> (% w/w)	LiNO <sub>3</sub> (% w/w)	NaNO <sub>2</sub> (% w/w)	Liquidus T (°C)	Maximum T (°C)	notes
46	54				221 <sup>1</sup>	nr	eutectic
60	40				238 <sup>2</sup>	550 -600 <sup>3</sup>	binary solar salt
7	53			40	141 <sup>4</sup>	450-538 <sup>4</sup>	HITECH® salt
15	43	42			133 <sup>3</sup>	480 <sup>3</sup>	reported eutectic <sup>2</sup>
23	46	30			140 <sup>2</sup>	505 <sup>3</sup>	
17	59		23		120 <sup>2</sup>	550-600 <sup>5</sup>	reported eutectic <sup>2</sup>
18	53		30		nr	550 <sup>6</sup>	
Nr	nr	nr	nr		95 <sup>2</sup>	500 <sup>6</sup>	quaternary mixture

nr= not reported, sources: <sup>1</sup>Zhang (2003), <sup>2</sup>Siegel (2010), <sup>3</sup>Bradshaw (1990), <sup>4</sup>Coastal Chemical Co., <sup>5</sup>ENEA data, <sup>6</sup>Bradshaw (2008)

The only long term tests on molten salt nitrates (60 Na – 40 K wt%) have been carried out at ENEA facilities (PCS and MOSE): In the PCS (Solar trough test facility) plant, the molten salt mixture has been continuously recirculated since 2004 for more than 60000 hours. The only variation detected in the molten salt composition, compared to the initial one, was nitrite formation at a concentration of around 2% (wt%). The production of this species is a typical behavior of nitrates in air atmosphere. Stainless steel alloying components were detected in the salt mixture at ppm concentrations, with no measurable effect on molten salt thermo-physical properties. No Na and K oxides were detected and the only gas production consisted of small quantities of oxygen at the beginning of the experimental campaign.

The first industrial plant with molten salt, Archimede solar power plant (5MWe) of ENEL electric company, is running since mid 2010 but no data are available at the moment.

ENEA and ENEL plants adopt the typical technical grade composition of molten salts as stated in Table 5. The use of anticaking agents is not accepted.

Table 5: Chemical composition specifications of molten-sat

Name	Mix potassium nitrate + sodium nitrate	
Composition	Sodium nitrate NaNO <sub>3</sub>	60 %
	Potassium nitrate KNO <sub>3</sub>	40 %
	Minimum nitrate %	99 %
<b>MAX PERCENTAGE OF IMPURITIES</b>		
Nitrite		0.20 %
Chloride		0.03 %
Carbonates		0.05 %
Sulfates		0.15 %
Alcalinity hidroxile		0.04 %
Perchlorates		0.04 %
Magnesium		0.04 %
Calcium		0.04 %
Insoluble		0.06 %

### Typical Test Procedures

Typical tests for thermal oils and molten salts include:

- Investigation of their **composition** and possible changes due to contact with typical system materials or other fluids (steel, water/steam) or operating conditions and **aging**.
- Thermophysical **properties** (density, heat capacity, etc.)
- Particular **phenomena** such as formation of hydrogen or solid compounds.

Other than the above methods for fluid characterization, these chapters also include a concise literature review of previous work on thermal oil and molten salt as a HTF in CSP application with focus on HTF chemistry.

## 4. Tower

Solar power towers generate electric power from sunlight by concentrating solar radiation on a tower-mounted heat exchanger (receiver). It uses an array of moveable mirrors (called heliostats) to focus the sun's rays upon a collector tower (the target). The high energy at this point is transferred to a heat transfer fluid to either store the heat for later use or directly generate steam for driving a Rankine cycle. When the HTF is pressurized air, the system can be coupled to a Brayton cycle in a gas turbine.

Tower systems are composed of different subsystems that can be evaluated independently in order to obtain partial efficiencies that can be combined to obtain the overall efficiency of the plant. These subsystems are:

- Solar field: composed of hundred to thousand heliostats
- Receiver.

## 4.1. Component Performance Evaluation

### 4.1.1. Heliostats

#### Optical Performance (Flux Mapping)

The optical performance of single heliostat is determined by the accuracy of the normal vector as this parameter governs the reflection. Deviations of the normal vector can be measured by means of photogrammetry, deflectometry and/or flux mapping. The first two methods are described in the chapter on shape measurement (chapter 13) because they are general for every kind of concentrator, whereas the flux mapping methodology is particular for the optical characterization of heliostats and is described below.

A characterization of heliostats by flux mapping conventionally translates as a quantification of heliostat errors determined by an analysis of their relative intensity distribution. To this end, they are aimed at a target normal to the direction of propagation of the reflected beam plane. This flux distribution is captured and stored by a digital camera. Thus, it is presented in its final form as a two dimensional array of numbers representing the spatial distribution of intensity (digital image), and can be characterized mathematically by the so-called image descriptors, in particular the central moments.

$$\mu_{pq} = \sum_x \sum_y (x - \bar{x})^p (y - \bar{y})^q f(x, y)$$

In case of a heliostat the central moments of order 1 and 2 are of particular interest, which can be expressed as follows:

$$\mu_{20} = \sum_x \sum_y (x - \bar{x})^2 f(x, y)$$

$$\mu_{02} = \sum_x \sum_y (y - \bar{y})^2 f(x, y)$$

$$\mu_{11} = \sum_x \sum_y (x - \bar{x})(y - \bar{y}) f(x, y)$$

Finally, the statistics that describe the digital image is defined in terms of the central moments as:

$$var(x) = \frac{\mu_{20}}{\sum_x \sum_y f(x, y)}; \mu_x = \sqrt{var(x)}$$

$$var(y) = \frac{\mu_{02}}{\sum_x \sum_y f(x, y)}; \mu_y = \sqrt{var(y)}$$

$$covar(x) = \frac{\mu_{11}}{\sum_x \sum_y f(x, y)}$$

The variables  $\mu_x$  and  $\mu_y$  are called standard deviations of the digital image based on the XY axes. The covariance of the distribution of intensity  $covar(x, y)$  quantifies the degree of correlation between the pixels of the image function, which helps to detect possible ellipticities, for example.

The above considerations lead to the most useful description of the image, which requires knowledge of their standard deviations according to the principal axes UV of the intensity distribution, which are those orthogonal axis for which  $covar(u, v) = 0$ , that is, these axes indicate the directions of maximum expansion of the image (Figure 6).

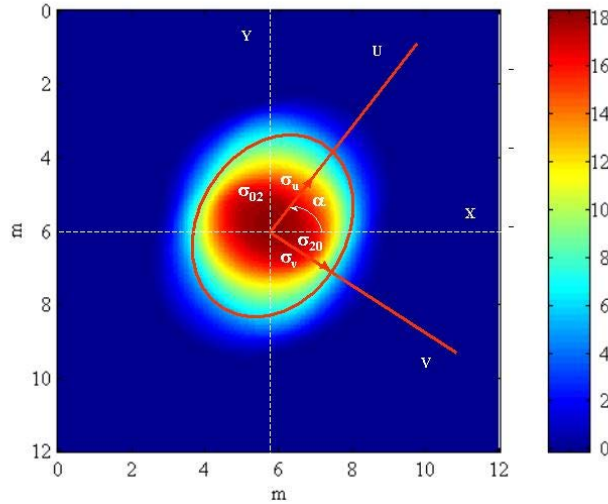


*Figure 6: Measured flux density of a heliostat with superimposed flux mapping analysis*

The basis vectors of these axes are the eigenvectors  $\{e_u, e_v\}$  associated with the eigenvalues  $\{\lambda_u, \lambda_v\}$  of the covariance matrix  $C_{XY}$  of the region pixels:

$$C_{XY} = \begin{pmatrix} var(x) & covar(x, y) \\ covar(x, y) & var(y) \end{pmatrix}$$

And principal standard deviations are defined as:

$$\mu_U = \sqrt{\lambda_U}; \mu_V = \sqrt{\lambda_V}$$

where  $\lambda_u, \lambda_v$  are the eigenvalues of the covariance matrix or variances of the image according to U and V axes.

The resulting shape of the Sun's image produced by a heliostat is influenced by various effects, such as the characteristics of the solar disk, the astigmatic aberration of the image, and the errors inherent in the heliostat. The impact of these effects on the statistical study of the image are independent. From a formal point of view, it can be demonstrated that statistically independent descriptors can be combined to an overall effective value according to the mathematical relationship:

$$\mu_{real}^2 = \mu_{sun}^2 + \mu_{astigm}^2 + \mu_{surface}^2$$

where  $\mu$  represent the standard deviations associated with the actual image of the heliostat ( first member ), solar disk , astigmatic aberration, and heliostat's surface errors. This can be resolved to yield the characteristics of the surface

$$\mu_{\text{surface}}^2 = \sqrt{\mu_{\text{real}}^2 - \mu_{\text{theor}}^2} \text{ where } \mu_{\text{theor}}^2 = \mu_{\text{sun}}^2 + \mu_{\text{astigm}}^2$$

$\mu_{\text{surface}}$  has units of length, as a standard deviation it quantifies the degree of dispersion of the impact of the beam with respect to its center  $(\bar{x}, \bar{y})$  and includes only errors originating from the heliostat shape. This value can be expressed in angular units (the angle subtended from the center of the heliostat) and is called error dispersion of the reflected beam and numerically expresses the optical quality of the heliostat in mrad:

$$\sigma_{\text{optical quality}}^2 = \sqrt{\sigma_{\text{real}}^2 - \sigma_{\text{theor}}^2} \text{ where } \sigma_{\text{theor}}^2 = \sigma_{\text{sun}}^2 + \sigma_{\text{astigm}}^2$$

This value is comparable to the normal deviation determined by the others shape measurement methods.

### *Tracking accuracy (Optical)*

In the same way, it is possible to calculate the standard deviation of the angular deviations of the center of the radiation spot reflected by the heliostats due to the inaccuracies of the tracking mechanism. This error is independent of the error calculated above and can be correlated in order to calculate the total heliostat error.

### *Solar Field Efficiency*

Solar field efficiency describes the ration of the power of solar radiation collected by the total surface of mirrors of the solar field to the power delivered at the receiver aperture. Basically, it depends on the heliostat layout on the solar field and the relative position of the receiver and the sun. As the sun position is changing continuously along the day and along the year, this value is instantaneous or can be determined as daily, monthly or annual average.

Main losses mechanisms included in the solar field efficiency are:

**Mirror Reflectance.** Mirror reflectance describes the fraction of the radiation absorbed by the glass which the mirrors are made of. Reflectance should be measured according the method described in chapter 10.1 .

**Cosine Effect.** This effect depends on both the Sun's position and the location of the individual heliostat relative to the receiver. The heliostat is positioned by the tracking mechanism so that its surface normal bisects the angle between the sun's rays and a line from the heliostat to the tower. The effective reflection area of the heliostat is reduced by the cosine of one-half of this angle.

**Shadowing and Blocking.** Shadowing occurs at low sun angles when a heliostat casts its shadow on a heliostat located behind it. Therefore, not all the incident solar flux is reaching the reflector. Blocking occurs when a heliostat in front of another heliostat blocks the reflected flux on its way to the receiver. The amount of shadowing and blocking in a particular field layout is a function of the heliostat spacing, tower height, and sun angle.

**Atmospheric Transmittance.** Many factors in field layout suggest that the field should extend far to the north of a very high tower. One major limitation on the distance a heliostat is placed away from the tower is the attenuation of the reflected beam as it travels from the heliostat to the receiver.

**Spillage.** This is the solar radiation that is not impinging the receiver surface but delivered on its surroundings. This factor depends on the distance between the heliostats and the receiver and on the optical and tracking accuracy of the heliostats.

Finally, the **total solar field efficiency** can be calculated as:

$$\eta_{\text{solar field}} = \eta_{\text{reflectance}} \eta_{\text{cosine}} \eta_{\text{Shadow and blocking}} \eta_{\text{Attenuation}} \eta_{\text{Spillage}}$$

Values of solar field efficiencies are usually computed by means of raytracing simulations of the heliostats layouts for a particular moment of the year or an annual average.

#### 4.1.2. Receiver

##### Delivered Power Calculation

To evaluate the efficiency of the receiver on a solar tower plant the thermal power output of the solar system is to be calculated from the change in enthalpy in the receiver working fluid. Across the inlet/outlet points, the delivered thermal power can be computed from:

$$P_{\text{meas}} = \dot{m}_{\text{HTF}} \cdot \Delta h_{\text{rec}}$$

#### 4.2. System Performance evaluation

The thermal power output of the solar field during a short-duration test period will vary primarily with the magnitude of the solar resource and the time of day and season. The purpose of the Power Test is to measure the thermal power output of the solar system under clear-sky conditions over a short period during which thermal steady-state equilibrium conditions exist, and to compare the measured results to performance model projections for those parameters.

Secondary impacts on power output result from variations in wind speed and ambient dry-bulb temperature. Thermal steady-state conditions can be expected for power tower systems at most times of the year for short test-run durations. Acceptable systematic uncertainties are the dominant consideration.

##### Typical Test Procedures

The key characteristics of the test methods are provided immediately below for both the short-duration thermal Power Test and multi-day long-duration continuous Production Test. The essence of these tests and their relevant characteristics are described below.

##### Short-Duration Steady-State Thermal Power Test (Power Test)

- Clear-day tests run at a thermal equilibrium condition
- Tests akin to ASME performance tests are run on equipment with a steady energy source
- Requirements specifying that equipment shall be operated within the pressure, temperature, and flow limits specified by the equipment vendors
- Comparison of measured performance to model projection
- Requirement to repeat tests over hours/days to prove replicability

##### Long-Duration Production Test (Production Test)

- Length of duration is specified in the contract, ranging from several days (e.g., up to 15) to months to years
- Test covers complete operation from morning startup to evening shutdown, and overnight parasitic thermal and electrical losses
- Extra factors are included that are not part of the short-duration Power Tests, e.g., startup transients, freeze protection, variable irradiance, inclement weather conditions, and shutdown transients
- Equipment shall be operated within the pressure, temperature, and flow limits specified by the equipment vendors

Used appropriately, there are two other specific uses of the Power Test tests, namely in the Capacity Test and in the calculation of solar system thermal efficiency.

#### Capacity Test

- Short-duration Power Test to prove design capacity
- Test to be run at specified minimum solar conditions, or higher
- No comparison to model projection unless required
- Typical duration is over a number of hours within a period of several days

#### Solar system thermal efficiency calculation

- Derived from the results of the Power Test by normalizing with the solar power to the heliostat field (specifically, the DNI times the tracking heliostat area)
- To be examined if designated by the Parties to the test
- Measured efficiency performance to be compared to model projection

The tests are to be run on clear days during any time of year. Even with a high DNI, which can be experienced on a clear winter day, the important solar resource term that dictates the thermal energy input into the receiver is found to be relatively steady during midday periods throughout the year.

During the performance test period, the solar systems should not be operated beyond their specified or suggested operating limits for solar resource, ambient temperature, or wind speed as provided by the solar system supplier(s).

Calculation of the mass flow typically requires measurement of the volumetric flow rate and knowledge of the working fluid density (i.e., that of molten salt, water-steam, or gas) as a function of temperature. Calculation of the thermal power requires knowledge of the enthalpy.

In the case of an indirect molten salt receiver system, these properties of the working fluid are recommended to be measured prior to the test.

### *Literature*

D. Kearney (2013): Utility-Scale Power Tower Solar Systems: Performance Acceptance Test Guidelines, NREL Technical Report.

### 4.3. Chemical test

This section describes the test and evaluation of receiver-reactors used for solar thermochemical processes. In those processes concentrated solar radiation is used to provide high-temperature process heat for endothermic chemical reactions. So-called receiver-reactors act on the one hand as a receiver for absorption of the incoming solar irradiation and on the other hand, they provide the reaction room for the chemical reaction.

Different types of thermochemical reactions can be carried out in receiver-reactors, e.g. solar steam and dry reforming, cracking, gasification as well as thermochemical cycles. The goal of those processes is the production of solar fuels, i.e. hydrogen or synthetic gas, as a means of storing solar energy in a chemical form. All those processes have in common that they need high temperature process heat to drive the endothermic chemical reaction.

### 4.4. Performance of Solar Receivers

In general, the performance of such receiver-reactors is characterized by their solar-to-fuel energy conversion efficiency. Romero and Steinfeld defined it as the maximum amount of work extracted from the reaction products at 298 K,  $\Delta G$  divided by the solar power input from the concentrating system,  $Q_{\text{solar}}$  as

$$\eta_{\text{solar-to-fuel}} = \frac{-\Delta G}{Q_{\text{solar}}}$$

With this definition they established a base for evaluating and comparing different solar thermochemical processes for ideal, closed cycle systems.

For open material cycles, in which carbonaceous feedstocks are being solar-upgraded, they defined the solar-to-fuel energy conversion efficiency as

$$\eta_{\text{solar-to-fuel}} = \frac{-\Delta G}{Q_{\text{solar}} + HHV_{\text{reactants}}}$$

where  $HHV_{\text{reactants}}$  is the high heating value of the feedstock being processed.

Furler et al. defined the solar-to-fuel efficiency based on  $\Delta H$  instead of  $\Delta G$

$$\eta_{\text{solar-to-fuel}} = \frac{\Delta H_{\text{fuel}} n_{\text{fuel}}}{Q_{\text{solar}} + E_{\text{penalties}}}$$

where  $\Delta H_{\text{fuel}}$  is the high heating value of the fuel produced,  $n_{\text{fuel}}$  is the total amount of fuel produced,  $Q_{\text{solar}}$  is again the solar power input and  $E_{\text{penalties}}$  are system specific energy penalties such as those derived from the consumption of electricity, inert gas or pumping work for promoting the chemical reaction. Analogous to the third equation the second is sometimes reported based on  $\Delta H$  instead of  $\Delta G$ .

When comparing the efficiencies of solar receiver-reactors, especially when citing literature data, attention should be paid to the definitions used. Where required, the efficiencies must be converted with the corresponding factor to ensure comparability.

Note that in all definitions above, the solar-to-fuel efficiency does not include the optical efficiency of the solar concentrating system. Higher  $\eta_{\text{solar-to-fuel}}$  lead to lower required solar collection areas for production of a given amount of solar fuel, which directly translates into lower solar fuel costs. As in solar thermal electricity production plants, the costs for the solar collection and concentrating infrastructure make up the main part of the total investment costs.  $\eta_{\text{solar-to-fuel}}$  can be regarded as a means of characterizing solely the receiver-reactor, but not the process or the solar fuel production plant as a whole.

#### 4.5. Heliostat Field Control for Solar Chemical Processes

In contrast to solar thermal power plants, solar fuel production plants often require different control strategies. The challenge of those chemical processes is, to keep the reaction temperature constant, in order to avoid unwanted side-reactions.

In the following, an example of a heliostat field control will be discussed. The process chosen is a two-step thermochemical cycle powered by concentrated sunlight from a solar tower system. This process is an attractive path to the production of hydrogen from water. The particular challenge of this process lies in its two process steps that run at different temperature levels and thus require different power inputs:

- In the first process step the redox system, a ferrite coated on a monolithic honeycomb absorber, is present in its reduced form while the concentrated solar energy hits the ceramic absorber. When water vapor is fed to the honeycomb at 800 °C, oxygen is abstracted from the water molecules, bond in the redox system and hydrogen is produced. When the metal oxide system is completely oxidized it is heated up for regeneration at 1100–1200 °C in an oxygen-lean atmosphere.
- Under those conditions, in the second process step, oxygen is set free from the redox system, so the metal oxide is being reduced and after completion of the reaction again capable of water splitting. Since the overall process consists of two core reaction steps, which need to be carried out sequentially in a reactor unit at two different temperature steps, a special process and plant concept had to be developed enabling the continuous supply of product regardless of the alternating nature of the solar reactor operation.

The challenge of the process control is to keep the two core reaction temperatures constant and to ensure regular temperature switches after completion of the individual process steps, independent of the weather conditions, like DNI fluctuation, clouds and wind speed. Also start-up, the fast switching after completion of half-cycles and the shutdown must be controlled. A process control of this pilot plant needs to ensure the following aspects:

- Ensuring the realization of the necessary absorber temperature levels.
- Keeping the absorber temperature as constant as possible over a half-cycle considering the “disturbance” of varying DNI.

- Keeping the solar flux distribution on the aperture as homogeneous as possible over a day considering the “disturbance” of varying elevation and azimuth of the sun.
- Ensuring the cycling of operational temperature between the levels mentioned above.
- Ensuring the initiation of a switch after achieving a defined degree of completion of the reaction.
- Ensuring short switching times between two half-cycles.
- Ensuring a reliable start-up and shut-down of the plant.

Manual switching of heliostats to fulfil those control tasks is considered state of the art. The thermal reduction step of the thermochemical cycle is endothermic and performed at 1150–1200 °C. The water splitting step is slightly exothermic and performed at 800–850 °C. Therefore, the regenerating module needs more solar power and a higher solar flux density than the one for water splitting. For the first process step still somewhat power is needed, since in a reactor of this size the heat provided by the exothermic splitting reaction is not sufficient to compensate the heat losses due to non-ideal insulation and reradiation. The low temperature process step only needs a low amount of solar power to compensate heat losses. This means, the flux density has to be changed when the status of the cycle in the related reaction chamber is switched from thermal reduction to water splitting and vice versa. This can be realized by partitioning the heliostat field. In the present case this means that different groups of the SSPS heliostat field need to be defined and used for the following purposes (Fig. 1). One group of heliostats is responsible for the base load for both modules ( $G_{\text{prod M1}}$  and  $G_{\text{prod M2}}$ ) needed to keep the required temperature level of the water splitting. A second group of heliostats ( $G_{\text{reg M1+2}}$ ) is flexible and is switched from one module to the other after each half-cycle. This second group provides the power needed for the regeneration at higher temperatures. A third group of heliostats ( $G_{\text{heatup}}$ ) is responsible for the heating phase, in order to change the temperatures from 850 to 1200 °C in a sufficiently short period of switching time. This latter group provides an extra amount of power only during those switching periods and is used in addition to the other two groups. A fourth group ( $G_{\text{spare M1+M2}}$ ) consists of some heliostats which are responsible for the daily fluctuation in DNI and weather conditions. The mentioned heliostat groups do not consist of adjacent heliostats in one specific part of the field but are rather distributed over the whole field. By that means day-time dependent differences of cosine-losses and flux distributions, which are influenced by the set of positions of the heliostat subgroup chosen, can be kept low. In a previous analysis it turned out that the heliostat field is the set-parameter of choice to control the central operational parameter, the absorber temperature (Roeb et al. 2009). Other parameters like temperature of the feed and mass flow and the reactants cannot be used for this purpose.

It was decided to develop a control and simulation program, and to optimize the operational strategy. A simulation program, which on the one hand allows fulfilling the mentioned control tasks and which on the other hand, enables to predict operational behavior in certain scenarios was developed. The results of the simulation model were evaluated by comparing and validating them with experimental data from the Hydrosol 100 kW pilot plant at the Plataforma Solar de Almería in Spain (Säck et al. 2012). Because of the promising results the system model is currently being extended to enable a use as a control model with controller for the temperature control of the two core reactions in the process.

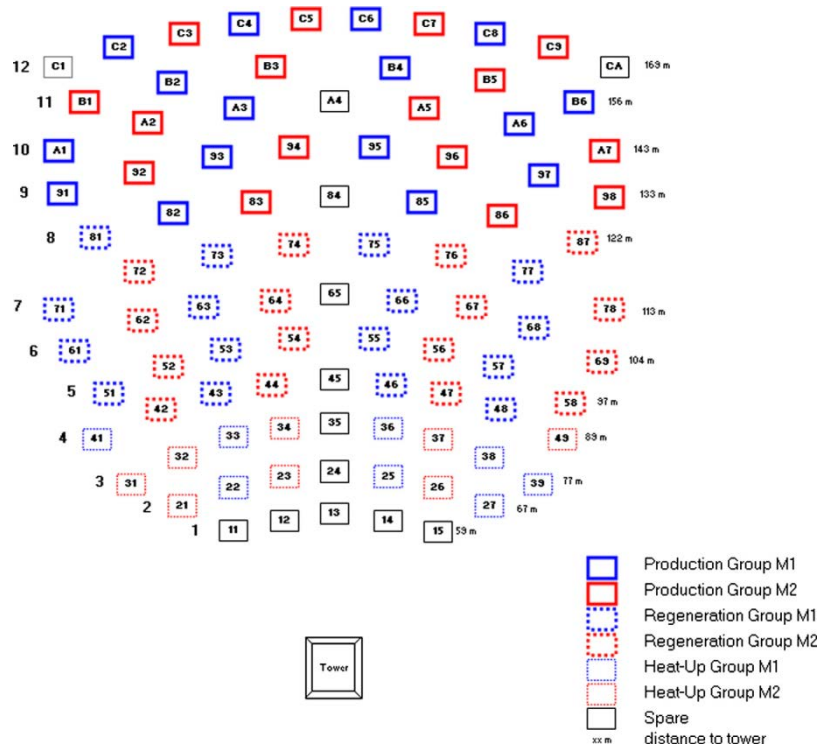


Figure 7: Defining of different groups for the control of the chemical process

### Typical Test Procedures and Necessary Measurements

For calculation of the solar-to-fuel conversion efficiency the solar power input  $Q_{\text{solar}}$  and the total amount of fuel produced  $n_{\text{fuel}}$  must be determined. While the solar power input can be measured directly, it is usually not possible to measure the molar flow rate or mass flow rate of the desired reaction product directly.

Usually, the product gas leaving the reactor is a mixture of unreacted educt gases, reaction products and if applicable inert gas. For example in the case of solar steam reforming, the product gas contains remaining water vapor and methane plus the reaction products hydrogen and carbon monoxide. Other reaction products such as carbon dioxide can be present as well. Therefore, the molar flow rate of the desired product is calculated from the product gas composition and the total flow rate.

The molar flow rate of a component  $i$  can be calculated as a product of the molar ratio and the total molar flow rate

$$\dot{n}_i = x_i \cdot \dot{n}_{\text{total}}$$

where  $\dot{n}_i$  is the molar flow rate of a component  $i$ ,  $x_i$  is the molar ratio of component  $i$  in the gas mixture and  $\dot{n}_{\text{total}}$  is the total molar flow rate of the product gas stream.

The corresponding mass flow rate can be calculated by using the Molar Mass  $M_i$ .

$$\dot{m}_i = \dot{n}_i \cdot M_i$$

The produced amount of a certain desired product within a defined time span is calculated by integration of the molar flow rate over time  $t$ :

$$n_{\text{fuel}} = \int \dot{n}_{\text{fuel}} dt$$

Thus for calculation of the solar-to-fuel efficiency, the following variables have to be measured during testing and characterization of solar receiver-reactors.

- Solar power input from the concentrating system  $Q_{\text{solar}}$
- Molar flow rates of product gas stream  $\dot{n}_{\text{total}}$
- Product gas composition  $x_i$

Beside, other values of interest often are

- Temperature of the reactants inside the receiver-reactor
- Pressure inside the receiver-reactor

Other parameters can be of interest for characterization of a solar receiver-reactor. These have to be determined, dependent on the individual process. In any case, care should always be taken when comparing different literature data. Up to now, no consistent qualification and characterization methods exist for comparing fuel production processes among each other. An overview of measurement devices and methods typically used to determine the above mentioned key variables is given in chapter 19.

### *Literature*

*M. Romero and A. Steinfeld (2012): Concentrating solar thermal power and thermochemical fuels. Energy & Environmental Science, 5(11): p. 9234 - 9245.*

*P. Furler, J. Scheffe, M. Gorbar, L. Moes, U. Vogt and A. Steinfeld (2012): Solar Thermochemical CO<sub>2</sub> Splitting Utilizing a Reticulated Porous Ceria Redox System. Energy & Fuels, 26(11): p. 7051-7059.*

*M. Roeb, M. Neises, J.-P. Säck, P. Rietbrock, N. Monnerie, J. Dersch, M. Schmitz and C. Sattler (2009): Operational strategy of a two-step thermochemical process for solar hydrogen production. International Journal of Hydrogen Energy, 2009. 34(10): p. 4537-4545.*

*J.-P. Säck, M. Roeb, C. Sattler, R. Pitz-Paal and A. Heinzl (2012): Development of a system model for a hydrogen production process on a solar tower. Solar Energy, 86(1): p. 99-111.*

## 5. Dish

### 5.1. System Performance evaluation

The relevant energy flows between the subsystems of a dish/Stirling unit and the typical losses of these components are as follows:

The sun light is reflected by the mirrors of the parabolic concentrator towards the focal point. Some parts of the concentrator are shaded by structural elements and the power is reduced also by the reflectance of the mirrors. Only a portion of the concentrated sun light enters through the aperture of the cavity. Inside the cavity only part of the remaining power is directly absorbed by the receiver. Another part is reflected back through the aperture or to the cavity walls where it might be absorbed or reflected again. The hot surfaces inside the cavity cause radiation and convective losses through the aperture and conductive losses through the isolated cavity walls. The thermal power transferred to the working gas inside the receiver is partly converted to mechanical power by the Stirling cycle. The cooling water stream transports the other part of the heat to the air radiators or another heat sink of the Stirling unit. Some additional thermal losses are caused by the warm engine surfaces by means of radiation and convection. Finally, the generator converts a big part of the mechanical power to electricity and dissipates the residual part into the Stirling engine's housing. The gross output of the power conversion unit is reduced by the parasitic power consisting of the consumption of the cooling and the tracking system, controls and other necessary parts to operate the system resulting in the net electric power output.

The overall system efficiency is defined as:

$$\eta = \frac{P_{\text{useful}}}{P_{\text{input}}} = \frac{P_{\text{electric,net}}}{P_{\text{sun on dish aperture}}}$$

It is the useful electrical output of the system in relation to the solar power entering the aperture area of the concentrator. This efficiency is the product of all component efficiencies in the conversion chain described above. It depends on the ambient conditions because wind can increase thermal losses, the ambient temperature has an important effect on the conversion efficiency of the Stirling engine and the sunshape can influence the distribution of the concentrated sun light on the absorber of the engine.

### 5.2. Component Performance Evaluation

#### 5.2.1. *Measurement of environmental conditions*

Measurement of the complete environmental conditions is crucial for the evaluation of the system performance as well as for many of the procedures for the evaluation of components performances. The relevant measurement procedures are described in chapter 7.

To produce comparable data some limits were defined in the literature (Stine, IEA) for direct normal insolation, wind speed and cooling water temperature when evaluating system performance:

- DNI about 1000W/m<sup>2</sup>

- Wind speed should be lower than 4.5m/s
- Cooling water temperature closed to 15°C

The proposed insolation limit is not achievable for many test sites and therefore cannot be established as a hard requirement for comparable test conditions but tests should be performed at high insolation to avoid unnecessary extrapolation. Using only performance data with wind speed below the proposed limit should be possible for all sites. About the necessity for a limit regarding cooling water temperature there are different opinions. Definitely Dish/Stirling system power output and efficiency depend considerably on the temperature of the available cooling water. But usually, in a Stirling PCU the cooling and radiator system is an integral part and if only data is compared with an equal cooling water temperature a comparison between different radiator systems is not possible. Best practice in this case should be to report cooling water temperature and ambient temperature always together with the performance data.

### ***5.2.2. Mirror Reflectance***

Reflectance should be measured according the method described in section 10.1.

### ***5.2.3. Optical quality of dish concentrators***

The optical quality of the dish concentrator can be evaluated with different methods.

Indirect flux measurement as described section 11.2 formerly was the only method to qualify dish concentrators by evaluating the distribution of the concentrated sun light in the aperture of receiver plane of the Stirling engine.

Today, deflectometry as described in section 13.2 is a powerful tool that allows analyzing the concentrator surface in detail. Together with raytracing algorithms this method can produce flux maps with similar precision as the traditional method but gives the possibility to identify the reasons for imperfections and to consider possible corrective actions.

The surface of the concentrator also can be measured with photogrammetry as described in section 13.3 but normally with much lower spacial resolution compared to deflectometry and therefore with the need to interpolate between the measurement point.

Deflectometry and photogrammetry can also be used to detect and correct misalignment when analyzing faceted dish concentrators.

Most of the above methods just produce data for a specific tracking angle and should therefore be combined with finite element methods to evaluate all relevant operation angles and wind load scenarios for the dish system.

### ***5.2.4. Intercept Factor***

As described already in an earlier section the intercept factor is the fraction of energy reflected from the concentrator to the energy that is reaching the solar absorber surface (receiver surface). For cavity receivers the intercept factor depends on the aperture size of the cavity but is also highly

affected by the concentrator optical errors, tracking accuracy, mirror and receiver alignment accuracy, and the apparent size of the sun (sun shape).

The intercept factor can be calculated from the results of the analysis of the concentrator quality as described in the section above or it can be measured directly using a calorimeter (see also section 0 on calorimetry) with an aperture of the desired size and position. A calorimeter should be designed to absorb all the radiation entering its aperture and convert it to thermal energy that increases the temperature of a well-defined cooling fluid (mostly water). Applying precise measurement methods for temperature increase and mass flow as described in sections 8.1 and 9 the power entering the calorimeter can be defined very well and related to the power reflected from the parabolic concentrator.

### **5.2.5. Engine efficiency**

The thermal power input into the Stirling cycle cannot be measured easily. But under steady-state conditions the power input and the sum of all power outputs must be equal. In particular the sum of mechanical shaft power and the thermal energy evacuated by the cooling system must be equal to the thermal power input to the working gas inside the solar receiver, when the rather small heat losses of warm engine parts are neglected (or included in the sum, calculating or estimating the heat transfer to the engine housing). This means that we can define the engine efficiency by just measuring the mechanical power at the engine shaft and the rise of the enthalpy of the cooling fluid passing through the engine.

Since the conversion characteristics of commercial generators are well documented, the measurement of mechanical shaft power can be replaced by the measurement of the electric power output as described in section 18.

Measuring the thermal power evacuated by the cooling system requires precise knowledge or measurement of the physical properties of the cooling fluid (heat capacity  $c_p$ ) and measurement of the fluid temperature at the inlet and the outlet of the engine as well as measurement of the fluid mass flow rate through the engine.

Measuring heat capacity is not described in this document and usually implies large uncertainties. Therefore, the easiest way to avoid problems is to use a well-known fluid, clean water (!), as coolant when the engine efficiency is to be analyzed.

Measurement of fluid temperature and mass flow require very high accuracy. Recommendations for temperature measurement in fluids can be found in section 8.1. To increase precision the usage of mixing chambers is recommended. The method for measuring mass flow is described in section 9.

## **Typical Test Procedures**

### **Test of tracking system**

The system performance can only reach the maximum level if - under all operation conditions – the biggest part of the power reflected from the concentrator enters into the PCU's aperture. This is only possible when the center of the receiver is perfectly aligned on the optical axis of the concentrator and this optical axis is pointing exactly towards the center of the Sun. Misalignment can occur either

originated by the motors, gears or positioning sensors that cause unreproducible positions or it can be caused by deformations of the systems structure by gravity or wind load.

The electromechanical system can be easily tested sending the drives to specific coordinates from different starting positions and check if the result is always reproducible and the precision of reproducibility is within the desired limits.

The overall tracking precision can only be measured by an indirect flux measurement campaign. Flux images that have to be taken throughout a desired observation period can be analyzed for the 'deformation' of the flux distribution or the movement of the 'center of gravity' of the flux density which corresponds to the misalignment of the Stirling's solar receiver in the specific operation position and under a specific external load.

### Short term power testing

As described in the earlier chapter **Fehler! Verweisquelle konnte nicht gefunden werden.** the objective of a short term power test run is to demonstrate the power output of the system under specific stable ambient conditions. All subsystems are supposed to work close to their design point to achieve highest efficiencies. For a power test all system parameters and ambient conditions must be monitored to be able to analyze the operation behavior of all subsystems and to be able to define the system efficiencies as described at the beginning of this chapter.

### Long term testing

When a dish/Stirling system is under long term testing, the focus changes to 'real life conditions'. The system will then undergo transient conditions, will warm-up in the morning and cool-down in the evening, it might run during a dust storm or with a wet concentrator after a rain shower. As explained already in chapter **Fehler! Verweisquelle konnte nicht gefunden werden.** the objective is to record all necessary parameters to be able to understand their influence on the long term output and the reliability of the system and to predict the systems production over time even considering system availability.

### Literature

*W.B. Stine, and M.A. Powell (1992): Proposed guidelines for reporting performance of a solar dish/Stirling electric generation system. In 28. intersociety energy conversion engineering conference, Atlanta, GA (United States),8-13 Aug 1993.*

*W.B. Stine and R.B. Diver (1994): A compendium of solar dish/stirling technology. Albuquerque, NM and Livermore, CA: Sandia National Laboratories.*

*W. Reinalter, S. Ulmer, P. Heller, Th. Rauch, J.-M. Gineste, A. FerrièreAlain and F. Nepveu(2008): Detailed Performance Analysis of a 10 kW Dish/Stirling System. Journal of Solar Energy Engineering (130). American Society of Mechanical Engineers.*

## 6. Furnace (CNRS)

### 6.1. Presentation

Literally speaking, solar furnaces cover any optical system using solar energy to heat a process: from the flat panels on the roof to produce hot water to research installations with complex optics to reach high concentration of the solar energy.

However, we reduce here the solar furnaces to the double reflection installations with a fixed focus:

- First reflection on the flat heliostat(s) which track(s) the sun and collect(s) the solar energy
- Second reflection by the fixed concentrating optic (parabolic, spherical, ellipsoidal...) towards the focal point.

This optical design allows a fixed focus in space, easing notably the fixation and the wiring of the process using the concentrating solar energy. Additionally, the furnaces with off axis concentrators do not impose high requirements on the size of the process as it doesn't intercept the solar light, for a slightly reduced theoretical solar concentration: see for example the DLR Cologne solar furnace.

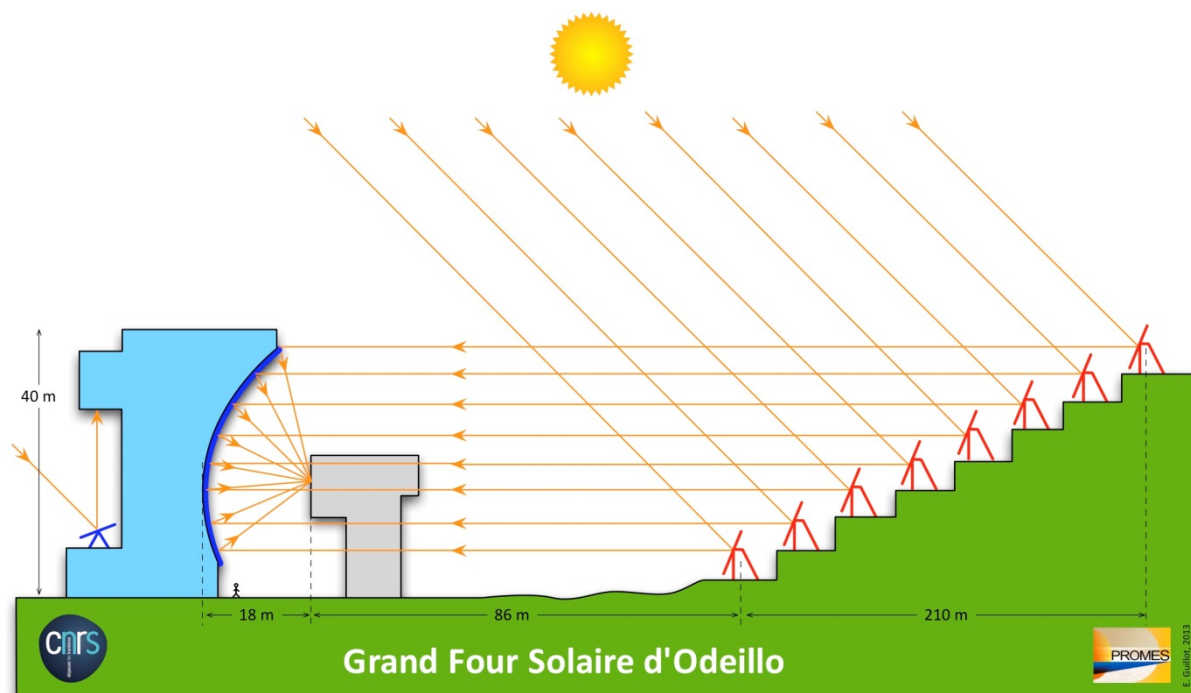


Figure 8: Typical solar furnace: on the right the flat heliostats which track the sun to collect the solar energy and send it to the non-moving parabola on the left for usage at the non-moving focus in the gray tower in the middle left.

### 6.2. Applications

Solar Furnaces are typically used for high temperature processes, beyond 1800K: the fixed concentrating optic typically is of a high optical quality as its fixed mechanical structure is easier and cheaper to make stiff and precise compared to moving optics.

This high optical quality of solar furnaces leads to high concentration ratios that in turn, lead to high achievable temperatures depending on the process at focus: for example, beyond 3500K for a concentration factor of 10 000 at CNRS Odeillo's Big Solar Furnace to synthesize carbon nanotubes.

The high temperatures possible are typically used for chemical processes or for testing:

- Synthesizing materials: ceramics, nanoparticles...
- Producing energy carriers such as solid or liquid fuels: hydrogen, hydrocarbons, coke...
- Testing materials in harsh temperature or flux conditions: aerospace, nuclear reactors...
- Testing new processes in numerous conditions thanks to the flexibility of the solar power: R&D for any high temperature process, solar or not, for example innovative coatings application, nuclear waste vitrification...

Currently, all solar furnaces known to the authors are used by R&D centers for the aforementioned applications, no commercial solar furnace is known for purely commercial operation such as production of electricity or materials synthesis.

### 6.3. Testing

The performance of a solar furnace is estimated by **determining the available flux power density in different planes** near the focal point and their stability in time by mapping the concentrated solar beam. The typical methods for heat flux measurements are described in chapter 11. Direct and indirect methods are advised as they typically reduce the uncertainty on the results. Calculated methods typically have greater uncertainties than for the other CSP technologies due to the high concentration factor that increases the sensitivity on the uncertainty of the determination of the optical performance, both at macro scale (tracking errors, canting or shape deviation determined by deflectometry or photogrammetry) and at micro scale (soiling and mirror properties as determined by bidirectional reflectance distribution measures).

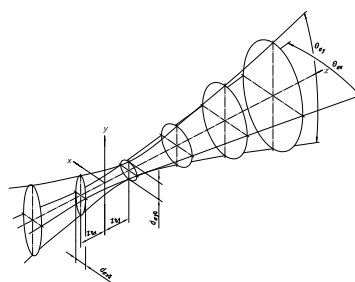


*Figure 8 Inspiration from ISO 11146: description of a laser beam by elliptical Gaussian distributions. This approach can be used for initial or simple modelling to reduce the quantity of data characterizing a solar furnace*

The description of the beam can be inspired by what has been normalized for lasers: ISO 11146 describes vocabulary, plans in space, diverging angles, waist size, moments distributions... Usually, each R&D center devises its own formatting of the results depending the requirements of each project. The heat flux data can be **reduced to Gaussian distributions** as described in this ISO, but that

is often just good enough for initial or simple modeling, actual use of the complete flux map as boundary conditions in finite element software is common.

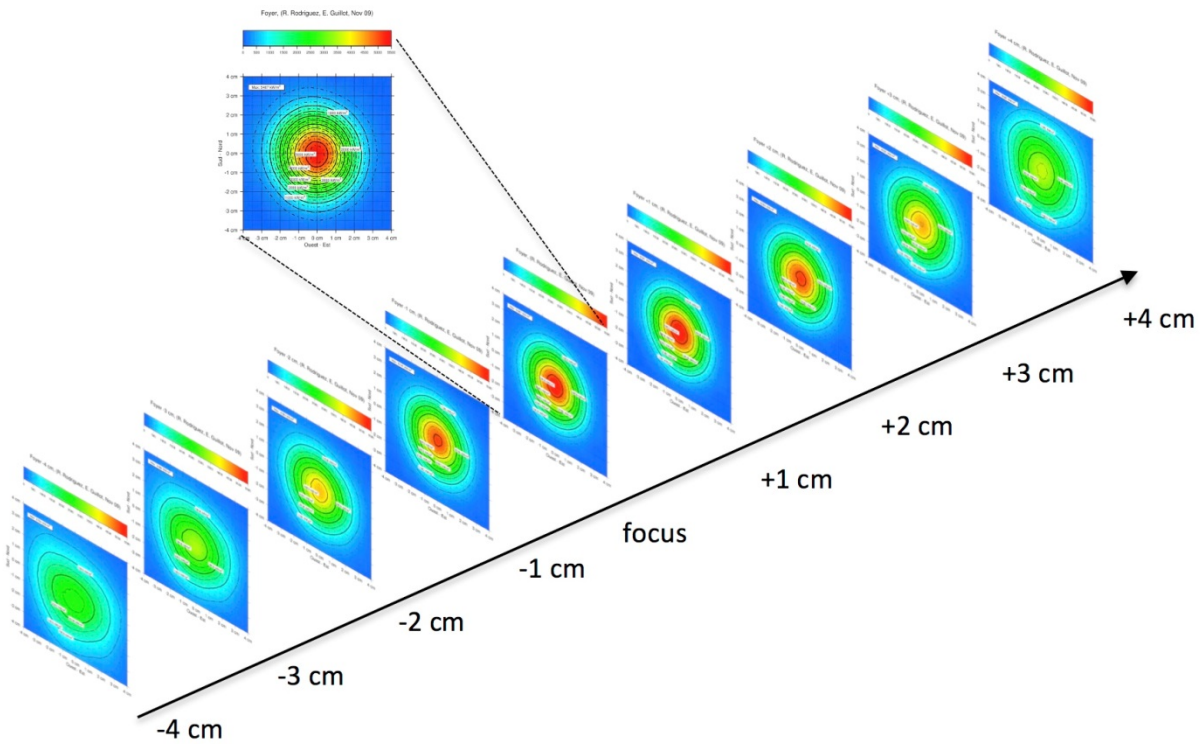


*Figure 9: Real characterisation of a solar furnace: flux mapping with a calibrated camera has been done along the focal axis for different planes.*

Another important characteristic is the flexibility with which one can control the flux power density both in space and in time. The performance of a solar furnace is therefore determined by flux measurements, either direct, indirect or calculated methods.

The **achievable temperature is not a characteristic of a solar furnace itself**, but a characteristic of the combination of the solar furnace and the process operated at its focus. It depends on the provided solar flux density and the thermal balance of the process taking into account energy used by the process and energy lost either by radiation or conduction/convection at its boundaries. Consequently, poorly insulated walls of the reactor or a poorly designed receiver cavity lead to high losses hence lower temperature for the same given solar furnace.

# Part 2

## Measurement Methods

---

## 7. Solar Resource and meteorological Data Measurement

Several meteorological parameters have to be monitored during testing of concentrating solar power systems depending on the type of the experiment. The chapters of PART 1 on the test procedures for the different CSP technologies refer to various meteorological quantities. The measurement procedures for these quantities are described in this chapter.

The measurement of meteorological parameters for purely meteorological purposes is well described in the Guide to Meteorological Instruments and Methods of Observation by CIMO (Commission for Instruments and Methods of Observation) [WMO, 2010]). In addition to this guide there are international and national standards for such measurements. However, the existing documents do neither consider the specific requirements nor the boundary conditions for CSP testing. Here, we are interested in characterizing the meteorological conditions that affect the test object. This means that the influence of surrounding objects (buildings, vegetation, ...) has to be included in the measurements, although these influences should be excluded for purely meteorological purposes. In the following, we will refer to the CIMO guide and standards whenever possible and present information that is required for their application to CSP testing. If not specified otherwise, the recommendations from [WMO, 2010] apply.

### 7.1. Irradiance

In particular, CSP testing involves the measuring direct normal irradiance (DNI), but also diffuse horizontal irradiance (DfHI) and global horizontal irradiance (GHI). All three irradiance components refer to shortwave broadband solar irradiance with wavelengths between 300 nm and 3000 to 4000 nm.

In the strict sense of the definition, DNI is the irradiance on a surface perpendicular to the vector from the observer to the center of the sun caused by radiation that did not interact with the atmosphere [e.g. WMO 2010]. This strict definition is useful for atmospheric physics and radiative transfer models, but brings along a complication for ground observations: It is not possible to measure whether or not a photon was scattered if it reaches the observer from the direction in which we see the solar disk. Therefore, DNI is interpreted differently in the world of solar energy. Direct solar radiation is understood as the “radiation received from a small solid angle centered on the sun’s disk” [ISO 9060, ISO, 1990]. The size of this small solid angle for DNI measurements is recommended to be  $5 \cdot 10^{-3}$  sr (corresponding to  $2.5^\circ$  half angle) [WMO, 2008]. This recommendation is approximately 10 times larger than the radius of the solar disk itself (yearly average  $0.266^\circ$ ). This is due to the fact that instruments for DNI measurements (pyrheliometers) have to be tracked to follow the path of the sun and small tracking errors have to be expected. The large field of view (FOV) of pyrheliometers reduces the effect of such tracking errors. In these guidelines, we understand DNI as the experimental DNI measured with a pyrheliometer according to the typical usage in solar energy.

Corresponding to the above understanding of DNI the diffuse horizontal irradiance (DfHI) is the irradiance caused by solar radiation from a solid angle of  $2\pi$  sr above a horizontally levelled surface excluding the radiation that is interpreted as DNI. GHI is the irradiance caused by solar radiation from a solid angle of  $2\pi$  sr above a horizontally levelled surface. In accordance with this definition, the GHI can be calculated from DNI and DHI using the solar elevation angle, calculated by a sufficiently accurate algorithm [e.g. Michalsky, 1988].

For the correct use of the DNI measurements in CSP testing, circumsolar radiation plays an important role. Due to forward scattering of direct sunlight in the atmosphere, the circumsolar region closely surrounding the solar disk looks very bright. The radiation coming from this region is called circumsolar radiation. For the typical field of view of modern pyrhemometers ( $2.5^\circ$ ), circumsolar radiation contributes to the DNI measurement. This contribution can be quantified if the radiance distribution within the solar disk angle and the circumsolar region and the so called penumbra function [Pastiels, 1959] of the pyrhemometer is known. Such quantification is of particular interest for CSP as the contribution of circumsolar radiation to the yield of most concentrating plants is smaller than its contribution to the DNI measurement. This effect has to be considered in the testing of concentrating collectors in order to avoid an overestimation of the intercepted irradiance of a system.

For CSP testing under clear skies with low aerosol load the sunshape might be estimated with acceptable accuracy e.g. based on information given in the appendix of ISO 9059. Then only a small additional uncertainty has to be considered for the experiment. For tests during high aerosol loads or even during the presence of clouds, the sunshape should be measured and the effect has to be included in the experimental evaluation to avoid systematic underestimation of the collector performance. Such measurements are still subject of research activities (e.g. in WP13.1 of this project). For more details on circumsolar radiation, please refer to [CNRS/DLR, 2012] and [Wilbert, 2013].

### *Description of method*

#### **Direct Normal Irradiance (DNI)**

DNI can be determined directly with pyrhemometers or indirectly from GHI and DfHI measurements. GHI and DfHI measurements are explained in the following paragraphs.

Pyrhemometers consist of a sensor element that is positioned at a well-defined distance behind an aperture. Thus, only radiation from the above mentioned angular region reaches the sensor element as described by the penumbra function. For the often harsh conditions at CSP test sites, mostly field pyrhemometers are used. Such instruments have entrance windows in the aperture in order to protect the instrument, e.g. of dust and rain. Field pyrhemometers usually use blackened thermopile sensors, which allow a broad spectral response of the instrument. Thermopiles generate a voltage that is proportional to the irradiance that is absorbed by the sensor surface. The voltages are in the order of  $10 \mu\text{V} / (\text{W} / \text{m}^2)$  and a calibration constant is required to transform the output voltage into a DNI signal. There are also photoelectric pyrhemometers using photodiodes instead of thermopiles. They usually do not provide the spectral range required for pyrhemometers in the WMO and ISO 9060 definition of the term pyrhemometers [ISO 9060, ISO, 1990; WMO, 2010] and typically exhibit a greater sensitivity to ambient temperature that should be corrected.

Another type of pyrhemometers is the absolute cavity pyrhemometer. It usually consists of a radiometer head with two blackened cavities and a control unit. Absolute cavity pyrhemometers are operated on the principle of substituting radiative by electrical power and hence measuring radiation as electrical power in absolute in units of  $\text{W}/\text{m}^2$ . While in operation, the front cavity is orientated towards the sun and heated up by radiation incident through a hole with an exactly defined size during the “open phase”. Its back being connected to a heat sink yields a temperature difference across the thermal impedance, which is proportional to the incoming radiative power and which is measured. In a following “closed phase”, this power is then substituted by an integrated electrical

heater controlled to obtain the same temperature difference. Hence the cavity has to be irradiated and shaded alternately, meaning that the instrument cannot be operated continuously but in chopped mode with the measurement taken at the end of every phase. In order to compensate for changes in heat sink temperature, a second equivalent back cavity, viewing the ambient without being irradiated, is included with the temperature difference measured across a second thermal impedance likewise. The open cavity, the higher price and discontinuous operation make absolute cavity pyrhemeters unsuitable for field operation. They are important for the calibration of field irradiometers because they can serve as reference instruments.

### **Global Horizontal Irradiance (GHI)**

Instruments measuring GHI are called pyranometers. Field pyranometers usually use blackened thermopiles as sensor elements that can receive short wave radiation from the complete hemisphere above the sensor. There are also photoelectric pyranometers that use photodiodes instead of thermopiles. They usually do not provide the spectral range required for pyranometers in the WMO and ISO 9060 definition of the term pyranometers [ISO 9060, ISO, 1990; WMO, 2010]. The sensor is positioned below an entrance window or a diffusor disk. For thermopile sensors, mostly one or two glass domes form the entrance window. Two domes are used in order to reduce thermal offsets mainly due to wind. An additional ventilation unit with heating is optional but usually advised to further reduce thermal offsets of thermopile sensors: ventilation also reduces the sensor soiling and the time that dew, rain drops or snow cover the dome.

The most accurate way to determine the GHI is by deriving it from accurate measurements of the DfHI and the DNI. The direct GHI measurement is ideally only used as a quality check by comparing the direct measurement to the calculated GHI.

### **Diffuse Horizontal Irradiance (DfHI)**

DfHI is measured by diffusometers. Diffusometers consist of a pyranometer and a shading structure that blocks the direct radiation on its way to the sensor. Corresponding to the definition of the experimental DNI, penumbra functions can be defined for instruments that measure DfHI [Major 1992]. The penumbra function is given by the geometry of the shading element, its position relative to the sensor and the size of the sensor surface. Shadow balls, shading disks, or shading rings are used. Shading rings also block a considerable part of the diffuse radiation so that correction functions are necessary to determine the DfHI. The penumbra functions of diffusometers depend on the solar position as the shading structure moves corresponding to the elevation while the sensor element is kept horizontal. The penumbra functions involved in DNI and DHI measurements should correspond to each other, when calculating one of the three components from the other two. If the penumbra functions of the pyrhemeters and the diffusometers deviate from each other, part of the circumsolar irradiance might be neglected or included twice in the calculation.

### **GHI, DHI and DNI from Rotating Shadowband Irradiometers**

Rotating Shadowband Irradiometers (RSIs) consist of a pyranometer and a shadowband that rotates e.g. once per minute around the pyranometer such that the sensor is shaded for some time independent of the solar positions. When the shadowband is in its rest position the GHI is measured. DfHI is measured during the rotation when the shadow falls on the sensor. DNI is then calculated using GHI, DfHI and the solar zenith angle. RSIs are often called RSRs or RSP, depending on the

instrument manufacturer. The notation RSI refers to all such instruments measuring irradiance by use of a rotating shadowband.

There are two types of RSIs: RSIs with continuous and discontinuous rotation. Currently, all RSIs with continuous rotation use photodiode pyranometers. This is necessary, because the sensors need a short response time, in order to measure the irradiance signal during the rotation of the shadowband.

### *Specifications for equipment to be used*

Different classes of pyrheliometers and pyranometers are defined in ISO 9060 depending on potential error caused by different sources (such as temperature changes, spectral selectivity, ...). These instrument properties with respect to these different sources should be known. The categories defined for pyrheliometers and pyranometers in ISO 9060 in order of decreasing accuracy are “secondary standard”, “first class” and “second class”. The classes are defined using the reached uncertainties caused by various relevant effects and the response time. For pyrheliometers, the traceability of the calibration to the World Reference Group is also considered for the classification.

For pyrheliometers the additional class “Primary Standard” is defined. This class refers to absolute pyrheliometers that closely reached the reference measurements in various “recognized pyrheliometers comparisons”. For pyrheliometers, the “Secondary standard” instruments are usually absolute pyrheliometers and the best commercially available field pyrheliometers are “First Class” instruments.

Pyrheliometer measurements require a solar tracker that precisely directs the pyrheliometer towards the sun. The tracking accuracy should be known and always well below the difference of the slope angle and the solar disk angle. The recommended slope angle for pyrheliometers is  $1^\circ$  so that the tracking accuracy must always be better than  $\sim 0.7^\circ$  (all half angles). However, such large tracking error should not be accepted as solar trackers with sun sensors reach much better accuracies when operated correctly ( $0.05^\circ - 0.1^\circ$ ).

Preferably, the instruments used for CSP testing should be ISO 9060 “First Class” pyrheliometers and “Secondary Standard” pyranometers. However, for some test procedures the solar irradiance is not as crucial for the overall uncertainty budget and also other sensor types might be used. This holds especially if the irradiance is not used for calculations but rather for the rough specification of the experimental boundary conditions.

For the selection of the trackers the situation is similar. Automated trackers with sun sensors are recommended for testing whenever the DNI is used for more than the specification of the boundary conditions of the measurements. If no automated trackers are available, additional more frequent control of the pyrheliometers alignment including documentation is required. If misalignment is found, the experimental data since the last positive alignment check should be discarded.

For the highest requirements for the uncertainty of DNI, parallel measurements with absolute cavity pyrheliometers and field pyrheliometers can be considered.

The data logger systems should fulfill the accuracy requirements given for pyrheliometers calibration [ISO 9059].

### *Sensor calibration issues*

Calibration of the irradiance sensors is the key for precise irradiance measurements. The standardized calibration is described in detail in ISO, 9059 for pyrheliometers, and in ISO 9846 and ISO 9847 for pyranometers. The calibration should be traceable to the World Radiation Reference which represents the primary standard for solar irradiance measurements. Manufacturers usually sell their instruments including calibration and offer recalibration services. Often these calibrations are indoor calibrations that usually involve higher uncertainties than calibrations using solar radiation.

The calibration constants of thermopile sensors change with time so that a sufficiently frequent recalibration has to be guaranteed. The uncertainty of the irradiometers has to be adjusted with respect to the time passed since the last calibration.

Self-calibrating absolute cavity pyrheliometers have to be calibrated, too despite their name. Although the calibration constants of such instruments are connected to the size of the absorbing surface and rather constant compared to thermopiles the participation in pyrheliometer comparisons is recommended for such instruments.

### *Main error sources and expected precision*

One of the main sources of error for irradiance measurements is the misuse of the equipment. Even with state of the art instrumentation significant errors can occur. The most important examples for misuse are sensor soiling and misalignment of the instruments and/or the solar tracker. Also the electrical shielding and grounding has to be done thoroughly.

Another important source of uncertainty is the calibration of the instrument.

The expected precision of DNI measurements with well calibrated pyrheliometers is within 1 % and 2 % ( $1\sigma$ ) depending on the other meteorological parameters, the logger and the cabling. For well calibrated pyranometers lower accuracies are reached ( $\sim 2\%$ ). The accuracy of the DNI, DfHI and GHI determinations results from these accuracies and the selected setup (direct measurement or calculation from the other two components).

### *Recommendations*

Besides the above recommendations for the selection of the instruments, and the tracking control, the following should be considered:

- First of all the position of the sensors should be selected with care. For common irradiance measurements it is usually stated that no objectives around the sensors should have an elevation of more than  $5^\circ$  with respect to the sensor position [WMO, 2008]. The restrictions for testing are less restrictive as the measurements are usually not used for the meteorological characterization of the site. Thus we can formulate that the pyrheliometer measurements should never be used when something is in the instruments field of view. For the pyranometers the recommendation is more complex as the field of view is  $180^\circ$ . If DNI is determined from DHI and GHI, the diffuse component in the GHI measurement must

be identical to the DfHI. If the GHI or the DfHI is used for calculations assuming that the collector was exposed to this irradiance, the collector should also be exposed to the same DfHI. Furthermore, the DNI should reach the collector and the sensor positions completely. This means that objects reaching elevations of much more than 5° are acceptable for CSP testing if they are far enough away and affect the CSP component or system and the sensors in the same way. This thought is essential for the formulation of the recommendations for all meteorological parameters involved in CSP testing.

- The mounts for the sensors must be stable and thermal expansion of the mount due to temperature changes have to be considered. This might affect the tracking accuracy which has to be checked as stated above. The leveling accuracy of the pyranometers should be better than 0.1°, as specified for the pyranometer calibration in ISO 9847.
- It is important to make sure that cables conducting analog signals are positioned at some distance from power lines. Observation of signals with a high sampling rate can be used to discover 50 Hz noise. Applying integration times corresponding to the grid frequency can reduce errors significantly.
- The sampling period should be smaller than 1/e (the reciprocal value of the time constant) of the thermopile sensors (as recommended in [WMO, 2008]) and shorter than or 1 second for photoelectric devices. For the interpretation of the results the response time of the instruments has to be considered (often ~5s for thermopiles).

## 7.2. Other meteorological parameters

In the following, guidelines for the measurement of further meteorological parameters are formulated. The recommendations concerning cabling, datalogging for the irradiance measurement also hold for the auxiliary meteorological measurement.

### 7.2.1. Air Temperature and Relative Humidity

The air temperature is an important factor for the calculation of the receiver efficiency. The temperature of the air near the earth's surface (dry bulb temperature) is commonly measured in °C (or in ° Fahrenheit, depending on the country). Finally, temperatures have to be known in the thermodynamic scale of temperature, in Kelvin.

Relative humidity is a relevant parameter for cooling and receiver efficiency, depending on the technology. It can also affect optical temperature measurements. Relative humidity is the ratio of the observed vapour pressure to the saturation vapour pressure with respect to water at the same temperature and pressure [WMO, 2008]. It is usually given in per cent.

#### *Description of method*

Relative humidity is measured with hygrometers and dry bulb temperature with thermometers. From the various existing methods for temperature and humidity measurements we focus on recommended methods for CSP testing: electrical temperature measurement with temperature dependent resistors or band gap sensors and capacitive or resistive humidity measurements. The principle of operation of these sensors relies on the systematic change of the electric properties of the sensor material with the temperature or the relative humidity. Other methods are acceptable, too, if the method allows the automatic recording of the signal with a data logger.

Temperature and relative humidity sensors can be acquired as combined sensor (hygro-thermometers) including radiation shield and optional ventilation. Electrical thermometers or hygrometers have to be installed with a radiation shield, in order to avoid that the sensor is heated up artificially above the air temperature. For very low wind velocities measurement errors can occur if no active ventilation is used in order to exchange the air inside the shield with the ambient air.

### *Specifications for equipment to be used*

The sensors should be specified with the measurement method, the operation range and the accuracy for different intervals of the operating range. The response time of the sensors should be considered, too. Response times of thermometers are often several minutes long. Humidity sensors show response times of several seconds.

### *Sensor calibration issues*

Sensors should be calibrated following the manufacturers recommendations. For silicon CMOS sensors a typical drift of approximately 1 % per year has to be expected. Replacement of the sensors element with new calibrated sensors is usually the most convenient method for recalibration.

### *Main error sources and expected precision*

The sensors can be affected by dust, salt and water that might accumulate on the sensors outer surface (e.g. the ceramic cap on the sensor element). The surface has to be controlled at least monthly and cleaned or exchanged when necessary.

Typical accuracies of the described sensors are approximately 1 K for the complete range of natural terrestrial temperatures and below 0.5 K for temperatures between 5°C and 40°C.

The uncertainty for the relative humidity is typically around 2 % for 10 to 90 % relative humidity and 4 % for the complete range. With other measurement methods higher accuracies can be reached (see e.g. [WMO, 2010]), but this is usually not required for CSP testing.

### *Recommendations*

As stated above, the CIMO guidelines and the manufacturer's recommendations on cabling, maintenance and calibration should be followed. One deviation from the guidelines is that, in our case the ground properties below and around the sensors should be comparable to the ground below the CSP test object.

#### *7.2.2. Atmospheric Pressure*

The atmospheric pressure on a given surface is defined as the force per unit area due to the weight of the above atmosphere [WMO, 2008]. The atmospheric pressure is of importance for the receiver and power block efficiency (depending on the technology) and for cooling. Atmospheric pressure is usually given in hPa, mbar, or mmHg.

### *Description of method*

Atmospheric pressure can be measured with mercury barometers, aneroid barometers, hypsometers or electronic barometers. For CSP testing basically electronic barometers are of interest, due to the availability of automated data logging.

Electronic barometers consist of a transducer that creates an electronic signal depending on the state of a sensor element. The sensor element can be a piezoelectric material, an aneroid capsule that changes its shape or position due to the pressure, or a resonator that changes its mode of vibration with the pressure. The displacement of the aneroid capsule can be detected e.g. using capacity or resistance changes.

### *Specifications for equipment to be used*

The specifications for the sensors should include the selected measurement method, the mounting and the uncertainties achieved in different measurement ranges.

### *Sensor calibration issues*

Barometers should be calibrated following the manufacturers recommendations. Recalibration every year might be necessary depending on the instrument model. As some sensors (see e.g. [Campbell, 2007]) show only small drifts of 0.1 mbar per year, longer recalibration intervals can be accepted in these cases.

### *Main error sources and expected precision*

High temperature changes are a known source of errors for electronic barometers. Vibrations, electromagnetic field and the effect of wind and or ventilation are important sources of errors. The expected precision is around 2 mbar for temperatures between 0 and 40°C and pressures between 600 mbar and 1100 mbar.

### *Recommendations*

As stated above, the CIMO guidelines and the manufacturer's recommendations on cabling, maintenance and calibration should be followed. Electronic barometers should be mounted in a weatherproof case or inside a building in order to protect them from humidity, corrosion and solar radiation. If mounted inside a building or closed case the barometer should be coupled with the outside using its pressure connector and a hose. Temperature gradients have to be kept as small as possible. The distance to sources of electromagnetic fields (e.g. transformers) should be as high as possible and shielding should be provided for the cables and the housing. To reduce the effect of wind on the reading a static head should be used if additional measurement errors of approximately 5 hPa (see [WMO, 2010]) cannot be accepted. Shocks and vibrations have to be avoided.

#### **7.2.3. Wind Speed and Wind Direction**

Wind speed and wind direction are important for the evaluation of both the optical efficiency of the collector (deformation), and the receiver efficiency (convection). Wind speed and direction are often understood as the horizontal component of the wind velocity. For some applications in CSP testing also the three dimensional wind velocities are of importance.

The 2D horizontal wind speed is the absolute amount of the projection of the wind vector to the horizontal plane. Wind direction (2D) is reported by the direction from which the wind originates. It is usually measured in °N (geographical, not magnetic north).

### *Description of method*

Wind speed is measured with anemometers. The most common designs are cup anemometers and propeller anemometers. These instruments consist of a rotor that moves corresponding to the wind velocity and a signal generator that is connected to the rotor. There are several other anemometer types (see [WMO, 2010]). One of the most common other types are (ultra)sonic sensors. (Ultra)sonic anemometers measure the time that an ultrasonic signal needs to cross a constant measurement distance that is exposed to the wind. Combination of several measurement paths can be used to derive the wind direction and the wind vector. For the measurement of the convective losses of tower receivers also LIDAR, RADAR and SONAR techniques might be of interest.

The wind direction can also be measured with wind vanes. Wind vanes change their direction corresponding to that of the horizontal component of the wind vector. The position of the vane can be read e.g. by a potentiometer setup. Many ultrasonic sensors, and combined propeller anemometers also derive the wind direction directly.

### *Specifications for equipment to be used*

Anemometers and wind vanes should be specified with the measurement method, the operation range and the accuracy for different intervals of the operating range. Furthermore, the resolution, the response time and the sampling rate of the measurements have to be stated.

### *Sensor calibration issues*

Sensors should be calibrated following the manufacturers recommendations. The zero offset of ultrasonic sensors should be checked in order to determine whether or not recalibration is required. Complete mechanical anemometers and wind vanes or their moving components are often rather exchanged after 2-5 years than recalibrated. The lifetime of the sensors should be considered.

### *Main error sources and expected precision*

Mechanical parts of the sensors have to be checked periodically for proper functionality. Wrong orientation of the wind vanes has to be avoided, and the magnetic declination should be considered for the setup. The latter holds of course also for the setup up of solar trackers, but here it is of higher importance as small orientation errors will not be noticed. Cup and propeller anemometers react slower to decreases of the wind speed than to increases. This can lead to systematic overestimation of the wind speed.

Ultrasonic sensors reach accuracies of approximately 1-2 % for instantaneous measurements with high sampling rates (~50 Hz) and 0.1 % for integration times around 2 min. Typical accuracies for mechanical anemometers are approximately 1 %. Accuracies for wind direction are around 1°-2°.

## Recommendations

It is often impossible to measure wind velocity following WMO's CIMO guide close to CSP test sites. At CSP test facilities and in power plants other objects are usually too close to the test site. As said before, the idea is to measure the conditions that influence the test object. This can only be achieved approximately in most cases. In some cases, the position of the sensors might be selected such that this condition is fulfilled at least during most of the time, e.g. for the main wind direction(s). Also, wind measurements at multiple positions and heights must be considered. In order to make the measurements roughly comparable to wind measurements following the CIMO guide one sensor should be installed at 10m height.

Wind gusts should be measured, too if wind forces and their effects are considered in the CSP test. The wind gust is the maximum of the wind speed in a specified time interval.

High frequency wind data might be of interest to analyze the dynamic forces on the collector. If this is required, the response time of sensors has to be considered. The application of ultrasonic sensors or LIDARs might be necessary.

## Literature

*WMO (2010): Guide to Meteorological Instruments and Methods of Observation, WMO-No. 8, Seventh edition, updated 2010.*

*ISO-9060 (1990): Solar energy - Specification and classification of instruments for measuring hemispherical solar and direct solar radiation.*

*ISO-9059 (1990): Solar energy - Calibration of field pyrhemimeters by comparison to a reference pyrhemimeter.*

*ISO9846 Solar energy – Calibration of a pyranometer using a pyrhemimeter*

*ISO9847 Solar energy – Calibration of field pyranometers by comparison to a reference pyranometer*

*L. J. B McArthur (2005): BASELINE SURFACE RADIATION NETWORK (BSRN) Operations Manual Version 2.1. WCRP-121 WMO/TD-No. 1274 WORLD CLIMATE RESEARCH PROGRAMME.*

*T. Stoffel, D. Renne, et al. (2010): Concentrating Solar Power: Best Practices Handbook for the Collection and Use of Solar Resource Data (CSP), National Renewable Energy Laboratory (NREL), Golden, CO.*

*CNRS/DLR; SFERA Project report R13.2: Guideline for replication and installation of the developed sunshape device, 2012, available online  
[http://sfera.sollab.eu/downloads/JRA/WP13/R13.2\\_SFERA\\_WP13T1.pdf](http://sfera.sollab.eu/downloads/JRA/WP13/R13.2_SFERA_WP13T1.pdf) (visited 16.11.2012), 2012.*

*S. Wilbert, B. Reinhardt, J. DeVore, M. Röger, R. Pitz-Paal, C. Gueymard, R. Buras (2013): Measurement of Solar Radiance Profiles with the Sun and Aureole Measurement System (SAM), Journal of Solar Energy Engineering.*

*G. Major (1992): Estimation of the error caused by the circumsolar radiation when measuring global radiation as a sum of direct and diffuse radiation, Solar Energy, 48(4), pp. 249-252.*

*R. Pastiels (1959) : Contribution a l'étude du problème des méthodes actinométriques, Publications, série A. No 11. Institut Royal Météorologique de Belgjque. Bruxelles, Belgium.*

*J. J. Michalsky (1988): The Astronomical Almanac's algorithm for approximate solar position (1950–2050)," Solar Energy, 40(3), pp. 227-235.*

*Campbell (2007): Instruction manual for the CS100 BarometricPressure Sensor. Revision 5/07.*

## 8. Temperature Measurement

### 8.1. Optical Temperature Measurement

#### *Description of the method*

The temperature of test equipment can be determined by measuring the amount of radiative heat emitted, typically in the infrared spectrum. The **Planck Law** allows to calculate the power hemispherically radiated by a local point of a black body at a given temperature for any wavelength.

$$L_{\lambda} = \frac{2hc_{\lambda}^2}{\lambda^5} \cdot \frac{1}{\exp\left(\frac{hc_{\lambda}}{k\lambda T}\right) - 1}$$

$L_{\lambda}$  Angular spectral luminance ( $\text{W}\cdot\text{m}^{-2}\cdot\text{sr}^{-1}\cdot\text{m}^{-1}$ )

$\lambda$  Considered light wavelength

$T$  Surface temperature of the body

$c_{\lambda}$  Speed of light in the considered medium (m/s)

$h = 6.626\ 17 \times 10^{-34}$  J.s Planck constant

$k = 1.380\ 66 \times 10^{-23}$  J/K Boltzman constant

Conversely, by measuring the radiant flux over the complete hemisphere for a given wavelength, one can therefore determine the temperature of the black body.

However, **actual materials are not black** bodies and thus part of this theoretically calculated power is not emitted. The emissivity coefficient compensates for this reduced emission, it depends on the considered wavelength, the temperature of the equipment, its composition, its surface aspect (polished, grinded...).

#### *8.1.1. Instruments*

**Pyrometers** are used to determine the average temperature of the sensed surface and infrared cameras to determine local temperature maps. The user has to provide the suitable emissivity from reference books or measurements.

**Bi- or tri-color pyrometers** can be used without knowing the emissivity. These devices are pyrometers operating at 2 or 3 wavelengths, and under the assumption that the emissivity of the material is the same at all these wavelengths, the redundant measurements allow to determine the temperature. However, this assumption is not always true despite the usual precautions (nearby wavelengths). The tri-color pyrometers are used to at least check this assumption, whereas bi-color pyrometers would always provide a result without indicating if it is realistic or not.

**Bi-color pyro-reflectometers** are bi-color pyrometers that additionally measure the directional reflectivity of the material at both wavelengths. If the material is opaque and the bidirectional reflectance distributions are proportional between both wavelengths (whatever the incoming and outgoing radiation direction, the ratio is constant between the reflectivity taken at each wavelength), the system of equation can be solved to determine the temperature without knowing the

hemispherical emissivity. These assumptions, despite being weaker than for bi- or tri-color pyrometry are still not always validated, for example in case of coated materials.

Development is currently under way engineering **cameras** based on bi-color pyrometry and on pyro-reflectometer principles to determine temperature maps with fewer assumptions on the emissivity of the materials for more robust instruments than the current common single wavelength or bandwidth infrared cameras.

### 8.1.2. Solar blind pyrometry

If the equipment for which we want to know the temperature is irradiated by concentrated solar energy, the aforementioned instrument will measure both the self-emitted light from the equipment and reflected concentrated solar light. This is true even for apparently non-reflective materials or cavities (except if completely designed as a black body). If the intensity of the self-emitted light is relatively low even the poorly reflected intense incoming concentrating light can dominate it.

For such conditions, the wavelength for the measurements must be chosen for which there is no or little concentrated solar light. This is the case either in Earth's or Sun's atmosphere absorption bands, or on the concentrating optical system absorption bands as illustrated in Figure 10. Such measurements are called **solar-blind** as they don't see solar radiation per design.

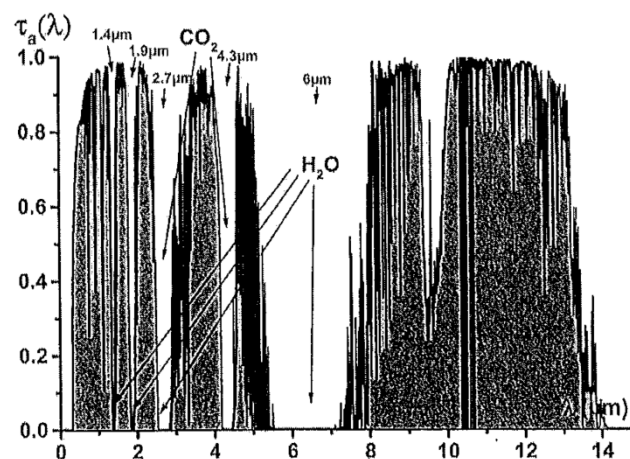


Figure 10: Atmospheric absorption bands in the infrared spectrum

### Specifications for equipment

To choose a pyrometer:

- Define your **temperature range**.  
Define both the minimal and maximal expected temperature. Few instruments are able to cover both very high temperature (> 2000K) and near ambient temperatures (< 500K)
- Define your **geometry**.  
Define both the desired probed spot size and the distance from which you will install the instrument. Be aware that low cost pyrometers (less than a few thousand euros/dollars) typically have a low quality alignment of the provided aiming lasers and the actual position of

the probed spot. You can check this by moving a diaphragm in the beam while probing a large hot surface such as a radiative plate.

The source to instrument beam characteristic is the etendue.

- Define your **wavelength(s)**.

Depending on both your material properties, the expected temperature and your environment condition, near or medium infrared are best suited.

Generally, the lower the temperature, the longer the wavelength due to the Planck law: the body will radiate more energy hence a higher signal. The **Wien's displacement law** can be used as an indication, as it gives the peak wavelength of the thermal emission of a perfect black body depending on its temperature:

$$\lambda_{max} \cdot T = 2898 \mu m \cdot K$$

$\lambda_{max}$  peak wavelength of the black body thermal emission in  $\mu m$

$T$  temperature of the black body in K

If you plan front side measurements, that is from the side irradiated by the concentrated solar energy, choose solar blind wavelength without reflected light. Typical solar blind wavelengths are 2.7  $\mu m$  (about 100 nm wide, due to water in the atmosphere) or 4.3  $\mu m$  (similarly narrow band due to CO<sub>2</sub> in the atmosphere) and 5 to 7  $\mu m$  (due to water and at the start to mirrors' glass absorption).

### *Calibration issues*

While calibrating your pyrometer with a black body or checking in it with a radiative plate:

- Always include the windows and filters that will be in your experimental setup.
- Reproduce as best as possible the geometry from your experiment such as distances, angles between the probed body and your instrument.
- Atmospheric conditions: especially for solar blind pyrometry, check accordingly the ground H<sub>2</sub>O or CO<sub>2</sub> levels during calibration to have them similar to those prevailing during your experiment.

### *Main error sources*

#### **Emissivity**

The emissivity is the ratio of light emitted by a body compared to the ideal black body. Ideally, the emissivity of your material should be measured. Tables from bibliography only give a possible range of the parameter, surface properties can make it change up to 50%, hence the determined temperature by similar ratio. Emissivity depends on:

- Chemical composition of the material.
- Physical state, including the crystal structure.

- Surface roughness: both low and high frequency shape compared to the pyrometer wavelength have an effect such as diffraction in the grooves.
- Temperature of the body.
- Coatings. Low thickness coating (a few microns) can be transparent or semi-transparent at your wavelength. You may measure emitted light from the coating, the body, or both; and there can be a thermal gradient between the body's surface and the coating's surface, leading to a complex mix of signals measured by the pyrometer.

### **Solar-blindness**

If your pyrometer is not completely solar blind (e.g. using an industrial pyrometer for the glass industry at 4.7 – 5  $\mu\text{m}$ ), residual reflected concentrated light will be added to the light emitted by your material. If the flux concentration and the material surface properties do not change, this can be dealt with as a systematic error and corrected, otherwise the temperature will be overestimated.

### **Dirt**

As any optical measurements, any dirt on the optics will change the results. As it is an infrared measure, there can be dirt not visible by the human eyes, such as residues from unsuitable cleaning liquids (soap...).

Alcohol based liquid are advised, preferably iso-propanol, but check the suitability with your windows materials (some infrared windows could be dissolved) and your working wavelengths (no residues).

### **Noise**

Parasite reflection can impede the optical measurement, notably for low temperature bodies. Electric noise should be reduced as always with proper grounding and shielding.

### **Multi color pyrometry**

Depending on the distance between the several wavelengths used by the pyrometer, all the above cited errors may be similar if the wavelength are near (no more than a few hundred nanometers) or the errors may be different if the wavelength are far from each other (several microns). In the latter case, the errors should be corrected or at least check individually for each wavelength used.

### **Literature**

*D. Hernandez, G. Olalde, J.M. Gineste, C. Gueymard (2004): Analysis and experimental results of solar blind measurements in solar furnaces; Journal of Solar Energy Engineering, Vol. 126, pp 645-653.*

*D. Hernandez, G. Olalde, A. Beck and E. Milcent (1995): Bicolor pyroreflectometer using an optical fiber probe ; Rev. Sci. Instrum., 66, 5548.*

*P.B. Coates(1977): Wavelength Specification In Optical and Photoelectric Pyrometry; Metrologia, 13, 1.*

*P.B. Coates (1981): Multi-Wavelength Pyrometry; Metrologia, 17, 103.*

*M. Schubnell, H.R. Tschudi and Ch. Muller; Temperature measurement under concentrated radiation; Sol. Energy, 58, 69, (1996)*

SFERA Deliverable R12.7: Report on solar blind and active pyrometry system

Etendue: <http://en.wikipedia.org/wiki/Etendue>

## 8.2. Temperature Measurement with contact probes

### *Description of method*

Almost all tests of CSP components or systems involve measuring either heat transfer fluid or component temperatures or both. These temperatures are typically determined using contact probes. Among the available measurement principles with contact probes, two are particularly suited to temperature measurement in CSP applications due to both accuracy and response time:

#### **Thermocouples**

Thermocouples operate on the basis of the fact that any junction of dissimilar metals produces an electric potential related to temperature. Thermocouples for practical measurement of temperature are junctions of specific alloys which have a predictable and repeatable relationship between temperature and voltage.

#### **Resistance Temperature Devices (RTD's)**

RTDs measure temperature by correlating the resistance of the RTD element with temperature. RTD elements are made from a pure material, typically platinum, nickel or copper. The material has a predictable change in resistance as the temperature changes.

Both measurement principles directly produce measurable variations of an electrical quantity.

When measuring fluid temperature the sensors are often not in direct contact with the medium but enclosed in a thermowell for reasons of durability, leakage and process safety.

### *Specifications for equipment to be used*

#### **Thermocouples**

There are different types of thermocouples depending on the pair of alloys used for the junction. Types J and K are suitable and recommended for typical temperatures levels of CSP applications ranging from 250 to 1500°C. In terms of sensor accuracy, class A thermocouples are superior and should thus be selected for CSP test applications.

The compensating cable connecting the thermocouples to the data acquisition system (DAS), must be of the minimum length required. The temperature of the cold junction must be monitored in real time and compensated for mathematically to avoid errors in the temperature determination. In case of longer distances between a measurement point and the DAS signals should be transferred via a digital bus (i.e. HART protocol).

The response time of thermocouples depends on the thermowell diameter (and resulting wall thickness) they are installed in, ranging from 1s (for diameters of 0.25mm) up to 9-15s (for diameter of 10mm).

### Resistance temperature devices

RTD's are more accurate, have better stability and higher response linearity than thermocouples. On the other hand, the cost of the sensor is higher than that of thermocouples. PT100 are most common and suitable for CSP applications, with a temperature range up to 650°C.

Concerning the accuracy of the sensor, class A (or DIN 1/3) RTD's are the more accurate ones and thus preferable for CSP applications.

In order to eliminate the influence of the temperature dependence of the cabling resistance, 4-wire connections must be used to connect the sensors to the DAS. Similarly to thermocouples for long distance signal transmission a digital bus protocol is preferred.

The response time of typical RTD sensors is longer than that of thermocouples (around 30s) due to the larger mass (of the sensor sheath) and thus the typical use of standard RTD's is measuring steady-state conditions or temperatures of fluids/components with long residence times/high thermal inertia. Small RTD sensors can be used for faster signals, with response times around the second, but their small size makes it more difficult to have proper mounting with low parasitic thermal gradients.

Table 7 shows a summary of RTD's and thermocouples main characteristics relevant for CSP testing.

*Table 7: Comparison of type J or K thermocouples to RTD Pt100 sensor for CSP testing*

Kind of sensor	Thermocouple J or K	RTD PT100
<b>Class</b>	Class A or better	Class A or better (DIN1/3)
<b>Temperature range</b>	up to 1250°C	up to 650°C
<b>Accuracy</b>	1.5°C or 0.004*t (the bigger one)	0.002*t+0.15
<b>Repeatability</b>	good	very good
<b>Sensibility</b>	Punctual	various mm
<b>Stability</b>	poor	Good
<b>Robustness</b>	good	poor
<b>Cost</b>	low	2-3 times thermocouples cost

### *Sensor calibration issues*

Temperature sensors are calibrated using block calibrators providing a constant, controllable temperature environment. During calibration sensors are compared to a higher order traceable reference sensor. Calibrations should be carried out regularly for the operating temperature range of the sensors. Particular care is required when attempting to measure small temperature differences. In this case, not only should the sensors be calibrated with respect to an absolute reference but also relative to one another to minimize the impact of any systematic deviations..

### *Main error sources and expected precision*

Errors of temperature measurement by means of contact probes predominantly result from poor thermal coupling of sensors to the components or media, thus resulting temperature differences between actual temperatures to be measured and temperatures “seen” by the sensors. In this context the influence of (relatively cold) ambient conditions is an issue. In addition to the typical sensor element uncertainty characterized by its type and class further uncertainties have to be considered due to sensor stability, hysteresis, repeatability, A/D conversion of transmitters and their temperature drift and the resolution of the data logging device.

### *Recommendations*

Installation of temperature sensors, mainly thermocouples, must avoid direct concentrated solar radiation of the sensors and must assure the contact between sensor and medium or component.

### *Literature*

International standard with application on thermocouples and RTD's

*IEC 60584-1, 1995. Thermocouples Part 1 : Reference tables.*

*IEC 60584-2, 1982. Thermocouples Part 2 : Tolerances.*

*IEC 60751, 1.995 Industrial platinum resistance thermometer sensors.*

*IEC 61152, 1992. Dimensions of metal-sheathed thermometer elements.*

*IEC 61515, 1995. Mineral insulated thermocouple cables and thermocouples.*

*IEC 61520, 2000. Metal thermowells for thermometer sensors — Functional dimensions.*

## 9. Mass flow measurement

Any evaluation of receiver, collector or (sub)system performance or efficiency based on heat balances necessarily requires measuring the flow rate of a heat transfer medium. Typically, flow rates are measured at the cold inlet of the system under investigation.

Different measurement principles and sensors can be used to determine flow rates in CSP testing. Measurement principles and instruments are chosen according to the heat transfer fluid, flow rates, pipe diameter and specific uncertainty requirements as well as cost aspects. Large scale parabolic trough applications commonly use ultrasonic and vortex flowmeters whereas smaller units may use coriolis meters. Tower related applications often use vortex meters or pressure drop based devices depending on the heat transfer medium. For installation and handling, Performance Test Code PTC 19.5 norm must be followed, as well as indications of PTC 19.1 norm.

### *Specifications for equipment to be used*

#### **Ultrasonic flowmeters**

Ultrasonic flowmeters are based on measuring the travel time difference between ultrasonic signals travelling upstream or downstream. To this end, signals are created by a transmitter injected diagonally into the pipe or onto its surface, pass through the HTF (with or without reflection on the pipe walls) and are picked up by a receiver. When subtracting travel times of signals travelling downstream from those travelling upstream, the speed of sound in the HTF cancels out. The travel time difference is directly proportional to the HTF mean speed.

Sensors are bidirectional and can measure positive and negative flows (an arrow on the sensor marks positive direction). They are composed by the sensor itself and a signal converter that must be installed far from the sensor to prevent high temperatures on the converter.

There are two different kinds of sensor based on the installation: inserted directly on the pipe by means of a welded or flanged roll; or Clamp-on type mounted outside in the pipe.

Accuracy of wetted ultrasonic flowmeters as stated by the manufacturers is 1% or better.

Table 1 lists advantages and disadvantages of ultrasonic flowmeters.

*Table 1: Advantages and disadvantages of ultrasonic flowmeters*

<b>Advantages</b>	<b>Disadvantages</b>
No additional pressure drops on the pipes	High cost
Suitable for corrosive and dirty fluids	Weak signal for low flows rates
Portable models available	Not suitable for two-phase flows
Measure in both directions	Volumetric method, fluid density required
Signal Linearity	

## Vortex flowmeters

This measuring method is based on Von Kármán vortex street: a fluid passing through an internal tube element that partially blocks the pipe generates alternating vortex to both sides of the blocking element with opposite directions. The frequency of the wake vortex is proportional to the volumetric flow rate ( $f=k \cdot Q_v$ ), where the k factor depends only on the geometry of the equipment and is independent from fluid speed, viscosity or density.

Vortex flowmeters have no moving components, reducing the maintenance of the equipment. There are different types of bluff bodies such as wafer, lug or flanged. Capacitive transducers are the main technology used, due to the robust behavior when submitted to thermal changes and tube vibration.

The accuracy of these sensors as stated by the manufacturers is 1.5% or better.

Table 2 shows the advantages and disadvantages of Vortex flowmeters

*Table 2: Advantages and disadvantages of vortex flowmeters*

Advantages	Disadvantages
No moving parts	Not suitable for laminar flows and high viscosity fluids
Suitable for liquids, gases and steam	Reynolds number > 10000
Acceptable pressure drops	Pipe vibrations largely influence measurements
Low maintenance	Volumetric method, fluid density required

## Coriolis flowmeters

This measuring principle is based on generating a controlled coriolis force into the sensor: these forces appear when longitudinal and rotational movements are superposed. The magnitude of the coriolis force and resulting phase difference in vibration are proportional to the mass of the fluid that flows through the sensor and accordingly, to the mass flow rate of the fluid. The effect is independent from temperature, pressure, viscosity, conductivity and flow profile. Some additional corrections of sensor temperature and pressure may be done to compensate changes of the instrument characteristics with these conditions.

Coriolis flowmeters measure directly mass flow and no density corrections are needed. Sensor must be inserted in the pipes using flanged or welds.

Accuracy of these sensors as stated by manufacturers is 0.5% or better.

Table 3 shows the advantages and disadvantages of Coriolis flowmeters

*Table 3: Advantages and disadvantages of Coriolis flowmeters*

<b>Advantages</b>	<b>Disadvantages</b>
High accuracy	High cost
Direct measurement of mass flow rate	High pressure drops
Suitable for liquids, gases and steam	Not suitable for large pipe diameters
Wide measurement ranges	

### **“pressure drop” flowmeters**

Pressure drop flowmeters measure the pressure drop across a nozzle or orifice plate inserted in the fluid flow in terms of differential pressure. The flow rate is correlated with the differential pressure measured according to:

$$\dot{Q}_v = K \cdot \Delta p^{1/2}$$

Accuracy of these sensors as stated by manufacturers is 2.0% or better.

Table 4 shows advantages and disadvantages of “pressure drop” flowmeters

*Table 4: Advantages and disadvantages of “pressure drop” flowmeters*

<b>Advantages</b>	<b>Disadvantages</b>
Low cost	Accuracy depends on fluids conditions
Simplicity	High pressure drops
Suitable for liquids, gases and steam	Not suitable for high viscosity fluids
	Broad measurement ranges
	Volumetric method, fluid density required

### **Selection criteria**

Most adequate flowmeters for CSP applications below 400°C are ultrasonic and vortex ones. Coriolis is the best selection for small size pipes if both higher price and larger external size can be afforded. Above 500°C, pressure drop flowmeters are typically the easiest technology to use.

Parameters to have in mind in the selection of the adequate equipment are: accuracy, measurement range, pressure drops, cost, corrosion, maintenance, etc.

## *Sensor calibration issues*

All flow sensors require regular (re)calibration, preferably at operating conditions. Standard commercial calibrations are carried out using water at ambient temperature, however. The effect of such deviating operation conditions on the sensor performance depends on the individual measurement principle and characteristic behavior of the sensor and needs to be considered individually. Typical calibrations involve a fluid loop with reference flowmeters or a precise measurement of the volume that passes through the meter during a certain period of time.

## *Main error sources and expected precision*

All methods for volumetric flow rate measurement described above are based on the assumption of a fully developed flow profile at or rather just before the location of the sensor and no important upstream disturbances. This implies the need for sufficient unimpeded piping length upstream of the sensors. Should this assumption be violated important errors will occur when deducing the flow rate from the signal.

Furthermore, temperature and density information is required in order to calculate the mass flow rate from measurements of volumetric flow rate. Possible errors much depend on the quality of this information.

Individual measurement accuracies are stated with the measurement principles above, these named measurement principles typically exhibit a measurement precision of 0.2 to 0.5%.

## *Recommendations*

### **For any flowmeter**

To avoid measurement errors, it is necessary to keep straight distances before and after the sensor (indicated by the manufacturer and guidelines to assure fully developed flow profiles). Usually 10 and 5 pipe diameters upstream and downstream respectively (50 and 15 diameters respectively for small size pipes between 1 and 3 inches). Required unimpeded lengths depend on upstream and downstream obstacles and need to be carefully checked for every application individually.

Orientation can be horizontal or vertical with rising flow. Pipes must be filled completely without air inside to prevent signal losses or poor flow measurements. To avoid air in pipes, following considerations have to be in mind:

- Do not install sensors in pipe's high point.
- Install sensor in upward slope horizontal pipes.
- Guarantee a minimum flow speed to avoid air in pipes.
- Do not install sensors in vertical pipes with downwards flows because full pipes cannot be guaranteed.

### **Additional recommendations for Vortex flowmeters**

These sensors are highly affected by pipe vibrations and thus, these must be avoided in order to obtain correct flow readings. At the same time, the flow profile must be stable to improve precision.

In case of installation of temperature and pressure sensors to convert volumetric flow to mass flow; they must be installed far away from the sensor in order not to affect generated vortex.

### **Additional recommendations for Coriolis flowmeters**

These flowmeters do not require long straight pipe distance upstream in order to measure correctly and valves, elbow joints, etc. do not affect measurement process.

To prevent cavitation inside sensor pipes, it is necessary to maintain an over pressure in the sensor. For this reason, coriolis sensors must be installed in the impeller pipe of the pumps or in the lower vertical pipes points.

### *Literature*

International normative applicable to mass flow measurement are:

*ISO 5167:2003 Measurement of fluid flow by means of pressure differential devices inserted in circular cross-section conduits running full - Part 1: General principles and requirements.*

*ASME PTC 19.5-2004. Flow Measurement.*

*ASME PTC 19.1-2005. Test Uncertainty.*

*EMI/RFI "Susceptibility of Electronic Equipment Standard".*

*EN60079-10: 2004. Electrical Apparatus for Explosive Gas Atmospheres General Requirement.*

*IEC 60529. Grados de protección proporcionados por Envolverte (código IP) 2004.*

*IEC 61000. Electromagnetic compatibility for industrial process measurement and control equipment.*

*EN IEC 61010-1 first and second edition (safety requirements for electrical equipment for measurement, control and laboratory use part 1).*

*IEC 61000-4-2 - Electrostatic Discharge Requirements.*

*IEC 61000-4-3 - 2002 Electromagnetic compatibility (EMC). Part 4-3: Testing and Measurement Techniques-Radiated, Radio-Frequency, Electromagnetic Field Immunity Test.*

*Pressure equipment directive (Module H of 97/23/EC, full quality assurance).*

*ANSI B 16.5. Pipe flanges and flange fitting, 1988.*

*ANSI B 16.25. Butt Welding Ends.*

*ANSI/ASME B1.20.1. Pipe Threads, General Purpose (Inch).*



*D. Kearney (2011): Utility-Scale Parabolic Trough Solar Systems: Performance Acceptance Test Guidelines*

## 10. Optical Properties

### 10.1. Reflectance

Reflectance is the fraction of incident electromagnetic radiation that is reflected at an interface between two materials with different refractive index. In general it must be treated as a directional property that is a function of the incident direction, the reflected direction, and the wavelength.

Considering the reflected direction, reflectance is divided in the three components: specular, diffuse and hemispherical; the latter being the sum of the others two. In parabolic-trough application, the useful portion is the “near-specular reflectance”, that is the specular and that diffuse in the cone with apex angle  $\Phi$ , where  $\Phi$  is the receiver diameter, and L is the path length between the point where radiation is reflected and the receiver. The proper measurement and treatment of the near-specular reflectance is quite a complex issue, on which work is still going on (see for instance the activity in SolarPACES Task III). Therefore, in the following only the specular reflectance will be considered. The present guidelines well fit conventional mirrors based on glass, but less the most recent solutions based on first-surface mirroring, for which diffuse reflectance is not negligible.

Reflectance greatly depends on the wavelength; the spectral reflectance describes the behavior of the reflectance in a given wavelength range. For CSP purposes, the most important parameter is the reflectance averaged on the emission solar spectrum (300 – 2500 nm about); this gives the solar reflectance.

#### *Description of method*

Among the available methods for measuring reflectance, the most reliable is the one based on a spectrophotometer equipped with an integrating sphere; the hemispherical reflectance of the mirror is obtained by comparison with a calibrated reference sample. The use of the integrating sphere avoids artefacts on the readings due to differences in flatness and thickness between sample and reference.

#### *Specification for equipment to be used*

Reflectance measurements should be carried out using a top level double-beam spectrophotometer equipped with an integrating sphere with a diameter larger than 150 mm; the reflectance of the coating of the sphere should be not less than 0.9 in the solar wavelength range. The reference mirror must be specular, i.e. low diffusive.

#### *Sensor calibration issues*

Reference mirrors must be periodically recalibrated because ageing and soil modify their reflectance; the typical error on reference is  $\pm 0.005$ .

#### *Main error sources*

Reference and specimen are measured in sequence; the instrument baseline may change up to 0.002.

#### *Recommendations*

More recently, SolarPACES TASK III published the guideline “Measurement of solar weighted reflectance of mirror materials for concentrating solar power technology with commercially available instrumentation”.

Referring to this guideline and the cited literature, here only few golden-rules are recalled:

- The reflectance must be measured in the spectral range required by the chosen standard with a top-level double-beam spectrophotometer.
- The most reliable reflectance measurement is that at near normal incidence, i. e. incidence angle less than 10°.
- The most reliable accessories are the “relative” and the “integrating sphere”; for both, initially the instrument is calibrated with a reference mirror. The “relative” accessory is not suitable for non-flat specimen and the achieved results may suffer from thickness mismatching of the glass plate covering the reflecting surface when it is different for specimen and reference mirror.
- The ratio between reflectance values of specimen and reference must be well inside the dynamic range of the instrument.
- The diffuse reflectance of the reference mirror must not be greater than the instrument accuracy.
- The reference mirror must be periodically verified with a certified mirror.
- When the specimen surface shows oriented texture, repeat the measurement at least twice, orienting the texture parallel and orthogonal to the incidence plane.
- In the final report, the used standard, spectrophotometer, reflectance accessory, and reference mirror must be explicitly declared.

### *Literature*

Several standards treat the reflectance measurement as well the solar averaging:

*ISO 5740. Road vehicles -- Rear view mirrors -- Test method for determining reflectance*

*ISO 6719. Anodizing of aluminium and its alloys -- Measurement of reflectance characteristics of aluminium surfaces using integrating-sphere instruments.*

*ISO 7668. Anodizing of aluminium and its alloys -- Measurement of specular reflectance and specular gloss of anodic oxidation coatings at angles of 20 degrees, 45 degrees, 60 degrees or 85 degrees.*

*ISO 7759. Anodizing of aluminium and its alloys -- Measurement of reflectance characteristics of aluminium surfaces using a goniophotometer or an abridged goniophotometer.*

*ISO 9060. Solar energy -- Specification and classification of instruments for measuring hemispherical solar and direct solar radiation.*

*ISO 9845-1. Solar energy -- Reference solar spectral irradiance at the ground at different receiving conditions -- Part 1: Direct normal and hemispherical solar irradiance for air mass 1.5.*

*ISO 15368. Optics and optical instruments -- Measurement of reflectance of plane surfaces and transmittance of plane parallel elements.*

*ASTM G173 - Standard Tables for Reference Solar Spectral Irradiances: Direct Normal and Hemispherical on 37° Tilted Surface*

More recently, SolarPACES TASK III published the guidelines “*Measurement of solar weighted reflectance of mirror materials for concentrating solar power technology with commercially available instrumentation*”.

*SFERA deliverable R12.11 Procedure for diagnostic on optical-thermal properties and performance of CSP components*

## 10.2. Reflectance, absorptance and emittance of the absorber coating

The reflectance of the absorber coating can be measured in the laboratory using spectrophotometers. Using energy conservation absorptance can be calculated from reflectance. Using Kirchhoff-Law emittance can be calculated from absorptance.

### *Description of method*

Spectral properties of surfaces and samples like reflectance, absorptance, transmittance and emittance of samples are in general dependent on wavelength  $\lambda$ , temperature  $T$ , incidence angles  $\theta$ ,  $\varphi$  and in the case of reflectance, transmittance and emittance, exitance angles  $\theta'$ ,  $\varphi'$ .

Due to measurement difficulties, often direct-hemispherical reflectance is measured as a function of wavelength  $\lambda$  at near normal incidence and at room temperature and considered a good representation of the spectral properties. However, it shall be mentioned here that some materials exhibit a pronounced temperature dependence of reflectance, for example. Furthermore the angular dependency may not be negligible: For isolators typically normal reflectance is lower than hemispherical reflectance, for conductors typically normal reflectance is higher than hemispherical reflectance. Furthermore, often technical surfaces have special directions due to the production process. In these directions especially specularly of reflectance can differ dramatically from specularly perpendicular to the special direction.

The monochromatic spectral reflectivity of the absorber coating  $r(\lambda)$  can be measured in the laboratory at defined wavelengths by a spectrophotometer with integration spheres. Typical UV-Vis-NIR spectrophotometers work in the range of 300 to 2500 nm. FTIR spectrophotometers work in the IR range of  $\sim 2$ -15 or up to 40  $\mu\text{m}$ . These devices are typically operated using near normal incidence and an integration sphere for the collection reflected light.

From this measurement the (near normal, direct hemispherical) solar weighted reflectance can be calculated using the solar spectrum at the Earth surface  $I(\lambda)$  in ( $\text{W m}^{-2} \text{nm}^{-1}$ ):

$$\bar{r} = \frac{\int_{300}^{2500} r(\lambda)I(\lambda)d\lambda}{\int_{300}^{2500} I(\lambda)d\lambda}$$

For the solar spectrum typically ASTM 173d is used. Assuming negligible transmission through the absorber, the near normal solar absorptance of the cermet coating can be calculated using conservation of energy via  $\bar{\alpha} = 1 - \bar{r}$ .

Applying Kirchhoff's law  $\alpha(\theta, \varphi) = \epsilon(\theta, \varphi)$  near normal emittance can be calculated. Total normal emittance can then be calculated by weighing  $\epsilon(\lambda)$  with the Planck distribution  $M(\lambda)$ . Total hemispherical emittance typically deviates from total near normal emittance, hence a correction may be applied.

Typically, integration spheres on the market have sample ports for the measurement of flat samples. Measurements on curved surfaces can be performed also. However, geometrical issues tend to increase at curved surfaces. An adapter for precise placement and orientation is necessary.

### *Specification for equipment to be used*

Various spectrophotometers are offered on the market. The spectral sensitivities should be matching the task. Typically, multiple light sources, diffraction gratings and sensors are combined in one machine to achieve the large desired spectral sensitivity of 300...2500 nm of the UV-VIS-NIR range. The same applies for FTIR spectrophotometers.

For quantitative measurements it is recommended to use integrating spheres of at least 15 cm diameter.

### *Sensor calibration issues*

Calibration of the reflectance measurement is performed using reference standards. It is recommended to use multiple standards. References should be as similar to the samples as possible, hence typically standards of high and low reflectance diffuse and specular reflectance should be available. Furthermore, it is good practice to use two standards of each kind, a working standard for every day measurements and a master standard which is used to check reflectance of the working standard in regular intervals. The master standards should be calibrated regularly in certified laboratories in order to insure up-to-date NIST-traceability.

### *Main error sources*

A major uncertainty of the method arises from the various simplifications made described above. Absorbers are operated up to 400°C or even 550°C, but the measurement is performed at room temperature. Additionally there are simplifications concerning angular dependence of incidence or exitance.

Furthermore main contributions to uncertainty of the measurement are the calibration of the standard and geometrical loss at in the integration spheres ports, closed or open, and baffles. It should be insured that the direct reflection does fall on the normal sphere surface, not on baffles or ports.

In the measurement of emittance with the above described method an issue might arise with a limited spectral range of the measurement as the Planck distribution may have significant contributions outside the spectral measurement range.

### *Recommendations*

### *Literature*

*SFERA deliverable R12.11 Procedure for diagnostic on optical-thermal properties and performance of CSP components*

## 11. Heat Flux Measurement

Radiometers and fluid-heating calorimeters are basic devices that can be used for direct measurement of incident heat flux in a particular location within the focal region, incorporated in different ways that depend on the type of concentrator and the level of solar concentration. Alternatively, indirect measurement of heat flux is performed using remote cameras and reflective targets that are placed within the focal-region for detailed images of the heat flux density profile, sometimes calibrated using direct heat flux density measurement with radiometers. Ray tracing based on measurements of concentrator surface topology can also be used to create simulated heat flux density distributions, which can be used for further analysis.

### 11.1. Direct method using radiometers

#### *Description of method*

The description of system designed and operated by CIEMAT is given as reference of possible usage: multiple moving radiometers providing spatial flux mapping.

A direct heat flux measurement system(MDF), has been designed, constructed and mounted on top of the SSPS-CRS tower at the Plataforma Solar de Almería (PSA) to measure the concentrated solar power by a heliostat field onto the flat aperture of a solar receiver prototype under evaluation. The geometry of the receiver aperture determines the operation and analysis procedures to obtain the incident power onto the defined area. Today, everything is prepared to perform the direct heat flux measurement on the aperture of solar receivers: radiometer array, data acquisition system and software.

This system corrects the technical deficiencies of the previous direct heat flux measurement devices [1, 2]. A new type of radiometer with response times of microseconds allows nearly an instantaneous direct heat flux measurement [3, 4, 5, 6, 7]. Based on this principle, a moving bar with several of these heat flux microsensors, HFM, has been built. The spatial resolution in the vertical direction improves with the number of radiometers. The moving bar passes in front of the receiver aperture in a parallel plane pivoting in a fixed point placed under the receiver aperture, in the vertical line of the center (Figure 11).

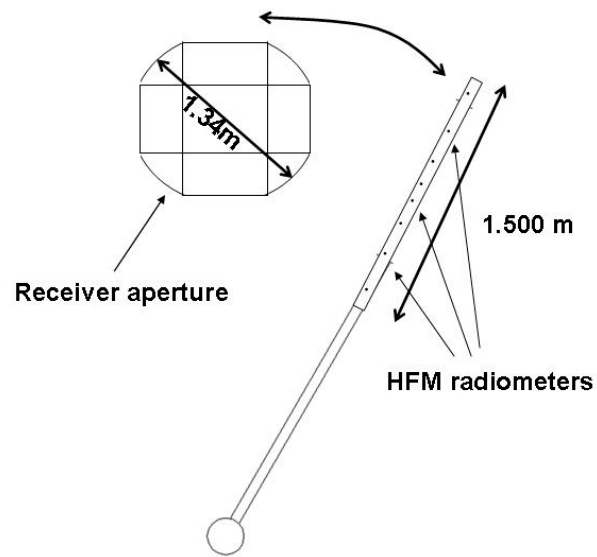


*Figure 11: Radiometer bar and receiver aperture in parallel planes*

Several interesting quantities such as the total incident power, the value of the heat flux peak and its positioning referred to the center of the aperture, are also obtained.

An example of measurement analysis is presented below. Figure 12 is a synthetic image obtained from a group of analog signals such as described before.

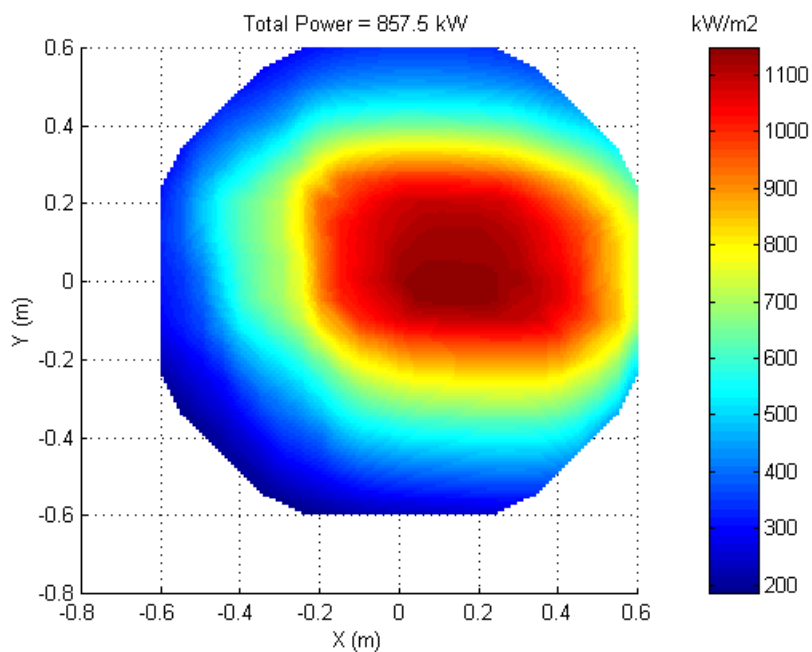


*Figure 12: 2D heat flux density distribution onto receiver aperture*

This example has been obtained by 45 heliostats aimed to obtain a uniform heat flux distribution. Several relevant quantities associated with these images are:

INSOLATION: 888 W/m<sup>2</sup>

Nº HELIOSTATS: 45

Number of measured data = 96

Heat flux density peak = 1147 kW/m<sup>2</sup>

xmax = 0.200 m

ymax = -0.050 m

Total Power = 857 kW

Power Error = ± 38 kW

Power Error = ± 4.5 %

Heat flux density average = 649 kW/m<sup>2</sup>

Energy = 0.44 kWh

Scanning Time = 1.86 s

### *Specifications for equipment to be used*

The MDF system has three four main components:

- Moving bar with eight HFM radiometers.
- Encoder.
- Acquisition card with 32 differential channels of 3 V of highest resolution, which represents a heat flux density resolution of 0.2 kW/m<sup>2</sup> and a power resolution of 0.006 W.
- Software for the data acquisition (Labview®) and for the analysis (Matlab®).

A fast data acquisition system for these radiometers and a convenient moving bar speed allow nearly instantaneous measurement of the heat flux distribution without water-cooling and improvement of the spatial resolution in the horizontal direction. These sensors are made using thin film processes [8, 9, 10]. Thin film construction gives the sensors many unique advantages:

- The industry's fastest response: 2-6 microseconds
- Minimal impact on the system under evaluation due to the small size of these radiometers of 6.32 mm diameter front face.
- Operation in temperatures up to 850°C, depending on the model, without external cooling.
- Measures both incident heat flux and temperature at the face of the sensor. The temperature is used to correct the heat flux measurement.
- Low electrical noise.
- Sensitivity: 15 μV/kW/m<sup>2</sup>

- Accuracy:  $\pm 3\%$

The signals from the radiometers are acquired by an acquisition card, which is integrated in a PXI/CPCI (National Instruments®) system placed in a rack at the top of the CRS tower. The transmission of the data to the PC in the operation room is performed by optical fiber.

### *Sensor calibration issues*

The Heat Flux Microsensor (HFM) are manufactured and calibrated by Vatel Corp. [10]. Because it is made with thin-film sputtering techniques, the entire sensor is less than 2 mm thick. The thermal resistance layer of silicon monoxide is also sputtered directly onto the surface. The resulting physical and thermal disruption of the surface due to the presence of the sensor is extremely small. Use of high-temperature thermocouple materials allows sensor operating temperatures to exceed 800 °C for the high-temperature models. They are best suited for heat flux density values above 1 kW/m<sup>2</sup>, with no practical upper limit. Because the sensor is so thin, the thermal response time is less than 10 ms, giving a good frequency response well above 1 kHz. A temperature measurement that is integrated into the sensor is very useful for checking the heat flux calibration and determining the heat transfer coefficient. The high temperature and fast time response capabilities are useful for aerodynamic applications, combusting flows in engines and propulsion systems, and capturing high-speed events such as shock passage. This rapid response also offers advantages in measurement of CST receiver transients.

The exposed face of the sensors is sprayed with a high-absorptance black coating to achieve absorption high enough to generate a significant signal. Zynolyte® is the preferred coating at Vatel because it creates a rough surface that improves heat absorption.

The current procedure for calibrating these sensors at Vatel [10, 11] is based on a dual-cavity black body, which is basically an electrically heated double-ended cylindrical graphite tube with a center partition that allows its internal temperature to be measured with an NIST-traceable pyrometer while the reference transducer is being calibrated. When the selected temperature of 850°C has stabilized, the transducer is quickly inserted into the cavity opposite the pyrometer. The Stefan-Boltzman law supplies the resulting irradiance value of about 90 kW/m<sup>2</sup> on the front face of the sensor, assuming hemispherical irradiation. Calibration of the reference heat flux sensor is performed with this single-point technique. This calibration is transferred to the commercial sensors by comparison in a calibration furnace with a graphite plate that radiates evenly and symmetrically when an electrical current passes through it [10, 11]. The calibration constant obtained with this method translates voltage to irradiance on the front face of the sensor. The manufacturer states that the accuracy of gages calibrated in this way is within  $\pm 3\%$  with a repeatability or precision of  $\pm 1\%$  [10].

### *Main error sources and expected accuracy*

At 850°C the spectral radiance of a black body is significantly different from the solar spectral distribution and a systematic error arises due to the difference in power absorbed by the coatings under these two dissimilar electromagnetic spectral distributions. The systematic error from measuring solar irradiance with these gages has been estimated from all this information. If the

sensor coating is Zynolyte<sup>®</sup>, the sensor overestimates the solar irradiance by 3.6% [11]. The main error source of this measurement system is the heat flux density measurement accuracy of the HFM sensors which is  $\pm 3\%$ . Obtaining the power on the receiver aperture involves other uncertainties related to the integration of the heat flux density map, positioning sensors and the receiver area of interest. Therefore, it is possible to obtain an estimation of the solar power measurement accuracy of about  $\pm 6\%$ .

### *Recommendations*

Experience with this heat flux measurement system is limited to the last 10 years at PSA to evaluate several solar receivers of less than 1.5 meters diameter front face and heat flux density levels below  $1500 \text{ kW/m}^2$ . The scaling of this measuring system to assess larger receivers under higher heat flux density levels is not obvious. The receiver aperture and the bar are tilted by the same angle. The moving bar passes in front of the receiver aperture at a distance of 250 mm in a parallel plane pivoting in a fixed point. This is placed under the receiver aperture, in the vertical line of the center. Using an acquisition rate of 10 data per second for these radiometers, which is concordant with the sampling of 10 readings per second of the bar angular position, and a moving bar speed of  $0.21 \text{ rad s}^{-1}$  allow the heat flux density distribution to be measured almost instantaneously, without forced cooling requirement. The resulting spatial resolution in the horizontal direction ranges from 10 to 13 mm. It is possible to improve the resolution in this direction by increasing the data acquisition rate and the number of readings per second of the bar angular position. The entry and exit positions of the bar onto the receiver aperture are defined by two angular encoder references. These two angular references delimit as well the useful data from the radiometers to obtain the heat flux density distribution onto the receiver aperture. The speed of the bar is considered constant because an alternating current motor drives the bar. When the bar reverses to the parking position vibrations are initiated. For this reason the estimation of the heat flux measurements for the return are not considered. The incident radiant power on the aperture is obtained by integrating the heat flux density distribution over the aperture area. A more detailed heat flux density distribution with a higher resolution is desirable. For this reason an interpolation with spacing of 50 mm has been performed with an inverse distance method with a consequent minimal error due to the small variations of the heat flux density distribution.

### *Literature*

- [1] F. Diessner (1981): *Operation manual for the measurement activities with Heat Flux Distribution (HFD) system, DFVLR (Deutsche Forschungs- und Versuchsanstalt für Luft- und Raumfahrt), Cologne, Germany.*
- [2] G. García (1988): *General description of the flux measuring system of the volumetric receiver, Plataforma Solar de Almería. Internal report R-15/88GG.*
- [3] J. Ballestrín (2001): *Direct Heat-Flux Measurement System (MDF) for Solar Central Receiver Evaluation, Publicación-961 de C.I.E.M.A.T. 2001. Ref. ISSN:1135-9420.*
- [4] J. Ballestrín (2002): *A non-water-cooled heat flux measurement system under concentrated solar radiation conditions, Solar Energy (PERGAMON), Vol. 73, No. 3, pp. 159-168. ISSN: 0038-092X*

- [5] J. Ballestrín, R. Monterreal (2004): *Hybrid Heat Flux Measurement System for Solar Central Receiver Evaluation*, *Energy (PERGAMON)*, Vol. 29, pp. 915-924. ISSN: 0360-5442.
- [6] J. Ballestrín, J. Valero and G. García(2010): *One-click heat flux measurement device*, 16<sup>th</sup> *SolarPACES International Symposium*. Perpignan, France, 21-24 September 2010.
- [7] K Lovegrove (2012): *Concentrating solar power technology. Principles, developments and applications*, *Woodhead Publishing Series in Energy No. 21 (October 2012)*. Chapter 18: *Heat flux and temperature measurement technologies*. pp 577-601. ISBN: 978 1 84569 769 3
- [8] J. M. Hager, S. Simmons, D. Smith, S. Onishi, L. W. Langley, T. E. Diller(1991): *Experimental Performance of a Heat Flux Microsensor*, *Trans ASME*, Vol 113, pp 246-250.
- [9] H. L. Peabody(1997): *Evaluation of a Heat Flux Microsensor in a Transonic Turbine Cascade*, PhD Dissertation, Faculty of Virginia Polytechnic Institute and State University.
- [10] *Vatell Corporation Thermatechnology (2000): Annual technical magazine on heat flux sensors.* <http://www.vatell.com/newsletter.htm>.
- [11] J. Ballestrín, M.Rodríguez-Alonso, J. Rodríguez et al: *Calibration of high-heat-flux sensors in a solar furnace*, *Metrologia (Institute of Physics)*, Vol. 43, pp. 495 – 500, 2006. ISSN: 0026-1394

## 11.2. Flux density measurement: indirect measurement method

### *Description of the method*

The most commonly used method to measure the flux distribution of solar concentrators is the indirect measurement method using a diffuse reflecting 'lambertian' target that is placed in the beam path of the concentrated solar radiation and a camera that takes images of the brightness reflected from this target. The brightness, represented by the 'greylevel' of each camera pixel can be calibrated to a flux density value with the help of a radiometer that measures in parallel at one point on the target. When the total power on the target is well known (like in many cases when measuring dish-systems) the total power also can be used to calibrate the images.

The measurement method can be applied using a stationary lambertian target that is illuminated by the concentrating system (parabolic dish, solar tower, trough,...) or it can be used with a small target that is moved through the beam path of the concentrating system (in operation) in the plane of interest (mostly closed to the aperture plane). In this case a series of pictures is taken during the movement of the target through the concentrated sun light under stable solar conditions. The raw image of the flux distribution is assembled cutting out the illuminated target from each picture and fitting these parts together. Later this assembled picture can be treated as described above.

Depending on the particular measurement system the picture needs to be rectified in several steps before it can be calibrated to a flux distribution. The measured signal of each pixel might need to be corrected for a non-linear camera response function and the dark current signal (caused just by the thermal condition of the camera chip) might have to be subtracted from the signal. Furthermore, the lens system or the camera chip might cause a location-dependent signal that needs to be corrected

(‘shading correction’) and of course depending on the camera view angle a geometrical correction of the image is necessary. For some specific measurements the dependency of the reflectance from the incident angle must be considered as well as the dependency of the signal from the available solar spectrum.

### *Specifications for equipment*

#### **Lambertian Target**

The Lambertian target must have the following properties

- High reflectance for solar radiation
- Reflectance should be independent from the wavelength in the range of sensitivity of the CCD-Camera
- Reflectance should be independent from incidence angle
- Cosine distribution of the emitted radiation (Lambert law)
- Surface resistant to temperature with reflectance independent from temperature
- Mechanically resistant

Commonly used are stationary targets that are placed in the beam path in the desired measurement plane or moving (bar) targets that are moved through the beam path in front of a solar receiver during the operation. For stationary targets normally a water-cooled, metal body with a thin, diffuse reflecting and temperature resistant coating (ceramic material) is used whereas for moving targets water cooling is not required in most cases because the exposure time of the target is quite short and temperature increase of the target material is acceptable. In this case normally a temperature resistant, white paint is used.

#### **Camera**

Best suited cameras for flux density measurement are using CCD-Sensors (Charge Coupled Device) with slow read-out of the sensors pixel information (slow scan). Flux measurement cameras must have a linear characteristic (brightness → pixel grey value) and should have a good signal to noise ratio to be able to evaluate also the big areas with low brightness which are typical for flux density images that usually have a very bright but rather small peak and a big area with low brightness that still has a significant contribution to the overall power.

Most important parameters found in the specifications for cameras are:

- **Linearity** is a very important characteristic of a CCD imaging system for photometric applications. The digital signal should be proportional to the number of incoming photons.
- **Dark current** of a CCD image sensor is an important factor for sensitivity. It results from the temperature-dependent thermal generation of electrons. Dark current must be considered during image evaluation and can be reduced and controlled by temperature controlled imaging sensors (Peltier cooling).

- **Signal to Noise Ratio**
- **Quantum Efficiency** is defined as the percentage of the generated electronic charges by the incoming photons and is dependent of the wavelength of the light. This dependency must be considered in the image evaluation.

### **Radiometer**

Commercially available radiometers for heat flux measurement usually work according a design developed by R. Gardon in the 1950th. A thin metal foil made of constantan is attached to the sensors cylindrical body made of copper so that they form an 'outer' thermocouple. A copper wire is then connected to the foil's center forming a second 'inner' thermocouple. When this sensor is exposed to a heat flux and the sensors body is cooled at the same time a temperature difference between the center of the foil and the sensor body occurs that produces an electrical signal by means of the two thermocouples that is proportional to the heat flux on the sensor surface. In a calibration procedure the voltage signal can be correlated with the heat flux density with typical precisions of about 3% for applications with highly concentrated sun light.

### **Optical filters**

The pixels of a CCD sensor accumulate an electric charge that is proportional to the incoming light. After the integration time the charge is transferred to the conversion zone of the chip and finally converted to a digital signal. Each pixel has a maximum of electric charge that it can hold. When there is more light available more electrons (charge) are produced but the signal cannot increase any more. This effect is called saturation and must be avoided when using a CCD as a measurement device. For a flux density measurement system to reduce the intensity of light on the sensor and to avoid saturation, neutral density (ND) filters are necessary even when the integration (exposure) time is reduced to very short periods. ND filters are supposed to reduce the intensity of the light independently from the wavelength. Since this is not completely right, the transmission characteristic of all used filters should be exactly known and should be considered during the evaluation of heat flux images.

As demonstrated by Ulmer the measurement result highly depends on the available solar spectrum which changes even during the measurement day. The spectrum is mainly influenced by the length of the path of the light when traveling through the atmosphere. The air mass was defined as the parameter that describes the different conditions.

The right combination of optical filters can significantly reduce the signal's dependency from the air mass and can contribute to a much higher precision of the results of heat flux measurement.

### ***Calibration issues***

Issues regarding the calibration of the heat flux sensors were already described and discussed in section **Fehler! Verweisquelle konnte nicht gefunden werden..** Frequent sensor calibration by the manufacturer and also participation at the comparison campaigns can increase measurement precision and comparison of the results from different measurement systems.

### *Main error sources and expected accuracy*

Expected total accuracy for an indirect heat flux measurement system are in the range of 5%, but can increase easily to much higher values, when not all components are chosen thoroughly. As the main error sources, we can identify the reading of the radiometer and the dependency of the measurement result from the available spectrum.

### *Recommendations*

As mentioned before the available spectrum and the spectral properties of all components of the measurement system must be considered to produce more precise results. Furthermore the physical location where the radiometer is placed in the concentrated light is also critical. The radiometer always should be placed in an area with low gradient because this reduces the possible error due to a dislocated reference value.

### *Literature*

*S. Ulmer (2004) Fortschritt-Berichte VDI: Messung der Strahlungsflussdichte-Verteilung von punktkonzentrierenden solarthermischen Kraftwerken. 6 (510). VDI Verlag. 121 S. ISBN 3-18-351006-5. ISSN 0178-9414*

*A. Neumann, R. Monterreal (1992): „Measurement of Concentrated Solar Radiation with the HERMES II System at the PSA”, 6th International Symposium on Solar Thermal Concentrating Technologies, Mojacar, Spain, 28. Sept. - 02. Oct. 1992.*

*J. Giral, N. Boulet, G. Hernandez (2000): OBELIX: Flux Mapping System using a Video Camera, Proceedings of the 14th Task III Meeting within IEA SolarPACES on Solar Technology and Applications, SolarPACES Technical Report No. III-2/00, Sydney, Australia.*

*Theta System, Glossaery for SIS system specifications, THETA SYSTEM Elektronik GmbH, Rathausstr. 13, D-82194 Gröbenzell, Germany*

## **11.3. Calculated method: raytracing**

In addition to measurement, it is possible to calculate the flux distribution of concentrating solar systems or facilities using the usual geometrical optical laws, mainly **Snell's law**. However, the application is not trivial as concentrating solar plants typically consist of a large number of mirrors of different orientation, shape, size, canting, reflectivity characteristics, shading and blocking etc. Furthermore a fine **discretization** of the optical system is required to describe all these local properties, leading to a large amount of data and/or statistical description of the optical system, and then integration techniques must be applied to calculate the flux distribution in the plane of interest of the system/facility.

To this end, two integration approaches are used to calculate the flux distribution, sometimes mixed along the path of the solar rays:

- Integration by convolution

- Monte Carlo integration

Commercial software is readily available for both approaches. Integration by convolution is much faster and can be used for design optimization or parametric sensitivity studies more easily. Monte Carlo techniques allow finer modeling of real optical system with much finer details, but at the cost of much longer computing time. Different variations of the Monte Carlo formulation can lower the computing cost while keeping the versatility advantages, such as the integral formulation Monte Carlo algorithm presented in [Piaud 2012] which allows fast sensitivity studies to help designers.

*Table 5: Comparison of optical integration approaches*

	<b>Convolution</b>	<b>Monte Carlo</b>
<b>Speed</b>	The fastest, due to simpler mathematics and optimized FFT algorithms	Slow to fast, depending on the optimisations (multicore, GPU...) and the mathematical formulation (naïve, lost rays handling, integral formulation...)
<b>Precision of the results</b>	Low to medium, as based on statistical descriptions rather than fine discretisation	The highest, can use fine actual measurements data of the optical system
<b>Parametric studies</b>	Easy	Depending on the software speed and mathematical approach

### *Description of method*

#### **Analytical Integration**

Analytical integration was the only possibility method for raytracing before ample computing capacities became widely available. As the objective is to lead to a mathematical formulation which can be solved with low computing capabilities or even without computers, simplifications of the description the optical system must first be performed.

Typically, the ideal geometrical description is kept (shapes, orientation in space of the mirrors...), and statistical functions are used to include the real errors of the optics such as microscopic errors of the normal or the reflectivity of the mirrors, shape variations (waviness...), orientation errors from tracking and canting or thermal effects etc. All these optical errors can be described as Gaussian distributions that widen the beam reflected by any point of the system, as described in [Lipps 1976]. At the end, a convolution product is written between the luminance of the source, the local normal distribution of the considered mirror and all the distribution of the optical errors considered. This convolution product is easily calculated nowadays thanks to the availability of extremely fast FFT algorithms.

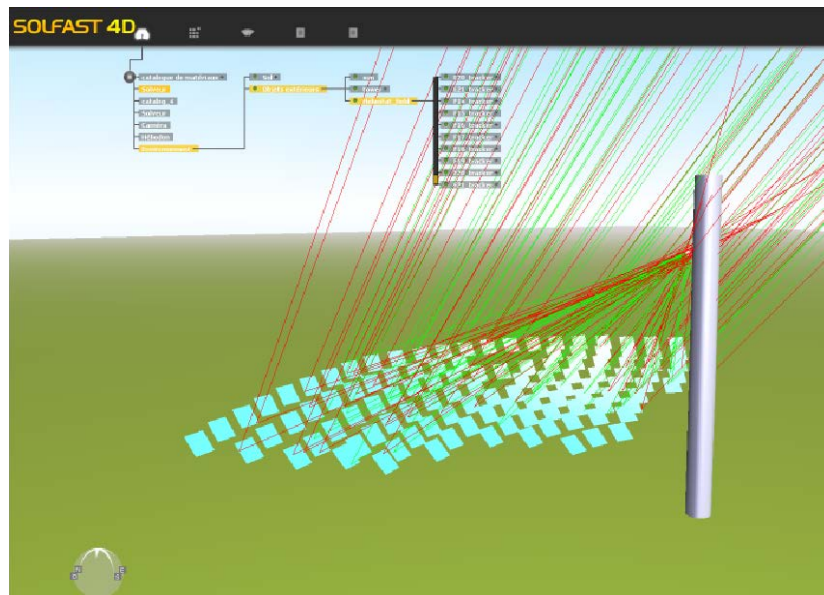


Figure 13: Screenshot from an exemplary Monte Carlo software (HPC SolFast 4D) showing a simplified model of tower, with rays reaching the receiver in green and the other rays in red.

### Monte Carlo Integration

In a nutshell, Monte Carlo ray tracing consists of simulating gazillions of individual solar rays and following their journey along the optical system. At the end, the number of rays reaching the area of interest is counted. Different approaches exist to achieve this simulation: launching rays either from the source or from the target, different types of random approaches used as well as ways to discard lost rays. The choice of the simulation direction leads to mathematics and algorithms more or less simple, and then to more or less heavy computing power requirements. For example, by inverting the distribution functions of the reflectivity and/or sun surface luminosity one can greatly reduce the number of useless calculated rays increasing the speed by several orders of magnitude in some cases, as described in [Piaud 2012].

### *Specification of the equipment to be used*

Even if the computing approaches are not specific to concentrating solar energy, mainstream optical software is typically not suited as only few allow suitable modeling of our source, the sun, and also few can cope with optical systems spreading on square kilometers. In addition, specialized CSP optical software typically includes tools speeding up design of solar facilities, such as libraries with ready to use heliostats, furnaces, troughs etc.

The following software can be used to simulate solar facilities:

- **SolFast 4D** (Integral Formulation Monte Carlo, HPC & CNRS)  
<http://www.hpc-sa.com/fr/products/solfast4d>
- **Tonatiuh** (Monte Carlo, CENER)  
<https://code.google.com/p/tonatiuh/> (free and open source)

- **SolTrace** (Monte Carlo, NREL)  
<http://www.nrel.gov/csp/soltrace/> (free)
- **STRAL** (Monte Carlo, DLR)
- **SPRAY** (Monte Carlo, DLR)
- **HELIOS** (convolution)
- **WINDELSOL** (convolution)
- **ZEMAX** (Monte Carlo)  
<https://www.radiantzemax.com/en> (used for design at focus, not complete facilities)

### ***Literature***

*Frederick W. Lipps (1976): Four different views of the heliostat flux density integral, Solar Energy, Volume 18, Issue 6, 1976, Pages 555-560*

*Benjamin Piaud, Christophe Coustet, Cyril Caliot, Emmanuel Guillot and Gilles Flamant (2012): Application of Monte-Carlo sensitivities estimation in Solfast-4D, Proceedings SolarPaces 2012. [http://www.hpc-sa.com/sites/default/files/Solfast4D\\_Solarpaces2012.pdf](http://www.hpc-sa.com/sites/default/files/Solfast4D_Solarpaces2012.pdf)*

## 12. Calorimetry

### *Description of method*

Calorimetric methods are currently the most accurate available means of determining the power or the flux density of a concentrating solar facility. Intercomparisons with other methods including Gardon type radiometers can be found in [Kaluza 2001] and [Neumann 2006].

Calorimetric methods are based on devices that heat a fluid with radiative energy. Typical devices are **water-cooled cavities** as shown in Figure 14 for which one measures the temperature elevation and the flow rate of the water to calculate the radiative heat transferred to the fluid.

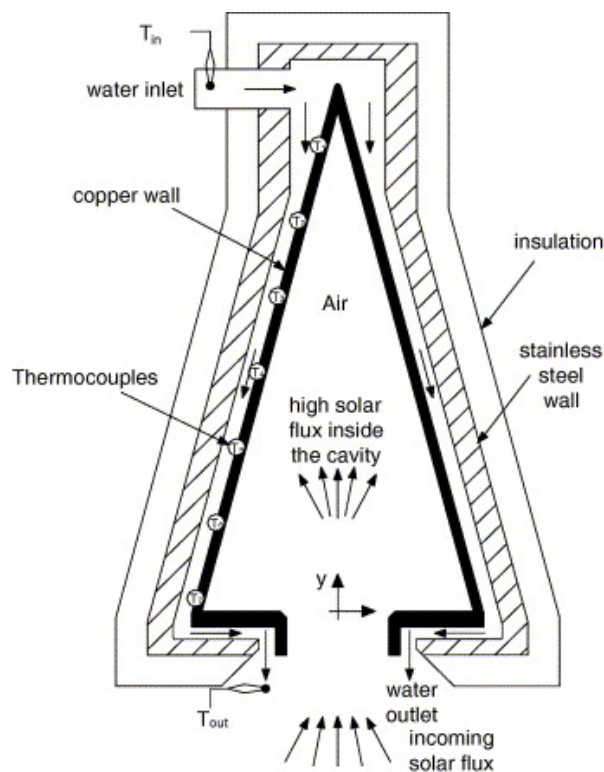


*Figure 14: CAVICAL conical calorimeter: in the paper, the authors describes their calorimeter and its study with FLUENT of the heat transfer in the cavity [Perez 2006]*

The calorimetric device or sensor can be used either for total or for partial power evaluation:

- Evaluation of the total power if the sensitive area is bigger than the concentrated beam. This is usually reasonable for low power facilities or/ and with high concentration ratio. Such devices are named “total calorimeters”.
- Evaluation of the flux density if the sensitive area is smaller than the concentrated beam, including mapping space by moving the sensor.

As an example for high precision instruments, one can refer to the Kendall radiometers, commercially available in the past for low flux density and described in the patent [Kendall 1971].

## Specification of the equipment to be used

In calorimetric evaluations three main parameters must be measured:

- The **temperature elevation** of the fluid:  $\Delta T$
- The **mass flow** of the fluid:  $\dot{m}$
- The instantaneous **direct normal irradiance**:  $DNI$

The power transferred to the fluid is calculated with:

$$P = \dot{m} \cdot c_p \cdot \Delta T$$

$P$  : measured power in *Watts*

$\dot{m}$ : fluid mass flow rate in kg/s

$c_p$ : mass heat capacity of the fluid in  $\frac{\text{J}}{\text{kg} \cdot ^\circ\text{C}}$

$\Delta T$ : temperature elevation of the fluid in  $^\circ\text{C}$

For the best accuracy, additional parameters should be measured:

- The absolute mean temperature of the fluid in the calorimeter
- The thermal losses of the calorimeter
- The circumsolar ratio CSR

With the absolute mean temperature of the fluid, one can compensate for the changes of the heat capacity of the water with the following formula suitable for distilled water:

$$c_p = 4 \cdot 10^{-2} \frac{\text{J}}{\text{kg} \cdot ^\circ\text{C}^3} \cdot T^2 - 2.65 \frac{\text{J}}{\text{kg} \cdot ^\circ\text{C}^2} \cdot T + 4220 \frac{\text{J}}{\text{kg} \cdot ^\circ\text{C}}$$

$c_p$ : mass heat capacity of the fluid in  $\frac{\text{J}}{\text{kg} \cdot ^\circ\text{C}}$

$T$ : mean temperature of the fluid in  $^\circ\text{C}$

### Temperature elevation of the fluid $\Delta T$

Temperatures probes must be inserted in the fluid pipes as close as possible to the calorimeter. Insertion lengths in the fluid must be at least 10 times the diameter of the probe: if 1,5 mm diameter probes are used, the wet length must be at least 15 mm. Longer lengths are recommended, especially if the pipes have high conductivity such as metallic piping versus plastic pipes.

Either RTD or thermocouples can be used. Low uncertainty **RTDs are advised** due to their higher stability and best off-shelf accuracy, such as 1/3 or 1/10 DIN, but small probes should be chosen in order to have short enough response time. If thermocouples are used, E type is recommended to match the expected temperature range while delivering high signal due to high Peltier effect. Moreover, the thermocouples should be connected in series in order to directly measure  $\Delta T$  with a single input channel on the data acquisition system.

Temperature data acquisition should be chosen to exhibit excellent short-term stability in order to have low uncertainty on the  $\Delta T$  determination. Typical care should be applied: short wires, adequate shielding, adequate signal filtering and integration.

Refer to chapter 8.2 for more information about temperature measurements with probes.

### Mass flow of the fluid $\dot{m}$

High accuracy mass flowmeters are required: Coriolis flowmeters are most common for inline continuous high accuracy mass flow measurements. For non-continuous measurements, weighting a filling tank can achieve very high accuracy as well. However this an acceptable method only for very stable power conditions as the mass flow rate is determined at a very low rate, typically at most a few times per minute.

The use of volumetric flow meters such as electromagnetic flow meters and high precision balanced turbines is possible if the density of the fluid is well known for the used temperature range. For pure water, the following correction can be used from 0°C to 40°C according to the recommendations by the International Committee for Weights and Measures (CIPM) based on the reference measures by [Tanaka 2001]:

$$\rho = a_5 \cdot \left( 1 - \frac{(T + a_1)^2 \cdot (T + a_2)}{a_3 \cdot (T + a_4)} \right)$$

$\rho$ : density of water between 0 and 40 °C in kg/m<sup>3</sup>)

$T$ : temperature of water in °C

$a_1 = -3.983035$  °C

$a_2 = 301.797$  °C

$a_3 = 522528.9$  °C<sup>2</sup>

$a_4 = 69.34881$  °C

$a_5 = 999.974950$  kg/m<sup>3</sup>

Refer to chapter 9 for more information about flowmeters.

### Instantaneous direct normal irradiation DNI

Refer to chapter 7 for information on DNI measurements.

### Mean temperature of the fluid $T$

Absolute temperature probes at the inlet and outlet temperatures are needed to calculate the mean temperature of the fluid in the calorimeter in order to apply the fluid mass heat capacity and density corrections, such as proposed upper in the text.

For better accuracy, multiples probes can be inserted on the fluid path in order to properly integrate these two corrections over real temperature gradient. The author has not seen such method being used for solar calorimetry but for radiation doses calorimetry where the calorimeter can be mapped with tens of thousands of temperature sensors to achieve extremely high accuracy and sensitivity: the best calorimetric dosimeters can exploit  $\Delta T$  in the milli if not micro Kelvin range, that means useful signals several orders smaller than the typical 3-20 K  $\Delta T$  as exploited for solar calorimeters. Refer for example to [Robert 2006], who describes several temperature measurement techniques for

very high accuracy, claiming realization of a sub-microKelvin thermometer for biological micro calorimetry applications.

### **Thermal losses of the calorimeter**

The main thermal losses of the calorimeter should be reduced as they are the biggest error of the device.

For any calorimeter the three usual thermal transfer modes should be studied carefully:

- Convection losses: either from the cavity (keep its aperture “small”, pay attention to the wind, orientate the aperture towards the ground if possible to limit natural convection) or the calorimeter walls (generously insulate them, for example with polyurethane foam except for the aperture area which may become too hot if exposed to stray concentrated solar energy).
- Conduction losses: fluid pipes and probes wires should have low thermal conductivity. Usage of plastic materials such as PVC pipes and small or thin wires will reduce these losses [Radu 2010].
- Radiative losses: at least two points should be studied.  
First, the cavity geometry and coating should be designed in order to have a very high absorptivity, as near as possible to 100%. The calculated apparent absorptivity at the aperture of the cavity should be higher than 95%. This is the most crucial part, as this parameter cannot be measured thus corrected from a real evaluation, it can only be derived from theoretical models which are hard to confirm.  
Then, the radiation losses from inside the cavity to the environment should be limited by avoiding high temperatures of the fluid: if its temperature is kept around ambient temperature, the exchanged power will be very low.

Electrical self-calibration of the calorimeter allows the compensation for convection losses, conduction losses and part of the radiation losses (only from the internal cavity, not reflection losses), if calibrated in similar environmental conditions as while measuring solar power. Self-calibration of the calorimeter can be realized if an electrical heating element has been integrated in the wetted part during construction: the user can then substitute a known electrical power to the incoming radiative solar power and determine this power with the usual heat flow transfer to the fluid. The difference between the measured power from the fluid flow and the injected electrical power represents the current sum of all the thermal losses, except the reflection losses under solar flux.

### ***Calibration issues***

#### **$\Delta T$ calibration**

A special calibration of the  $\Delta T$  measuring chain is required as the manufacturer’s specifications usually don’t cover the setup used for calorimetry: absolute accuracy over long periods of each probe or channel is not the useful parameter. Indeed, we rather need to know the relative uncertainty of each temperature determination during the measurement campaign. Absolute uncertainty

underestimates the accuracy of the setup: we need to evaluate each components stability, drift effects (mainly from ambient temperature), multiplexing effects... over the short time of measurement campaign.

For example, class I T type thermocouples have an uncertainty of  $\pm 0.5$  °C (the lowest per standard manufacturer specifications), which would lead to  $\pm 0.7$  °C uncertainty on the  $\Delta T$ . This calculation is correct, but far too high as the typical  $\Delta T$  should be kept around 10 °C to limit the thermal losses. This standard industrial uncertainty is high in order to compensate for the material fluctuations during the production at the manufacturer, in order to allow replacement of thermocouples over the years and delivering consistent temperature readings. But the same thermocouples can be calibrated for short term period and simultaneous use in order to achieve completely different uncertainty, well below 0.5°C.

### Main error sources

An exemplary investigation of the main errors for the realization of the DLR SunCatch calorimeter can be found in details in [Groer 1999].

#### Reflection losses — apparent absorptivity

The main error is typically caused by radiative losses from reflections through the aperture. To get an apparent absorptivity as high as possible, one usually designs cavity sensors coated with diffusive black paints. Internal reflections of the incoming beam are evaluated by raytracing or integral methods to assess the optical efficiency of the calorimeter, such as in [Groer 1999].

A similar problem has been studied in great detail in order to build real black bodies: how to reach high apparent emissivities of cavities, which is similar to high apparent absorptivity required for calorimeters. The literature in this field is more extensive, such as [Berry 1981], [Sapritsky 1992], [Ono 1986] and can be a source of inspiration for the calorimeter designers (see Figure 15).

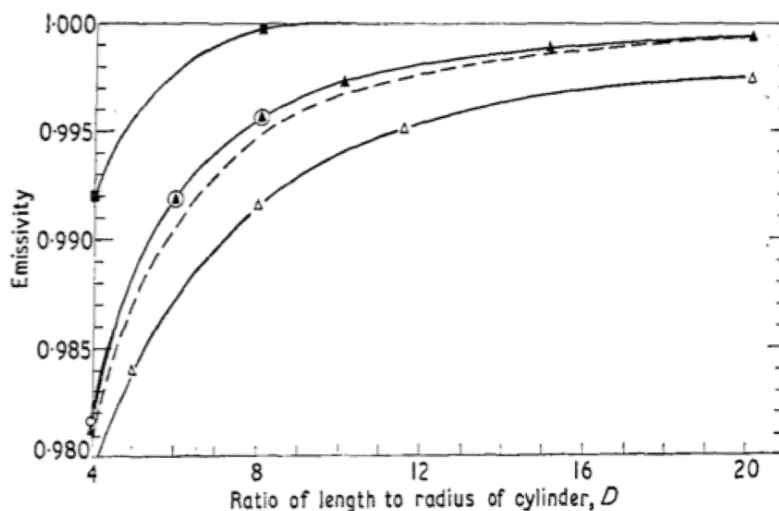


Figure 15: The emissivity of a cylinder with one end open and diffusely reflecting walls of emissivity 0.75, calculated according to Buckley (squares), Quinn (closed triangles) Sparrow (circles) and Gouffé (open triangles). The broken curve is the emissivity of a sphere having similar walls whose ratio of diameter to radius of aperture equals  $D$ . [Berry 1981]

This optical efficiency requires the correct match of the following parameters to the characteristics of the solar furnace, dish or central point receiver:

- Spectral absorbance of the coating matches the spectra transmitted.
- Aperture versus depth ratio matches the shape of the incoming concentrated solar beam.

The shape of the incoming solar beam will suggest either using cylindrical or conical cavities, and the shape of the bottom of cylindrical cavities. Usage of grooves is also possible.

The apparent absorptivity of the calorimeter should then be calculated for each shape of the incoming solar beam, for example ideally individually for each heliostat, or at least for group of heliostats having similar contribution at the measured location.

### **Wall losses**

The typical second error term is due to the thermal insulation of the calorimeter. The thermal balance of the calorimeter has to be evaluated: how much of the absorbed radiative heat is transferred to the fluid and how much is lost to the surroundings.

The insulation of the external parts of the calorimeter and especially the front flange has to be adapted to the environmental conditions such as ambient temperature and wind (convection losses).

### **Cavity convection losses**

Depending on the cavity size, orientation (opening on top or side), internal wall temperature, convection losses due to the air from inside should be accounted, such investigated as in [Perez 2006]. Typical tools are CFD simulation software such as FLUENT.

### *Sensors uncertainties*

The temperature and flow measurements uncertainties have to be evaluated in classic state of the art ways: true fluid temperature vs. measured temperature of the sensor, flow stability, other usual acquisition uncertainties.

### **Calorimeter inertia**

Calorimeters are not immediate sensors: the water flow takes a few seconds to travel through the device, and stabilization of temperature depends on the thermal inertia of the wetted materials. This should be taken into consideration: basically, if the solar furnace conditions are not stable enough (clouds, wind changing the aerosols, tracking errors of the heliostats...), calorimeters should not be used.

An investigation of the response time of calorimeter is presented in [Soscia 1990]. The thermal inertia of the calorimeter leads to required warm up time in order to stabilize the calorimeter to the environment and cold fluid temperature.

For example, in summer where room temperature is about 20 °C and cold water temperature is about 15 °C, the CNRS SolCal 20 requires 10 to 30 minutes before stabilization of the  $\Delta T$  in idle conditions, depending on the flow rate used: high flow rate leads to fast warm up and short response time, but also to small  $\Delta T$  at a given solar power.

## Aperture geometry

If the calorimeter is used to get a local evaluation of the flux density, the geometric aperture real characteristics must be determined with adequate performance. Photogrammetric methods can be used with a high-resolution camera spatially calibrated. For example small dents on the aperture can matter for centimeter sized apertures.

### *General recommendations*

- Insulate generously the body of the calorimeter to limit thermal losses
- Design the cavity with a generous depth to aperture ratio to limit reflection losses
- Use matte black paint inside the cavity, check its ageing to limit reflection losses
- Use plastic pipes for the water piping to limit conduction losses
- Use short wires of small diameter for the temperature probes to limit conduction losses and achieve high resistance
- Wait for thermal stabilization of the calorimeter body before actual measurements to limit drift of the measures
- Use a close loop distilled water circuit to know the properties of the working fluid and have stable flow and pressure conditions
- Calibrate the temperature probes for both absolute measurement and  $\Delta T$  measurement

### *References*

*J. Kaluza and A. Neumann (2001): Comparative measurements of different Solar flux gauge types, Journal of Solar Engineering, vol. 123, no3, pp. 251-255.*

*A. Neumann and C. Willsch, SolLab Radiometer Intercomparison Campaign 2006 Cologne, DLR Report.*

*J. M. Kendall(1971): Primary absolute radiometer, U.S. Patent No. 3,601,611, 24 Aug. 1971*  
<http://www.google.fr/patents/US3601611>

*C.A. Pérez-Rábago, M.J. Marcos, M. Romero, C.A. Estrada (2006): Heat transfer in a conical cavity calorimeter for measuring thermal power of a point focus concentrator, Solar Energy, Volume 80, Issue 11, November 2006, Pages 1434-1442, ISSN 0038-092X,*  
<http://dx.doi.org/10.1016/j.solener.2006.03.006>.

*M. Tanaka, G. Girard, R. Davis, A. Peuto, A. and N. Bignell(2001): Recommended table for the density of water between 0 °C and 40 °C based on recent experimental reports, Metrologia 38, 301.*

*IAPWS (2009): Revised Release on the IAPWS Formulation 1995 for the Thermodynamic Properties of Ordinary Water Substance for General and Scientific Use.*

J. Ballestrín, M. Rodríguez-Alonso, J. Rodríguez, I. Cañadas, F. J. Barbero, L. W. Langley and A. Barnes (2006):, *Calibration of high-heat-flux sensors in a solar furnace*, *Metrologia*, Volume 43, Issue 6, pp 495.

O. Alcayaga (1977) : *Contribution à l'étude de la répartition de densité de flux énergétique dans l'espace focal d'un système concentrateur de rayonnement solaire*. PhD thesis, University of Poitiers, France.

K. H. Berry (1981): *Emissivity of a cylindrical black-body cavity with a re-entrant cone and face*, *J. Phys. E: Sci. Instrum.*, Vol. 14.

A. Ono (1980): *Calculation of the directional emissivities of cavities by the Monte Carlo method*, *Journal of Optical Society of America*, Vol. 70, Issue 5, pp. 547-554.

V. I. Sapritsky and A. V. Prokhorov (1992): *Calculation of the Effective Emissivities of Specular-Diffuse Cavities by the Monte Carlo Method*, *Metrologia* 29, doi:10.1088/0026-1394/29/1/003

A. Ono (1986): *Evaluation of the Effective Emissivity of Reference Sources for the Radiometric Emissivity Measurements*, *International Journal of Thermophysics*, Vol. 7, No. 2, pp. 443-453.

R. David (2006): *A Liquid-in-Glass Thermometer with Sub-MicroKelvin Resolution, and its Application for Calorimetry*, PhD thesis , Massachusetts Institute of Technology, Dept. of Mechanical Engineering, <http://hdl.handle.net/1721.1/38223>.

D. Radu A. S. Guerra C. Ionita and I. Astefanoaei (2010): *Heat loss through connecting thermistor wires in a three-body graphite calorimeter*, *Metrologia* 47 179.

U. Groer and A. Neumann (1999): *Development and test of a high flux calorimeter at DLR Cologne*, *Phys. IV France* 9, p 643.

M. Socia (1990) : *Calorimétrie laser: mesure de fortes puissances laser*, *Bulletin du Bureau national de métrologie*, no82, pp. 9-15.

## 13. Shape Measurement

Mirror panels of various geometries (size, shape, curvature) are used in concentrating solar technologies to reflect sunlight onto the specific receiver areas. In order to reach high optical efficiency values the reflectance of the mirrors must be high and the geometry of the reflector surface and the relative position of the absorber have to be precise. This refers in particular to the shape of the mirrors. The shape and relative orientation of the mirror used for concentrating the sunlight onto the receiver determines how much of the specularly reflected beam radiation hits the receiver. This fraction is denominated the “intercept factor” (IC). The intercept factor depends on the reflector geometry as well as on geometric parameters of the receiver (size, relative position) and on sun position and tracking system.

There are several approaches to determine the shape accuracy of mirror panels. Objective of all measurement methods is the acquisition of information about the deviation of the mirror slope from the ideal shape. If the measurement includes a mapping of the information over the mirror surface, it can be used for quality control and optimization of the mirrors. In previous works performed at different institutions active in CSP development, the surface slope has been measured with various strategies and technologies. Common techniques can be catalogued as:

- **Laser-scanner:** a laser beam is sent to a point of the facet surface; the reflected beam is intercepted by a screen; the partial derivatives  $\partial z/\partial x$  and  $\partial z/\partial y$  in the reflecting point are evaluated by trigonometry. The procedure is repeated on a suitable number of points homogeneously distributed on the facet surface (exemplary applications VSHOT, Optical Profilometer).
- **Deflectometry or fringe reflection:** The reflective surface is positioned so that it views the reflection of a target. A series of fringe patterns with different phase and pattern orientation is displayed on the target while images are captured of the reflected and distorted patterns. Using the captured information, digital image processing calculates the local normal vectors of the mirror surface and the according deviation to the ideal normal vectors (exemplary application QDec).
- **Reverse analysis:** the image of a linear object put in the focal line is observed in the near-field from a number of points distributed along the parabola abscissa. The shape deviation from the ideal parabolic profile is inferred from the object-image displacement from the theoretical one (exemplary applications VIS, TARMES)
- **3D point measurements:** photogrammetry is the fastest implementation of this approach.

### *General Considerations for all Shape Measurements*

#### **Measurement Accuracy**

The accuracy of the applied procedure should be checked either by:

- measuring a reference mirror with known surface properties. This can be a curved mirror with known surface slope (calibrated e.g. by mechanical high precision measurement system), or

- measuring the evenness of a water surface, or
- cross-checking with another independent measurement method with known measurement accuracy.

The measurement accuracy has to be stated for local evaluation values as well as for root mean square values.

### Measurement Boundary Conditions

The following boundary conditions greatly affect the final results and should be carefully documented:

- **Type of support frame for facet mounting:** Generally, facets are not perfectly rigid and their shape depends on the way they are mounted. Therefore, during the measurement the facet must be mounted to a rigid supporting structure. Any element of the supporting structure, potentially affecting the final position and shape of the facet, must be adjusted accurately enough to not downgrade the instrument accuracy.
- **Fixation to the support frame** (i.e. if the sample is fixed with screws to the support frame or not): In case of angular deviation of the mounting pads a significant difference in shape accuracy might occur. Since the facets are screwed to the collector structure in field, a laboratory measurement with tightened screws is to be preferred.
- **Aim angle or set up orientation:** Analogously, also the gravity may induce shape-deformations. For a better comparison of the results achieved with different set-ups, the aim angle of the parabola axis for the adopted configuration must be clearly reported. For the measurement of parabolic trough mirror panels either a vertical or a horizontal orientation is to be preferred.
- **Room temperature**

### Documentation of the Measurement Results

First of all, the descriptive characteristics of the investigated facet as listed in Table 1 have to be collected, and included in the final measurement report.

*Table 1: Descriptive characteristics of parabolic trough collector facets*

	Description of characteristic	Example/clarification
<b>Technology</b>	main characteristic of the adopted manufacturing technology	back silvered glass, 4mm thick
<b>Dimensions</b>	physical/nominal area area intercepting radiation	
<b>Typology</b>	depending of the technology, the single facet may the whole (P/1), one half (P/2) or one quarter (P/4) of the parabola aperture	inner or outer type facets

<b>Coupling</b>	coupling of facets to the supporting structure	by screwing in pad glued on the mirror back  reference frame to describe the ideal parabola according the canonical equation
<b>Cartesian coordinates of mounting points</b>	coordinate system, coordinates	$z = \frac{1}{4f} x^2$ with origin set to align one of the two facet curve-edges with $y=0$

In the final report, the local values (graphical representation), mean, root mean square (rms) and peak-to-valley values of the following parameters must be reported:.

- **slope deviation:** deviation of the facet-surface from the ideal shape expressed as the arctangent of the partial derivatives  $\partial z/\partial x$  and  $\partial z/\partial y$ , and, if available, of  $z$  (HD).
- **focus deviation:** distance between the reflected solar-beam and the focal line, FD and if available MFD.
- **intercept factor** - ratio of solar radiation reflected towards the receiver and geometrically captured by it. In the case an intercept factor is given all assumptions for its calculation have to be stated (i.e. sun shape, further collector errors).

Because of the high relevance, graphs of the mean value of the FD, MFD and IF versus the angle of incidence (in perfect tracking) should be reported as well as graphs showing their behavior versus tracking error at least for normal incidence of the solar radiation with the rotation axis of the collector.

Furthermore, the final report must document the following **evaluation boundary conditions**:

- Measurement method
- Sampling density or spatial resolution of local values
- Measured surface area
- Maximum neglected rim of measurement sample
- Accuracy of measurement method

### 13.1. 3D shape measurement using a laser-scanner

#### *Description of method*

Only two instruments belong to the laser-scanner class: VSHOT and the Optical Profilometer. These kinds of instruments are very accurate, but the measurement is quite time-consuming. As matter of

fact only one point is measured at time, and between two measurements the laser must be properly aimed.

Figure 16 shows the sketch of the Optical Profilometer in the parabolic-trough version.

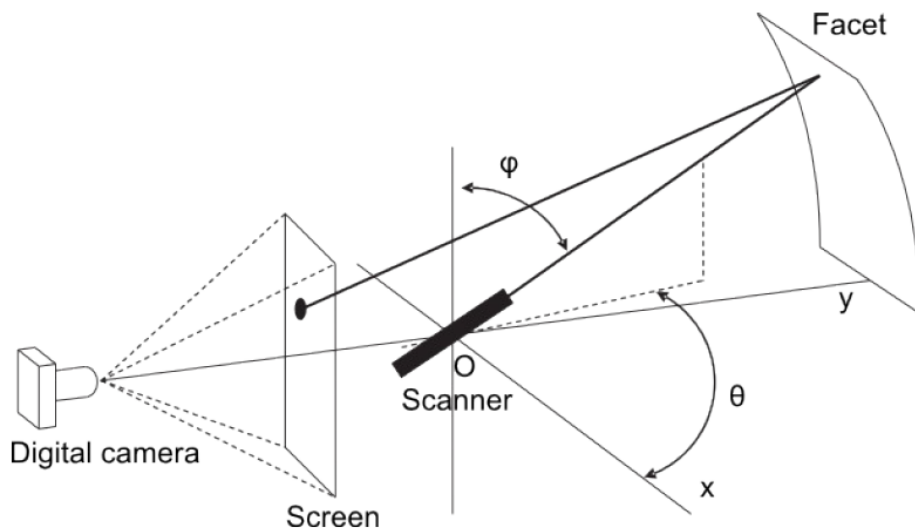


*Figure 16: Sketch of the Optical profilometer.*

The main component of the optical profilometer is the scanner, consisting of a HeNe laser and two high precision rotation stages. The mechanical support design ensures the light beam passing through the O point, the intersection point of the two orthogonal rotation axes. In this way, the two rotation stages allow the laser beam to be precisely directed everywhere in the solid angle according to the angles of the polar spherical coordinates in the laboratory reference centered in O.

The laser beam is aimed at a point of the facet; the reflected beam is captured by the screen; a digital camera captures the image of the screen. The coordinates of the spot S on the screen can be automatically evaluated provided the image was previously calibrated. For this purpose the laser is directly aimed at one of the points composing an ideal calibration grid, taking the picture of the screen and then processing the image. Both real and pixel coordinates of each calibration point are stored in a file that successively allows the conversion of the pixel coordinate to real world coordinates for any other point of a new image.

Laser-scanner, screen and camera are firmly mounted on a stiff structure; a couple of motorized rails allows to move the system along the x axis, and investigating a different vertical section of the facet.

The normal in the investigated point P of the facet surface is evaluated on the basis of the knowledge of the coordinates of the three points O, P, and S; initially the height in P is set at the value of the ideal parabola. The normal is computed over the all sampled points. Then more refined values of the height are obtained by integrating the partial derivative starting from one point where it is known (as an example a point over one of the fixing point of the facet); then the procedure is repeated until the successful convergence of z at any point.

### *Specifications for equipment to be used*

- HeNe laser with high stability point
- two high precision rotation stages
- sand-blast glass screen
- high resolution camera
- two motorized rails (only for parabolic-trough facets)

### *Main error sources and expected accuracy*

The method requires aligning/placing the set-up components with high accuracy, including the position of the supporting frame; any error affects the final results.

High deviation (HD) accuracy: < 0.02 mm

Slope deviation (SD) accuracy: < 0.015 mrad

### *Literature*

*A. Lewandowski, A. Gray (2010): Video Scanning Hartmann Optical Tester (VSHOT) Uncertainty Analysis, Proceedings of the SolarPACES International Symposium, 2010, Perpignan, France.*

*A. Maccari and M. Montecchi (2007): An optical profilometer for the characterisation of parabolic trough solar concentrators, Solar Energy, vol. 81, no. 2, pp. 185–194.*

## **13.2. Estimation of slope deviations of CSP reflectors using deflectometric methods**

### *Description of method*

Deflectometry is a digital photographic measurement technology with image analysis of the reflected image of a pattern taken by a high resolution camera. Main advantage of deflectometry as opposed to other methods is a high spatial resolution and fast measurement. The technique is also applied in other fields of application of surface analysis in quality control. No preparation of the sample other than cleaning is required. Dimming of surrounding light sources might be required for reliable measurements. By digital image processing local normal vectors of the mirror surface are calculated from the reflected patterns in the photos.

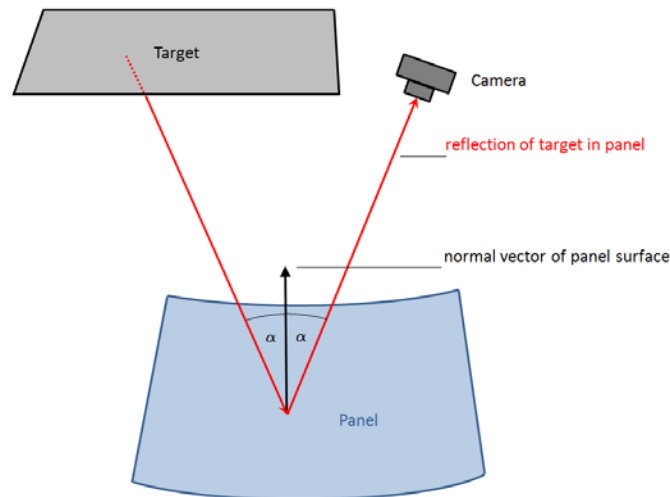


*Figure 17: Measurement principle of a deflectometric shape measurement*

There are different approaches to obtain the know pattern. The first one uses sinusoidal patterns of different phase and frequency projected on a white diffuse reflecting surface mounted above the mirror (set up see Figure 17). This method is used for all types of concentrators (heliostats, PTC modules and mirror panels and parabolic dish concentrators). Another approach for the qualification of transverse slope errors of parabolic troughs is called TARMES [13]. Here, the reflex image of the absorber tube edges is used to calculate local slope deviations. An images series with different perspectives is necessary to obtain sufficient information across the complete mirror surface.

### *Specifications for equipment to be used*

#### **Deflectometry**

- Digital SLR camera for Target Images
- Digital SLR camera for mirror Images
- White Lambertian (diffuse reflecting) target with sufficient size and position
- Projector to create patterns on target
- Supporting device for mirror/concentrator
- Device to accurately (< 0.3 mm) measure the relative positions of target, mirror and mirror camera (e.g. total station)
- Closed workshop to avoid disturbing daylight, alternatively outdoor measurements after sunset

#### **TARMES**

- Digital SLR camera for mirror images
- Device to measure the distance between camera and parabola vertex (e.g. Laser Distometer)

- Device to measure the current elevation angle of the collector for each image (e.g. Inclinometer)

### **Sensor calibration issues**

The camera distortion must be determined to enable a proper ortho-image creation from the raw images. The relative position of the involved components must be fix and known with superior accuracy (< 0.3 mm). The mirror must be cleaned before the measurement.

### **Main error sources and expected accuracy**

If the Sensor calibration issues are fulfilled, the expected measurement accuracies are:

Deflectometry local measurement accuracy:	< 0.5 mrad
Deflectometry global measurement accuracy:	< 0.2 mrad
TARMES local measurement accuracy:	< 1 mrad
TARMES global measurement accuracy (RMS error on SCE module level):	0.1 mrad

### **Recommendations**

none

### **Literature**

*T. März, C. Prah, et al. (2011): Validation of Two Optical Measurement Methods for the Qualification of the Shape Accuracy of Mirror Panels for Concentrating Solar Systems, Journal of Solar Energy Engineering 133: 031022.*

*S. Ulmer, T. März, et al. (2011): Automated high resolution measurement of heliostat slope errors. Solar Energy 85: 681-687.*

*S. Ulmer. et al. (2009): Slope Error Measurements of Parabolic Troughs Using the Reflected Image of the Absorber Tube. Journal of Solar Energy Engineering, Vol. 131, No. 1.*

*C. Prah, et al (2013): Airborne shape measurement of parabolic trough collector fields. Solar Energy, Volume 91, May 2013, Pages 68-78 Solar Energy 85: 681-687.*

## **13.3. Geometric analysis of solar concentrators with close range photogrammetry**

### **Description of method**

Because of its accuracy and flexibility, close-range-photogrammetry has been used as a qualification tool for CSP concentrator structures for both prototypes as well as for on-line quality assurance in production. Photogrammetry is appropriate especially for the measurement of the collector structure without mirrors, whereas complete collectors with mirror are rather measured by deflectometric approaches. Photogrammetry allows measuring the position of the mirror surface

relative to the focal line and the axis of rotation. Furthermore, a precise and high-resolution deformation analysis between different tracking positions and load conditions is possible.

The object of interest needs to be prepared for the measurement by applying target markers to the points of interest. The markers are recognized in a series of digital images of the object by photogrammetric evaluation software. That way, precise 3D coordinates of the points of interest are calculated from 2D image information, while the number and perspectives of the images must follow a certain system to obtain precise and reliable results.

An important step in the evaluation of CSP concentrator structures with close range photogrammetry is the post-processing. In this step, the arbitrary orientated 3D coordinates from the photogrammetric evaluation need to be transformed into the reference system of the design data and deviations between design and measured coordinates are calculated, graphically presented and compared to tolerance values.

### *Specifications for equipment to be used*

- High End digital single-lens-reflex camera with fix focal length (approx. 20 mm ) lens and a resolution > 12 megapixel
- Reference cross
- Self-adhesive circular targets to highlight the points of interest. For outdoor and daylight measurements, retro-reflective targets are recommended
- Ring flash if retro-reflective targets are used
- Scale bars to check and calibrate the 3D coordinates

### *Sensor calibration issues*

As the sensors of photogrammetric measurements are the camera and the target markers, calibration or accuracy issues should take into account their properties. Moreover, the selected perspectives and the target density have a significant influence on the measurement accuracy.

It is recommended to calibrate the camera during the evaluation which means that the distortion parameters of the cameras are calculated during the bundle adjustment.

The only way to independently check the measurement accuracy is to compare known distances of some selected targets to the distances returned by the bundle adjustment. With a proper setup, deviations of these distances in all dimensions should be below 0.5 mm on a length of 10 m.

### *Main error sources and expected accuracy/precision*

Main error source are:

- Insufficient number of images
- Insufficient target density

- Mechanical unstable camera (motion between lens and body)
- Bad contrast and sharpness of the images

Following good measurement practice measurement accuracies in the range of 0.5mm are achievable.

### *Recommendations*

The points of interest of a parabolic trough are usually the mirror surface, especially the mirror mounting points. In addition, the axis of rotation at both ends of the collector module and the absorber tube position are important.

The axis of rotation is mainly measured to define the Y-axis of the coordinate system and to enable a proper translation into the design data coordinate system.

Where points of interest are not directly accessible (e.g. Axis of rotation and absorber tube center), the (tube-) circumference can be measured by a sufficient number of targets, and the center may then be found by circle fit to these points.

### *Literature*

*T. Luhmann, S. Robson, S. Kyle, I. Harley (2006): Close Range Photogrammetry: Principles, Methods and Applications. (1st ed. ed.). Whittles: UK. ISBN: 1-870325-50-8.*

*K. Pottler et al. (2005): Photogrammetry: A Powerful Tool for Geometric Analysis of Solar Concentrators and Their Components. Journal of Solar Energy Engineering, Vol. 127(1), 94-101.*

*Roca-Pardinas et al. (2013): Validating a parabolic solar collector using close range photogrammetry. The Photogrammetric Record 28(142): 211-226 (June 2013), DOI: 10.1111/phor.12024.*

*M. R. Shortis, G.H.G. Johnston, K. Pottler, E. Lüpfer, (2008): Photogrammetric analysis of solar collectors. International Archives of Photogrammetry, Remote Sensing and Spatial Information Sciences, 37(5): 81-87.*

*E. Lüpfer, M. Geyer, W. Schiel, A. Esteban, R. Osuna, E. Zarza, P. Nava (2001): EuroTrough design issues and prototype testing at PSA. Proceedings of Solar Forum 2001. Solar Energy: The Power to Choose, Washington, DC, USA. 389-393.*

*E. Lüpfer, K. Pottler, S. Ulmer, K.-J. Riffelmann, A. Neumann, B. Schiricke, B. (2007): Parabolic trough optical performance analysis techniques. Journal of Solar Energy Engineering, 129(2): 147-152.*

*S. Garcia-Cortest, A. Bello-Garcia, C. Ordonez, (2012). Estimating intercept factor of a parabolic solar trough collector with new supporting structure using off-the-shelf photogrammetric equipment. Applied Energy. 92: 815-821.*

### 13.4. 3D shape analysis by reverse analysis: VISprofile

#### *Description of method*

A successful implementation of the reverse analysis approach is represented by the VISprofile set-up. Its main strengths are: superior accuracy, compactness and hardware simplicity.

The method is based on putting a suitable light source in/close to the focus and viewing the source image reflected by the facet at a number of different positions. Depending on the facet typology (long/short radius of curvature, double curvature or parabolic trough), light source and distribution of observation positions are set accordingly. Figure 18 shows the VISprofile arrangement to measure parabolic-trough facets, composed of

- linear array of point light sources
- camera, and
- motorized linear guide rail,

All these components must be conveniently aligned with respect to the facet [Montecchi et al. 2011]. The source array is placed along the nominal focus line of the parabolic-trough facet under test; in this manner, for perfectly parabolic-shaped reflectors, the observer  $C$  sees the point-source images, aligned across the panel width (in the flat direction,  $y$  axis), at his own abscissa, i.e.  $x = x_C$ . Otherwise, shape imperfections in the curved direction ( $x$  axis) result in displacement of the point-source images from  $x_C$ .

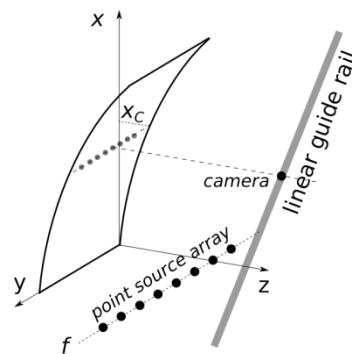


Figure 18 VISprofile sketch

The camera is installed on the motorized linear guide rail placed centrally in front of the specimen. The scan consists of capturing a number of frames varying the camera abscissa, so that during the scan the observed point-source-images span the whole facet-surface, from one linear edge to the opposite one. In summary, the surface is evaluated as follows:

Let  $S = (x_S, y_S, z_S)$  be a point light source with the image in  $P = (x, y, z)$  according to the observer  $C = (x_C, y_C, z_C)$ . The coordinates  $(x, y)$  are determined by referring the image to the facet width  $L$ , camera abscissa  $x_C$  and camera aiming;  $z$  is first set to that of the ideal parabola. Then, as shown in Figure 19, the normal to the surface in  $P$  is given by

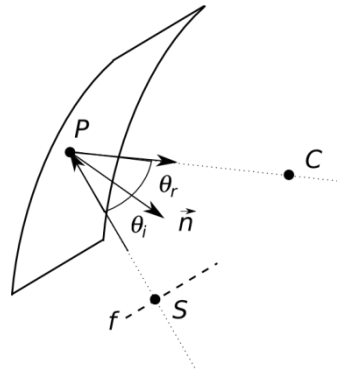


Figure 19: The observer  $C$  sees the point light source  $S$  imaged in  $P$  of the parabolic-trough facet-surface; position and normal to the surface in  $P$  have to fulfil the two reflection laws

$$-\vec{SP} + \vec{PC} \propto \vec{n}$$

where all the vectors are unit vectors, and  $\vec{n}$  is normal to the facet surface in  $P$ . It is easy to verify the relationship between  $\vec{n}$  and the partial derivatives of the surface in  $P$ :

$$\vec{n} \propto \left( \frac{\partial z}{\partial x}, \frac{\partial z}{\partial y}, -1 \right)$$

The normal is computed over the all sampled points, and a more refined  $z$  value is obtained by integrating the partial derivative starting from one point where  $z$  is known (as an example a point over one of the fixing point of the facet); then the procedure is repeated until the successful convergence of  $z$  at any point.

The advantages of the VISprofile lie in its high accuracy, limited dimensions and height ( $z$ ) evaluation.

### *Specifications for equipment to be used*

The method requires

- Linear array of point light sources (see [refVISprofile] for an easy and cheap manufacturing)
- High resolution high frame-rate camera equipped with low distortion objective
- Motorized linear rail with low yaw-pitch-roll
- Device to accurately ( $< 0.3$  mm) measure the positions of point source, support-frame for mirror and camera (e.g. total station)

### *Main error sources and expected precision*

The method requires aligning/placing the set-up components with high accuracy, including the position of the supporting frame; any error affect the final results.

Yaw-pitch-roll of the camera along the motorized rail if present must be properly corrected via software

The camera should be equipped with a low distortion objective. If image deformation occurs, it must be corrected via software.

High deviation (HD) accuracy: < 0.05 mm

Slope deviation (SD) accuracy: < 0.02 mrad

### *Recommendations*

None

### *References*

*A. Maccari, M. Montecchi (2007): An optical profilometer for the characterisation of parabolic trough solar concentrators, Solar Energy 81, 185-194.*

*M. Montecchi, A. Benetti and G. Cara (2011): Fast 3D Optical-Profilometer for the Shape Accuracy Control of Parabolic Trough Facets, SolarRACES International Symposium, Granada, Spain.*

## 14. Canting and alignment of CSP concentrators

### 14.1. General procedure

#### *Description of method*

The terms canting and alignment refer to the followings task during the assembly of concentrators and solar fields:

**Canting** is the orientation of single (pre-shaped) mirror panels within a single collector module (parabolic trough SCE or single heliostat). The quality of the canting depends on the position and orientation of the mirror mounting points of the collector structure. Since most collector (steel-) structures are mounted on a precisely erected jig, there is neither a need nor a possibility to improve the collector canting after commissioning.

**Alignment** is the relative orientation of different parabolic trough modules (SCEs) when the SCA is assembled. The goal of that process is, that the optical axis of all SCEs of one SCA point in the same direction with deviations smaller than  $0.1^\circ$ .

#### *Specifications for equipment to be used*

##### **Canting**

###### During collector assembly

It is recommended that heliostats and parabolic troughs be assembled on precisely erected mounting jigs. That way, the position and orientation of the mirror mounting points can be assured. The first concentrators as well as the jig should be checked during startup of the production by means of close range photogrammetry.

###### After commissioning in the solar field

Possible canting errors can be derived from shape measurements (close range photogrammetry, deflectometry or similar) or detected investigation of the flux spot of heliostats. If the concentrator structure allows for correcting the mirror mounting point positions, the shape can be optimized iteratively.

##### **Alignment**

For the alignment of parabolic trough collector modules, a reference line perpendicular to the optical axis (so called water level) is needed. This line virtual line can also be derived from the outer mirror edges. As SCA assembly takes place in zenith position, the orientation of the modules during assembly must be checked with inclinometers. Deviations of the water level from the horizon up to  $0.1^\circ$  can be tolerated.

#### *Literature*

*R. Top, B. Diver, T. A. Moss (2007): Practical Field Alignment of Parabolic Trough Solar Concentrators, Journal of Solar Energy Engineering, Vol. 129, 2007*

C. Andraka et al. (2011): AIMFAST: An Alignment Tool Based on Fringe Reflection Methods Applied To Dish Concentrators, J. Sol. Energy Eng. Vol. 133, Issue 3, 031018.

## 14.2. Check of the mutual optical alignment of receiver and concentrator in the field by reverse analysis (VISfield)

In field, the receiver itself can be used instead of a light source in a reverse analysis process. For a section of an ideal parabolic trough concentrator shown in **Fehler! Verweisquelle konnte nicht gefunden werden.** and the ray  $r$  parallel to the parabola axes;  $r$  crosses the point  $V$ , hits the parabola in  $P$ , is reflected towards the focus  $F$  and finally hits the HCE in  $R$ , which is aligned with the points  $P$  and  $F$ . Conversely (by reversing ray propagation), the ray emitted by  $R$  towards  $P$ , follows the same above described path and crosses the point  $V$ . An observer in  $V$  sees the image of the HCE spread between  $x_{\min}$  and  $x_{\max}$ , and in particular the point  $R$  imaged in  $x_v$  (the abscissa of  $V$ ). All rays emitted from any other point of the HCE and reflected in  $P$  do not reach  $V$ . When increasing the distance of  $V$  from the parabola to capture the far field image of the collector, it is clear that the ray  $r$  is very special because is the sole ray determining the far field image of  $P$ .

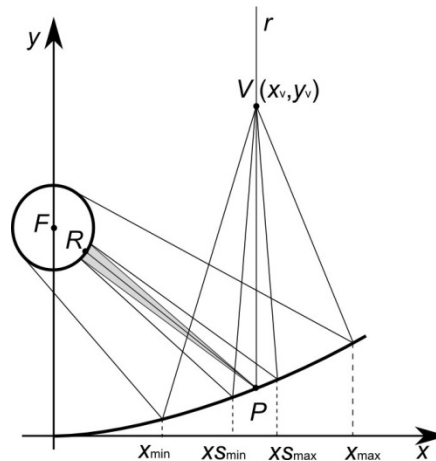


Figure 20: Reflected image of HCE observed from the view point  $V$ . A hypothetical solar spot of the solar radiation that would be reflected by  $P$  will appear spread in the HCE image between  $x_{s_{\min}}$  and  $x_{s_{\max}}$ .

Anyway, for the actual purpose the important concept is that the point of the HCE whose image is sight with  $x_v$  corresponds to the spot-centre of the solar-radiation that would be reflected by  $P$  and intercepted by the HCE in perfect-tracking condition; the spot-radius is  $s = FP \tan(\alpha)$ , with  $FP$  as optical path length between  $P$  and the HCE (as matter of fact, the HCE radius is much smaller than the focal length, then  $RP \approx FP$ ),  $\alpha$  is the half-angle of the cone across which the solar radiation is spread. From  $V$ , that hypothetical solar-spot will appear spread in the HCE image between  $x_{s_{\min}}$  and  $x_{s_{\max}}$ . As well  $x_{\min}$  and  $x_{\max}$ ,  $x_{s_{\min}}$  and  $x_{s_{\max}}$  can be determined by imposing the respect of the second law of reflection.

If for some reason the slope in  $P$  deviates from that of the ideal-parabola by  $\delta$  radians. The effect observed from  $V$  is the shift of the HCE image along the x-axis of about  $2M\delta FP$ . Where  $M$  is the image magnification,  $(x_{\max} - x_{\min})/2r$ ; this results is easily understood considering that due to the slope variation, the inclination of the reflected ray increases by  $2\delta$ , and consequently the impact point on the section of the HCE is shifted for  $2\delta FP$ ; on the other hand, by the principle of ray reversibility, the

image of the impact point remain sight with  $x_v$ , then the HCE image has to shift by  $2M\delta FP$ . A similar effect is caused also by deviation of the  $P$  ordinate, but at the typical values observed for good quality facet-mirror, about 1 mm, the amplitude is much less and therefore neglected.

The above considerations allow to get quantitative information about slope-deviation and local IF value (i.e. concerning the point  $P$  of the mirror) by the analysis of the position of the HCE image: Be  $\Delta$  the image shift, the slope deviation is  $\delta = \Delta / 2MFP$ , and with good approximation the local IF is given by the portion of the range ( $x_{S_{min}} x_{S_{max}}$ ) appearing superimposed to the HCE image. As an example Fig. x4 shows the frontal view of an experimental spare module 12 m long, oriented towards the horizon, from  $V$  in  $x_v = 1.5$  m and about  $y_v = 13$  m. In the picture the lines corresponding to  $x_{min}$ ,  $x_{max}$ ,  $x_{S_{min}}$  and  $x_{S_{max}}$  are also drawn. The lower half of the parabolic-trough is composed by ten facets only one of which only is correctly aligned, as shown by the position of the HCE image with respect to the expected position. All other facets should be adjusted for the reduction of the slope of about 19 mrad, being  $\Delta \approx M 2 r$  and  $FP = 1810$  mm. Considering the region delimited by  $x_{S_{min}}$  and  $x_{S_{max}}$ , the local IF along  $x_v$  is 1 through the correctly aligned facet and 0 elsewhere.

In order to get the most complete information, this analysis has to be repeated on a set of frames captured from different observation points, with  $x_v$  spanning the x-axis from the vertex to the external parabola border; the optimal step between one frame and the following is the digital resolution of the parabola surface, that is the side of the pixel-image. With this criterion the number of frames to be captured is some hundreds.

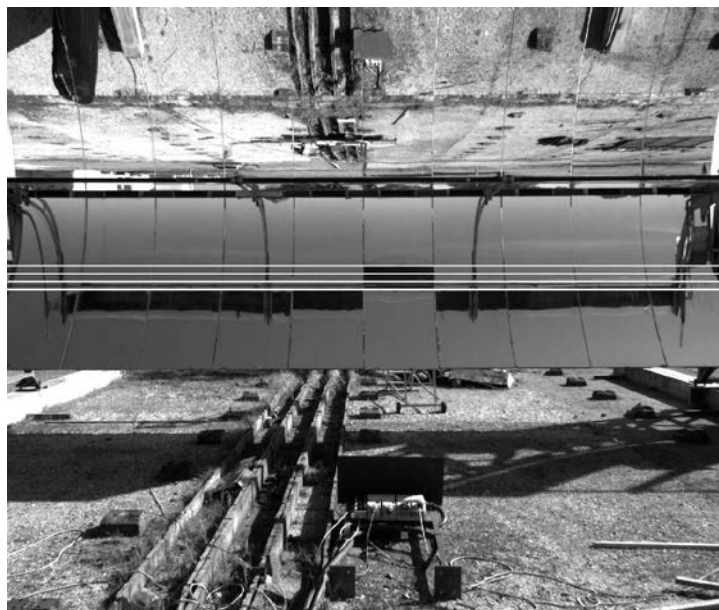


*Figure 21: Front view of an experimental spare module 12 m long, oriented towards the horizon, from in  $x_v = 1.5$  m and  $y_v = 13$  m about; from the top to the bottom the lines correspond to  $x_{min}$ ,  $x_{S_{min}}$ ,  $x_{S_{max}}$  and  $x_{max}$ .*

The VISfield allows to directly measure the actual intercept factor of one whole module at time. For this purpose the module must be precisely aimed at the horizon. A laser level, combined with the camera, allows finding, in the image, the reference line which is parallel to the rotation axis of the

module, and, if any, the off-set angle of the tracking monitor system, as well as aim deviation between different modules belonging to the same collector.

The VISfiled outputs are:

- contour map of the intercept factor,
- mean intercept factor for each facet (that represents the final quality check of facet in field)
- precise indication on how to improve the optical alignment by canting single facets.



Figure 22 shows the first prototype.

*Figure 22: First prototype of the VISfield made by Marposs*

### ***Specifications for equipment to be used***

- High resolution high frame-rate Camera equipped with low distortion objective
- Laser level
- Motorized linear rail with low yaw-pitch-roll installed on a steady platform.

### ***Main error sources and expected precision***

The most important parameter used in processing the sequence of frames is the reference line. It must be parallel to the rotation axis of the module, and its central point must have the same altitude as the camera. It must be set carefully. Because the reference line is unchanged during the camera travel along the motorized rail, yaw-pitch-roll should not cause image displacement greater than the image resolution itself; otherwise a suitable software correction is needed.

Another important parameter is the grey threshold allowing the automatic detection of the receiver image. Dusty mirrors and/or not uniform illumination of the module can require tailoring grey threshold across the module surface.

Concerning the precision of the intercept factor, generally it is better than 1%; larger values were always found due to some actual modification of module and/or facets. As a matter of fact, in field the conditions are never perfectly steady.

The accuracy on module aiming check is better than 1 mrad.

### *Recommendations*

None

## 15. Mechanical testing procedures

### 15.1. Drive backlash ultimate strength

#### *Description of method*

The extent of **existing backlashes in the drive system** is tested by applying a torque strong enough to overcome friction in the system in one direction and measuring the reached angular position. Then, reversing the load, a new measurement of the angular position is performed. The difference between the two positions is equivalent in angular terms to twice the error which can be associated to the system backlashes. It should be mentioned that for most hydraulic parabolic trough tracking systems backlash is not an issue. However, gearbox based electro mechanical tracking system may suffer from increased backlash after some years of operation.

The objective of **ultimate strength tests** is to verify that the drive system is able to withstand, statically, to a load (torque) equal to the design limit.

This evaluation is performed by applying to the system, statically and without inversion, the ultimate torque and verifying that the system is not subject to catastrophic failure.

With **drive tests under high load** the capability of the drive system to rotate the collector even in the presence of a load (torque) of greater magnitude than assumed for its safe positioning can be verified. This evaluation is performed by applying to the system the required torque and verifying that the system is still capable of operating.

### 15.2. Tracking and Torsion of Parabolic Trough Collector Drives

#### *Description of method*

Repeated **tracking and cycling tests under load** aim at checking the accuracy of positioning of the drive system when subjected to a given applied load (torque) at the same time as assessing/performing a sufficiently high number of cycles to verify the durability of the system. The loads must be carefully selected and should represent the conditions met by the system under operations. Static and dynamic loads on the tracking system are (see Figure 23):

- Wind loads
- Static unbalance
- Friction of bearing and flexible tube connectors (e. g. Balljoints)

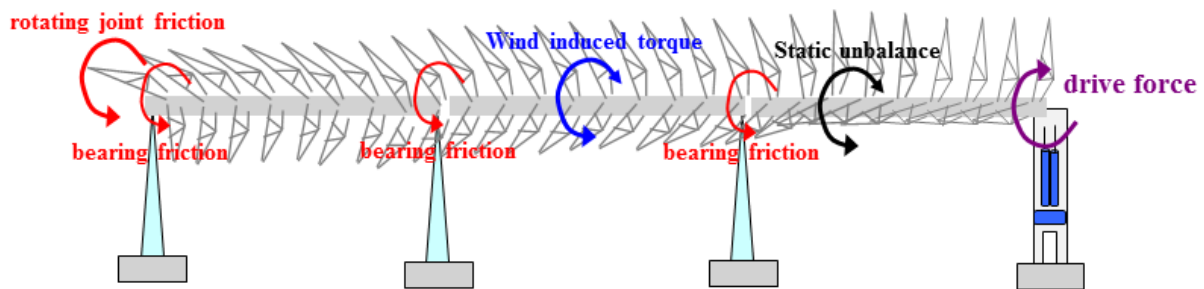


Figure 23: Typical static and dynamic load on parabolic trough tracking systems

Statistical analysis of the measured angular differences provides an estimate of the error which can be associated with the drive system under load. Instead, the performed number of cycles, the system time response and its wear conditions provide information about its durability. Both the positioning error and the durability of the drive system must be within the limits set by the adopted specifications.

The cycling of the drive system over time is obtained through an external device which sends a positioning signal to the drive system so that it follows a predefined path. This path consists of a simple linear variation of the angular position of the testing apparatus from  $-90^\circ$  to  $+90^\circ$ , in the lifting of the masses (loading), and from  $+90^\circ$  to  $-90^\circ$ , in the lowering of the masses (unloading). To assure realistic loads during the cycle test, the previously mentioned contributions (wind, unbalance and friction) should be estimated for a typical site and design and applied to the drive system.

To determine the equivalent work, i.e. the real years of operation simulated by the accelerated tracking, it is possible to assume a use of 1 cycle per day for 365 days per year with a utilization factor of 0.8, from which 292 cycles / year. So in 25 years of plant operation there could be about 7300 cycles.

### 15.3. Concentrator structure tests

The **backlash, flexibility and strength of the concentrator structure tests** aim at verifying the deformability of the reflective surfaces supports when subjected to normal operating loads and its failure resistance when subjected to ultimate loads (e.g. storm).

#### *Description of method*

The procedure to be used for the test strongly depends on the type of support. It should include the following steps:

1. With the system mounted without reflective surfaces, measurement of the correct positioning of the attachment points of the reflective surfaces relative to an appropriate reference system (e.g. by photogrammetry).
2. Measurement of the displacement of the attachment points of the reflective surfaces during the application of a load equivalent to the various principal operating conditions.
3. Verification of the correct behavior of the structure during the application of a load equivalent to the ultimate limit condition.

The test should be repeated on a sufficient number of components.

The objective of **backlash, slackness and stiffness of the receiver supports tests** is to verify the deformability of the receiver support and its mechanical connection to the torque tube/box when subjected to normal operating loads. For both measurements, it is sufficient to measure the relative motion of the receiver support to the outer mirror edge.

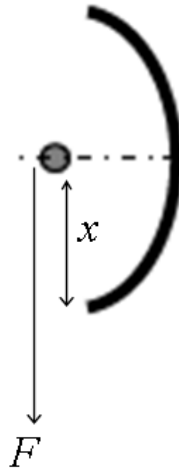


*Figure 24: Illustration of test set-up for backlash/slackness and lateral stiffness testing of parabolic troughs*

The proposed test procedure is as follows (see **Fehler! Verweisquelle konnte nicht gefunden werden.**):

Backlash/slackness:

- Apply an alternating force in x-direction large enough to overcome the dead load of receiver and receiver support. The resulting difference of the x-values measured for up- and downward force can be interpreted as slackness. Pivot based receiver supports may show slackness, while receiver supports based on spring-plates are less prone to lateral slackness

Lateral stiffness:

- Apply an increasing force in x-direction from 0 to approx. 500 N<sup>1</sup>. The resulting lateral deviation can be plotted vs. the applied force. Lateral deviations in this particular force range should not exceed 5 mm. Moreover, no plastic deformation should remain after the test!

---

<sup>1</sup>typical value for collectors with 4 m oil receivers, maximum value depends on the weight of one filled receiver

## 16. Performance Measurement

### 1.1. Thermal Performance Tests for Collector Modules

Thermal performance tests of collector units/modules are a means of assessing the interaction of the different components and its overall capacity to convert incident solar radiation into useful thermal power under specific boundary conditions.

The **total module or collector efficiency** denominates the ratio of useful power to effective solar power incident on the system in quasi steady-state operation. Its value strongly depends on operating conditions and is therefore further refined in designated tests with particular boundary/operating conditions:

**Peak optical efficiency** is determined from performance tests at near perpendicular incidence of solar irradiance on the collector aperture and mean fluid temperature near ambient temperature eliminating both angular dependent effects as well as thermal loss.

**Thermal efficiency** is determined at normal incidence for a range of operating temperatures.

The **Incident Angle Modifier (IAM)** is the ratio of optical efficiency at varying angles of incidence and peak optical efficiency. Consequently, testing requires low fluid temperatures and a sufficiently broad spectrum of incidence angles.

**Thermal losses** are usually measured with shaded collectors or at night time, so that they can be deduced from the temperature drop of the heat transfer fluid.

#### *Description of method*

The thermal collector performance is generally evaluated on the basis of an energy balance. To this end, the useful thermal power of a solar thermal collector unit is determined in short duration steady-state tests under clear sky conditions (stable weather conditions without cloud influences). The useful thermal power  $\dot{Q}_{coll}$  is calculated on the basis of the measured mass flow rate  $\dot{m}$  of the heat transfer fluid, its specific heat capacity  $c_p$  and the measured temperature difference between the fluid inlet and outlet temperatures  $T_{in}$  and  $T_{out}$ :

$$\dot{Q}_{coll} = \dot{m} \cdot c_p \cdot (T_{out} - T_{in})$$

The incident solar power on the collector is defined by the direct normal irradiance ( $DNI$ ), the cosine of the solar incidence angle  $\theta$ , the net collector aperture area  $A$ .

$$\dot{Q}_{in,sun} = DNI \cdot \cos(\theta) \cdot A$$

Wherever possible, it is desirable to carry out performance tests with clean collectors. Otherwise, the cleanliness needs to be measured and a cleanliness correction needs to be included. The mirror cleanliness is calculated as the quotient of the reflectivity of a soiled surface  $\rho_{soiled}$  and that of a perfectly clean surface  $\rho_{clean}$ .

$$\chi = \rho_{soiled} / \rho_{clean}$$

A typical cleanliness correction is multiplication by of the incident solar power by a factor of  $\chi^{3/2}$ . The cleanliness factor exponent accounts for the fact that the sun rays pass the solid glass concentrator surface twice and the receiver glass envelope once. Since the cleanliness of the receiver glass envelope is difficult to measure (curvature of glass envelope and position of receiver), equal soiling compared to the collector surface is assumed.

Typical performance figures characterize the collector in terms of relevant operating parameters/conditions:

General (module) **thermal efficiency** at any angle of incidence or temperature level is described by the quotient of the useful thermal power and the incident solar power

$$\eta_{th} = \dot{Q}_{coll} / \dot{Q}_{in,sun}$$

If the average fluid temperature  $\bar{T}_{HTF} = \frac{T_{in} + T_{out}}{2}$  corresponds to the ambient temperature  $T_{amb}$  thermal losses can be neglected. In this case, the measured efficiency of the collector corresponds to the **optical efficiency**  $\eta_{opt}$  at different angles of incidence.

$$\bar{T}_{HTF} = T_{amb} \Rightarrow \eta_{opt} = \dot{Q}_{coll} / \dot{Q}_{in,sun}$$

For perpendicular incidence of solar radiation (collector with East-West orientation at solar noon or two-axis tracked collector), no incident angle induced losses or cosine loss ( $\cos(\theta) = 1$ ) will occur. Under these conditions, the measurement of the **peak optical efficiency**  $\eta_0$  is possible.

$$\theta = 0 \Rightarrow \eta_0 = \eta_{opt}$$

The decrease in optical efficiency which depends on the incident angle for the solar radiation is described by the **incidence angle modifier** (IAM). An IAM characteristic  $\kappa(\theta)$  can be computed as the quotient of the optical efficiency at different angles of incidence to the optical peak efficiency (see **Fehler! Verweisquelle konnte nicht gefunden werden.**). For perpendicular incidence the IAM is equal to 1 ( $\kappa(0^\circ) = 1$ ).

$$\kappa(\theta) = \eta_{opt}(\theta) / \eta_0$$

Particular care is required when dealing with non-normal incidence testing of relatively short modules (compared to the length of the corresponding fullsize collector) as due to the increasing impact of end losses that need to be corrected for.

If the module/collector is not irradiated by the sun (e.g. at night), the **thermal losses of the unit** can be determined from **Fehler! Verweisquelle konnte nicht gefunden werden.** by observing the temperature drop from collector inlet to collector outlet. However influences like diffuse radiation, long wave atmospheric radiation and other heat/radiation sources should also be considered.

$$P_{loss} = \frac{\dot{Q}_{coll} + \dot{Q}_{rad}}{l} = \frac{\dot{m} \cdot c_p \cdot (T_{out} - T_{in}) + \dot{Q}_{rad}}{l}$$

Similarly to indoor receiver heat loss testing, the receiver heat loss is expressed per unit length.

### *Specifications for equipment to be used*

The determination of the useful heat power and the incident solar power require sensors for

- Mass/volumetric flow rate: Coriolis sensors that directly measure mass flow rate are preferable for high measurement accuracy and precision in flow rate measurement. All other flow meters measure volumetric flow rate that needs to be converted using an (uncertain) fluid density.
- Fluid temperature measurements should be implemented using Pt100 resistance temperature detectors. In direct contact with the medium their response time is reduced but the risk of failure by mechanical wearing is increased. Alternatively, thermowells protecting the sensor elements can be used. In any case, sufficient sensor/thermowell immersion depth is required to eliminate the effect of heat losses along the sensor sheath and the readings of the inlet and outlet sensors should be adjusted by calibration relative to one another.
- Direct normal irradiance is best measured with a high accuracy field pyrheliometer. The cleanliness of the pyrheliometer window during testing must be assured by regular cleaning.

### *Sensor calibration issues*

Thermal performance testing of parabolic trough collector modules among others involves testing a high fluid temperature. Flow meters are typically calibrated at low operating temperatures and therefore, adequate measures (temperature correction, zeroing at operating temperature) must be taken to ensure optimum measurement accuracy at elevated temperatures.

Relative calibration of inlet and outlet temperature sensors (in addition to an absolute calibration) assures high accuracy in temperature difference measurements. These calibrations should include the transmitters and data acquisition unit and can be carried out in a homogeneous fluid flow or using a block calibrator. The resulting significant increase in measurement accuracy is particularly relevant for small temperature differences and thus small test units, heat loss and optical efficiency testing.

Pyrheliometers used for performance testing should be calibrated shortly before testing due to possible sensor drifts. Outdoor pyrheliometer calibration procedures using absolute instruments are preferable to indoor calibration in terms of calibration uncertainty.

### *Main error sources and expected accuracy/precision*

All measured quantities are relevant in terms of uncertainty of performance results. The largest contributions to measurement uncertainty in performance testing are typically due to temperature difference and irradiance measurements and the uncertainty of thermophysical properties of the heat transfer fluid. While the former can be minimized by following the above calibration procedures, the latter result from laboratory characterization of the HTF (i.e. differential scanning calorimetry).

With a good measurement system uncertainties in the range 2-4% percentage points (for 95% coverage probability) can be achieved for optical and thermal performance. The uncertainty of heat

loss measurements is typically higher due to even smaller temperature differences. Furthermore, uncertainty budgets are usually dominated by systematic contributions resulting from calibration and individual sensor characteristics while the repeatability is high. This translates as much higher precision than accuracy of results which needs to be accounted for when deriving performance parameters from test results.

### *Recommendations*

Although cleanliness can be quantified in terms of reflectance, it is recommended to carry out performance tests on as clean collectors as possible. Clean mirrors and glass envelopes are the best reproducible state of the test system. The greater the degree of soiling and the more inhomogeneous the soiling, the more difficult it is to obtain representative values cleanliness from local measurements of reflectance. Thus a cleanliness correction always introduces an additional uncertainty and the impact of the cleanliness correction increases with decreasing values of cleanliness.

The use of the net aperture area is recommended for efficiency evaluation. In order to ensure comparability of results, the reference area used must be stated.

During test operation additional parameters such as wind direction, wind velocity and tracking angle should be monitored and any test peculiarities recorded for later review of the data base. The synchronicity of records is of particular relevance for thermal performance test as data matching is not possible at any later stage of the evaluation.

The size of collector units to be investigated with the steady-state tests described above is restricted by the capacities of available test facilities: Existing two axis tracking platforms can accommodate modules up to a length of 20 m and dissipate thermal power up to 100 kW. Test collectors or loops in turn are less flexible in terms of incidence angle testing and their balances of plant rarely sufficient for maintaining low HTF temperatures required for testing of peak optical efficiency and thermal efficiency tests at low temperature.

### *Literature*

*EN 12975-2(2006): Thermal solar systems and components - Solar collectors – Part 2: Test method.*

*ASTM 905 (2001): Standard Test Method for Determining Thermal Performance of Tracking Concentrating Solar Collectors.*

*E. Lüpfert, U. Herrmann, H. Price, E. Zarza, R. Kistner(2004): Towards Standard Performance Analysis for Parabolic Trough Collector Fields, Proc. 12th SolarPACES Int. Symposium, Oaxaca, Mexico.*

*D. Kearney (2010): Utility-Scale Parabolic Trough Solar Systems: Performance Acceptance Guidelines (April 2009 - December 2010), Tech. Rep. NREL/SR-5500-48895, National Renewable Energy Laboratory, Golden (USA).*

*P. Heller, M. Meyer-Grünefeldt, M. Ebert, N. Janotte, B. Nouri, K. Pottler, C. Prah, W. Reinalter, E. Zarza (2011): KONTAS – A Rotary Test Bench for Standardized Qualification of Parabolic Trough Components . SolarPACES 2011, Granada, Spain*

*N. Janotte, E. Lüpfert, R. Pitz-Paal, K. Pottler, M. Eck, E. Zarza, K.-J. Riffelmann (2010): Influence of Measurement Equipment on the Uncertainty of Performance Data from Test Loops for Concentrating Solar Collectors. Journal of Solar Energy Engineering, Vol: 132, Issue: 3.*

*S. Wilbert, N. Janotte, R. Pitz-Paal, L. van Wely, N. Geuder (2010) Reduced uncertainties of field pyrheliometers through improved sensor calibration. SolarPACES 2010, Perpignan (France).*

## 16.1. Measurement of the receiver heat loss vs. temperature

### *Description of method*

The heat loss of the HCE is typically measured by electrically heating the receiver to operating temperature. At steady state of constant temperature and heating power, heating power is equal to heat loss power.

Typically the heating power is controlled for the temperature of interest. In order to avoid controller oscillations it might be useful to also use periods of constant heating power. Typical temperature steps for oil receivers are 250 °C, 300 °C, 350 °C, and 400 °C. Intermediate temperatures can be calculated using spline interpolation. Result of the test is heat loss of the receiver in W or length specific heat loss in W/m.

Heat loss is the second most important performance parameter, besides optical efficiency, for judging the performance of a parabolic trough receiver. The test result can be compared to emittance measurements of the absorber coating and the vacuum quality in the annulus.

### *Specification for equipment to be used*

Two heating methods are in use: There is the electrical heating with heater cartridges inserted into the absorber and there is the direct Joule heating.

Heating with cartridges is typically realised with three heater zones, compare Figure 25: Heater configuration with cartridge heaters. Heat loss via the end-faces is not included in receiver heat loss. One homogeneous main heater of the length of the receiver provides the bulk of the heating power of 0.5 to 3 kW. This main heater is often further enclosed by homogenisation tube with high thermal conductivity, which enhances the temperature distribution at the absorber. Independently controlled bellows heaters at the position provide additional heating power in order to compensate for additional loss at the bellows and at the ends.

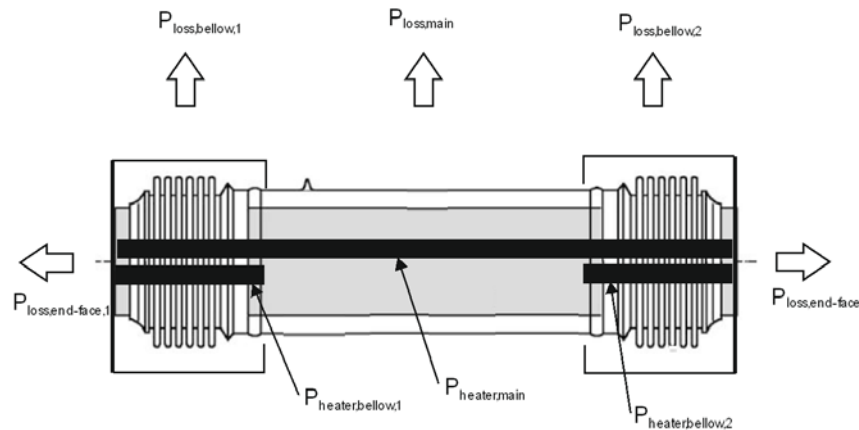


*Figure 25: Heater configuration with cartridge heaters. Heat loss via the end-faces is not included in receiver heat loss*

In a configuration with direct Joule heating the current flows directly through the absorber tube, which is made from stainless steel. The ends of the steel tube are blocked by electric clamps, so that it can be assumed that the axial heat loss through the steel tube is transferred to the ambient above all by the flange of the bellows. Two thermocouples have to be used for measuring the temperature of the flange of the two bellows. Due to the low resistance, high currents of 1000 A and low voltages 6V are typical. Additional heat loss at the bellows is also provided by cartridge heaters.

As heat loss via the end-faces, compare Figure 25, shall be excluded from the measurement in both configurations, thermal insulation is combined with either compensation heaters that lead to a negligible temperature gradient, or heat loss over the end-face is measured and included in the energy balance.

Temperature measurement is performed by thermocouples at various positions of the receiver, typically 6 to 12. Temperature distribution in circumference of the receiver shall be measured at 0° and 180° and optionally at 90° and 270°. Measurement of glass temperature is recommended.

During the measurement there must not be direct sunlight nor forced convection at the outside of the glass. Ambient temperature shall be recorded during the measurement.

### *Sensor calibration issues*

In the heater configuration with cartridge heaters and homogenisation tube the temperature measurement is susceptible for systematic measurement errors as the air and radiation temperatures in the annulus of homogenisation tube and absorber is systematically higher. Experimental means to minimize the effect are spring leaves for better force control and radiation shields. Furthermore, in state of the art test benches the temperature error is determined using a calibration tube. In this tube thermocouples are soldered or welded to the outside of the tube. Using the calibration tube with several insulation thicknesses, the temperature measurement offset of can be measured as a function of temperature and heating power, which in turn can be used to correct normal heat loss measurements.

### *Main error sources*

Compared to the temperature measurement, uncertainty of the heating power is typically negligible. Main contributions for the uncertainty stems from uncertainty of temperature offset measurement and correction and thermocouple calibration.

### *Recommendations*

None

### *Literature*

*P. Eichel et al. (2010): Heat Loss Testing on Parabolic Trough Receivers, SolarPACES 2010 International Symposium, Perpignan (France).*

## 17. Heat Transfer Fluid Properties and their Measurement

### 1.1. Thermal Oil

The characteristics of thermal oils can be described with the following parameters and related available standards methods:

**Table 2:** Thermophysical parameters and applicable measurement standards for thermal oils

Parameter		Available Standards
Ash (%)		DIN EN ISO 6245
Chlorine (%)		DIN 51577-3
Coke according to Conradsen (%)		DIN 51551-1 or DIN EN ISO 10370
Copper corrosion		DIN EN ISO 2160
Density	[ $\rho$ ]	ISO 3675; DIN 51757 ASTM D2717 95(2009)
Thermal conductivity	[k]	Standard Test Method for Thermal Conductivity of Liquids ASTM D2766 - 95(2009)
Heat capacity	[Cp]	Standard Test Method for Specific Heat of Liquids and Solids; DIN 51005
Thermal Diffusivity	[ $\alpha$ ]	ASTM Standard D2717-95
Thermal Expansion Coefficient	[k]	ASTM C 531
Enthalpy of vaporization	[ $\Delta H_{\text{vap}}$ ]	ASTM D3418-99
Enthalpy of fusion	[ $\Delta H_{\text{fus}}$ ]	Standard Test Method for Transition Temperatures of Polymers by Differential Scanning Calorimetry
Flammability		ISO 9772 and 9773
Flash Point (°C)		DIN EN 22719
Auto ignition temperature		ASTM Standard D2717-95, DIN 51794
Vapour pressure		ASTM Standard D2717-95
Boiling point		
Viscosity	[ $\mu$ ]	ISO 3104
Kinematic Viscosity (mm <sup>2</sup> /s)		DIN 51562-1 or DIN 53015
Neutralization number (mg KOH/g)		DIN 51558-1
Speed of sound on the fluids		ASTM Standard D2717-95
Impurities/degradation components		ASTM Standard D2717-95
Freezing point	[Tfp]	
Pourpoint (°C)		DIN ISO 3016
Sulfur (%)		DIN 51400-6
Thermal stability		DIN 51528, ASTM D 6743

Maximum working temperature [T<sub>wm</sub>]

Water (mg/kg) DIN 51777-1

---

## Literature

Recently the testing of thermal oils with respect to their chemical/thermophysical and degradation properties is reinvestigated by several groups due to the widespread use in solar thermal power plants.

The behavior of several thermal oils is described in

*Forristall (2003). Heat Transfer Analysis and Modeling of a Parabolic Trough Solar Receiver Implemented in Engineering Equation Solver NREL report, NREL/TP-550-34169*

Whereas the eutectic BP/DPO mixture as a HTF is focused on in

*Zeroual, B. Moummi, A. (2012). Design of parabolic trough collector solar field for future solar thermal power plants in algeria. Paper presented at the 2nd International Symposium on Environment Friendly Energies and Applications, EFEA 2012, 168-172.*

The chemical and thermophysical features of the most widely employed thermal oils are provided by their manufacturers and can be found by the respective web sites:

*Solutia, VP-1 Heat Transfer Fluid, Product Bulletin,*  
<http://www.therminol.com/pages/products/vp-1.asp>

*Solutia, Therminol 72, Product Bulletin,* <http://www.therminol.com/pages/products/72.asp>

*Dow Corning Corporation (1997), Dowtherm A Heat Transfer Fluid – Product Technical Data,* <http://www.dow.com/heattrans/>.

*Lanxess, Diphyl, Product data sheet.*

New experimental values of density, viscosity and thermal conductivity for different mixtures of diphenyl ether and biphenyl have been determined including the eutectic mixture by Lugo et al.:

*D. Cabaleiro, M.J. Pastoriza-Gallego, M.M. Piñeiro, J.L. Legido, L. Lugo, Thermophysical properties of (diphenyl ether + biphenyl) mixtures for their use as heat transfer fluids, J. Chem. Thermodynamics 50 (2012) 80–88.*

The measurement of heat capacity for therminol VP1 is discussed in:

*Gomez, J., Glatzmaier, G., Mehos M.. (2012). Heat Capacity Uncertainty Calculation For The Eutectic Mixture Of Biphenyl/Diphenyl Ether Used As Heat Transfer Fluid. Presented at SolarPACES 2012 Marrakech, Morocco, September 11–14, 2012.]*

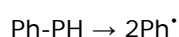
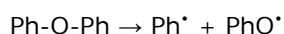
In 1962 Gäumann and Rayroux (T. Gäumann, J.-M. Rayroux, „182. Pyrolyse von Aromaten,“ in *HELVETICA CHIMICA ACTA, Volumen XLV, Fasciculus v (1962), 1962, pp. 1563-1571*) determined hydrogen as the prevailing degradation compound of biphenyl in the gas phase as well as methane and C<sub>2</sub> hydrocarbons. Benzene, isomeric terphenyls and quaterphenyls were found in the liquid phase. The authors suggested two primary reactions. The cleavage of biphenyl into phenyl radicals and the cleavage of C-H bonds. The formation of the aromatic degradation products was explained by chain reactions of the initially formed radicals. The authors also concluded that hydrogen atoms

would add easily to aromatic compounds and that this would support the degradation of these compounds.

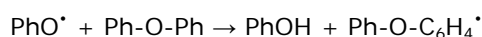
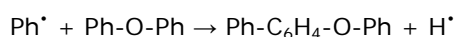
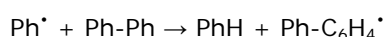
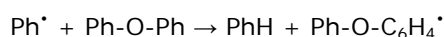
*Rainey and Yeatts (W. T. Rainey und L. B. Yeatts, „Studies on Pyrolysis Products of Pure Biphenyl,“ Oak Ridge National Laboratory, Oak Ridge, Tennessee, 1963)* investigated the accelerated aging of biphenyl at 425 °C for 12 h and 16 h. Their study confirms the previously found findings. Additionally, they found C3 hydrocarbons.

In 1968 two studies on the investigation of the eutectic mixture of BP/DPO were published that focussed on the application in an organic Rankine cycle (*A. W. Adam, R. E. Niggemann und L. W. Sibert, „Thermal Stability Determination of Biphenyl and the Eutectic of Biphenyl an Phenyl Ether in a Rankine Cycle System,“ in IECEC, Intersociety Energy Conversion Conference, Vol.1, pp. 398-406, New York, 1968; 21; G. S. Leighton, „The Organic Rankine Cycle,“ in IECEC, Intersociety Energy Conversion Conference, Vol.1, pp. 389-397, New York, 1968*). The fluid was operated for 10,000 hours at 371 °C. Besides hydrogen, benzene, an isomeric terphenyl the authors found phenol as degradation product.

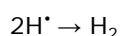
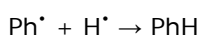
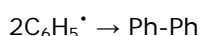
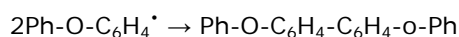
*Arnold* reported in 1978 an aging study of the eutectic BP/DPO mixtures at 400 - 425 °C for 120 hours (*C. Arnold, „Evaluation of Organic Coolants for the Transportation of LMFBR Spent Fuel Rods,“ Report No. SAND77-1486, 1978*). He reported a degradation degree of 8% for the 425 °C test. The gas phase consisted of 44% hydrogen. As the viscosity had increased he concluded that a polymerization had occurred. He suggested a reaction mechanism which is in accordance to *Gäumann* and *Rayroux*. As initiating reactions the interannular bonds in BP or DPO were cleaved which leads to phenyl (Ph<sup>•</sup>) and Phenoxy (PhO<sup>•</sup>) as radicals.



The aromatic degradation compounds were explained via radical chain reactions:



The reaction chain is terminated by the recombination of two radicals:



*Proksch* et al. reported kinetic data for the degradation of biphenyl (*E. Proksch, A. Strigl, M. Wagner-Löffler, W. Szinovatz, Chem -1ng -Tech 57 (1985) Nr 2, 148- 153*). They studied the degradation in the range of 420 - 465 °C and aimed at a degradation degree of 1%. The authors report as well on the formation of benzene, isomeric terphenyls and quaterphenyls.

*Cook* et al. report on the effect of impurities on the degradation (*B. R. Cook, B. B. Wilkinson, C. C. Culross, S. M. Holmes, L. E. Martinez, Energy & Fuels 1997, 11, 61-75*). They heated mixtures of biphenyl and alkanes at 450 °C and observed increased degradation. The authors

explained this effect via the formation of hydrogen atoms from the less stable alkanes. As *Gäumann* and *Rayroux* they concluded that hydrogen atoms would assist the cleavage of aromatic compounds due to an addition reaction.

In the older studies no detailed kinetic data on the formation of hydrogen or other degradation compounds were presented. The thermal degradation under accelerated aging conditions was examined recently. In this study the formation of gases and volatile compounds was examined in detail. A comparison of heat capacities of fresh fluid and HTF from a CSP plant (SEGS V) is given as well. For the first time the formation of water as a degradation product was described:

*Jung, C., Schmidt, V., Senholdt, M., (2012). Aging of Organic heat transfer media. Presented at SolarPACES 2012 Marrakech, Morocco, September 11–14, 2012.*

## 17.1. Molten Salts

Regarding the chemical/physical properties of molten salt mixtures, no standardized analytical methods have been agreed on to date. For this reason, the analytical methods employed by the ENEA laboratories are listed in **Fehler! Verweisquelle konnte nicht gefunden werden..** Clearly, in the next future, common criteria will be discussed with all the other interested organizations, in order to establish feasible standardized test methods.

*Table 6: Parameters and used characterization method*

Parameter		Employed Method
Chemical composition (anions/cations)		Ion chromatography
Alkaline impurities: carbonates, oxides		acidimetric titration
Other impurities:		Inductively coupled plasma-Atomic emission spectrometry (ICP-AES), flame atomic absorption spectroscopy (FAAS)
Density	[ $\rho$ ]	Achimedes' principle based method
Thermal conductivity	[k]	The experimental apparatus is under setting-up
Heat capacity	[Cp]	Differential scanning calorimetry, with sapphire as reference standard
Thermal Diffusivity	[ $\alpha$ ]	The experimental apparatus is under setting-up <sup>2</sup>
Thermal Expansion Coefficient	[k]	The experimental apparatus is under setting-up <sup>3</sup>
Enthalpy of fusion	[ $\Delta H_{fus}$ ]	Differential scanning calorimetry
Vapour pressure		Pressure measurement in autoclave
Melting point	T <sub>m</sub>	Differential scanning calorimetry

<sup>2</sup> Y. Nagasaka and A. Nagashima (1981), Absolute measurement of the thermal conductivity of electrically conducting liquids by the transient hot-wire method, J. Phys. E: Sci Instrum., vol14, 1981.

J. S. Powell, An instrument for the measurement of the thermal conductivity of liquids at high temperatures., Meas.SciTechnol 2 (1991) 111-117

<sup>3</sup> Detection of liquid level by laser technique

Viscosity	[ $\mu$ ]	Rheometry
Maximum working temperature	[ $T_{wm}$ ]	Molten salt thermal degradation is followed by ion-chromatography, produced gases evolution by gas chromatography.

---

## Literature

The following three references describe the employment of molten nitrates as HTF and HSM for CSP plants:

*G. J. Kolb, R. B. Diver (2008): Conceptual Design of an Advanced Trough Utilizing a Molten Salt Working Fluid, presented at SolarPACES 2008, Las Vegas, NV, Mar. 3-7.*

*J.E. Pacheco (editor) (2002): Final Test and Evaluation Results from the Solar Two Project, Sandia National Laboratories SAND2002-0120, January 2002.*

*R. W. Bradshaw, N. P. Siegel (2008): Molten Nitrate Salt Development For Thermal Energy Storage In Parabolic Trough Solar Power Systems - Proceedings of ES2008 Energy Sustainability 2008, August 10-14, 2008, Jacksonville, Florida USA.*

The chemical/physical characterization of various molten nitrates mixture is reported here:

*X. Zhang, J. Tian, K. Xu, Y. Gao (2003): Thermodynamic Evaluation of Phase Equilibria in NaNO<sub>3</sub>-KNO<sub>3</sub> System - Journal of Phase Equilibria. 2003. vol 24 No. 5, 441-446,*

*N. Siegel, G. Glatzmaier (2010): Molten Salt Heat Transfer Fluids and Thermal Storage Technology - CIMTEC 2010, 5th Forum on New Materials - Montecatini Terme, Italy June 13th-18th, 2010,*

*R. W. Bradshaw, D. E. Meeker, High-temperature stability of ternary nitrate molten salts for solar thermal energy systems, Solar Energy Materials 1990; 21: 51-60,*

*Coastal Chemical Co., L.L.C. – HITEC® Heat Transfer Salt technical brochure,*

A survey on the chemical/physical features concerning the binary mixture NaNO<sub>3</sub>/KNO<sub>3</sub>, named "solar salt":

*T. Bauer, N. Breidenbach, N. Pflieger, D. Laing, M. Eck (2012): Overview of molten salt storage systems and material development for solar thermal power plants - Paper presented at the World Renewable Energy Forum, WREF 2012, Including World Renewable Energy Congress XII and Colorado Renewable Energy Society (CRES) Annual Conference (2012), 2 837-844.*

Regarding density measurements:

*R. W. Bradshaw R.W. (2009): Effect of composition on the density of multi-component molten nitrate salts - SANDIA report SAND2009-8221, December 2009.*

Concerning heat capacity:

*K. Ichikawa, T. Matsumoto (1983): Heat capacities of lithium, sodium, potassium, rubidium, and caesium nitrates in the solid and liquid states - Bulletin of the Chemical Society of Japan (1983), 56(7)*

Viscosity determination:

*R. W. Bradshaw (2010): Viscosity of Multi-component Molten Nitrate Salts—Liquidus to 200°C, Sandia report - SAND2010-1129, March 2010,*

*J. L. Copeland, J.R. Christie (1971): On the constant volume viscous properties of molten alkali nitrates - The Journal of Chemical Physics, (1971), 55(10), 4925-4932,*

*V. M.B. Nunes, M. J. V. Lourenço, F. J. V. Santos, C. A. Nieto De Castro (2006): Viscosity of molten sodium nitrate - International Journal of Thermophysics, (2006), 27(6), 1638-1649.*

Thermal conductivity:

*L. R. White, H. T. Davis (1967): Thermal conductivity of molten alkali nitrates - The Journal of Chemical Physics, (1967), 47(12), 5433-5439*

Molten nitrates thermal stability:

*E. S. Freeman (1956): The kinetics of the thermal decomposition of sodium nitrate and of the reaction between sodium nitrite and oxygen - Journal of Physical Chemistry, (1956), 60(11), 1487-1493*

*E. S. Freeman (1957): The kinetics of the thermal decomposition of potassium nitrate and of the reaction between potassium nitrite and oxygen - Journal of the American Chemical Society, (1957), 79(4), 838-842]*

## 18. Measurement of Electric Power

CSP facilities are usually used to produce electrical power. The quantity and the quality of the produced electrical power is therefore important in the evaluation of the performance of the CSP plant.

As no CSP specific aspect has been highlighted, the reader can refer to broadly available guidelines for electrical power measurements such as the **IEC 61000-4-30** *Power quality measurement methods*, and the **IEC 62053** *Electricity measuring equipment (A.C.), particular requirements*, or European counterparts or complements such as **EN 50160** *Voltage characteristics of electricity supplied by public distribution systems*.

Some elements are presented here, but the reader is strongly encouraged to refer to the existing IEC or EN norms for details and practical applications, or comprehensive guidelines on the topic, for example *Modern Power Quality Measurement Techniques* edited by the European company Metrel and available on internet.

### *Description of the method*

Both the amount and the quality of the produced electrical power should be evaluated to determine the performance of the CSP process: ideally, the produced electrical energy is a set of pure sinusoidal voltages with a given nominal amplitude voltage, frequency and phase between the voltages.

However, practical electrical power production exhibits defaults that must be characterized in terms of :

- Frequency.
- Voltage: nominal voltage, dips (undervoltage), swells (overvoltage), interruptions, flicker, interruptions. Characterization should be made phase per phase and the neutral if present.
- Voltage unbalance between phases.
- Harmonics and interharmonics.

The IEC 61000-4-30 describes those parameters and the conditions for their evaluation. The norm also describes the performance requirements for class A and B evaluation, that is either for precise/contractual evaluation (class A) or diagnostics/troubleshooting purposes (class B).

Among the aspects to be checked, the time sampling and integration time should be well defined and presented in order to take into account the time variability of the parameters. For example, IEC 61000-4-30 requires “basic measurement time interval” that are 10 cycles long for 50 Hz power system or 12 cycles for 60 Hz. These measurement time intervals are then aggregated over 3 different time intervals depending on the considered parameter:

- 3 seconds interval (150 cycles for 50 Hz systems or 180 cycles for 60 Hz)
- 10 minutes interval
- 2 hours interval

Aggregation should be performed using the square root of the arithmetic mean of the squared values. The intervals are identified using absolute time that should have uncertainty lower than one

cycle:  $\pm 20$  ms for 50 Hz or  $\pm 16.7$  ms for 60 Hz. For example, IEC 61000-4-30 recommends to evaluate the harmonic voltages with 10 minutes values for at least one week and with 3 seconds values daily for at least one week: Annex A of this norm states the complete recommendations.

Instant evaluations of current and voltage is not a proper measurement of the delivered electrical power as both vary quickly with time, aggregation must be used.

### *Specification for the equipment to be used*

The reader can refer notably to the following documents:

- The annex A of IEC 61000-4-30 provides guidelines and possible issues for the required measurements.
- The abovementioned Metrel guide includes a complete measurement procedure and report on power quality.

When choosing a powermeter, the instrument should comply with the norms IEC 62053 or equivalent that define performance classes and allowed perturbations of the supply systems due to the instrument (for example losses due to shunt resistors).

### *Recommendations*

- Follow existing norms such as IEC 61000-4-30 or EN 51060.
- Aggregates measured instant values over significant length of time using the square root of the arithmetic mean of the squared values.
- Only authorized personnel should have intervention on live electrical components to install the required transducers.

### *Literature*

*Modern Power Quality Measurement Techniques, edited by METREL, Code No. 20 750 592,  
[http://www.shmcomms.co.uk/images/PDFs/AN\\_power\\_meas\\_tech.pdf](http://www.shmcomms.co.uk/images/PDFs/AN_power_meas_tech.pdf)*

*IEC 61000-4-30 Electromagnetic compatibility — Testing and measurement techniques — Power quality measurement methods.*

*IEC 61000-4-15 Electromagnetic compatibility — Flickermeter – Functional and design specification.*

*IEC 61000-4-7 Electromagnetic compatibility — General guide on harmonics and interharmonics measurements and instrumentation.*

*IEC 62053-11 Electricity metering equipment (a.c.) – Particular requirements – Electromechanical meters for active energy (classes 0,5, 1 and 2).*

*IEC 62053-21 Electricity metering equipment (a.c.) – Particular requirements – Static meters for active energy (classes 1 and 2).*

*EN 50160 Voltage characteristics of electricity supplied by public distribution systems.*

## 19. Measurement of the solar-to-fuel efficiency of solar receivers

### *Description of the method*

The efficiency of solar receivers is determined on the basis of the useful output in terms of energy stored in the products and solar energy input

$$\eta_{\text{solar-to-fuel}} = \frac{-\Delta G}{Q_{\text{solar}}}$$

To this end, a number of measurement quantities described in more detail in the following need to be determined.

#### **Solar power input**

The solar power input of the concentrating system  $Q_{\text{solar}}$  can be derived from solar flux measurements in the receiver-reactor aperture. Those measurement systems correspond to those used to characterize solar tower systems (compare chapter 11).

#### **Molar flow rate of reactants**

Often it is difficult to measure the product gas flow rate leaving the reactor, because the gas is still hot and calibration systems would have to be integrated directly into the system. Usually, the mass flow rates of the educts are measured before operation of the receiver-reactor. In case of reactions without a change of the molar amount, the molar flow rate of the educts is equal to that of the products. In case of changing molar amounts during the reaction, the product gas flow has to be calculated from the educt gas flow rate and the conversion.

Different gas flow calibration systems exist and are commercially available. For accurate measurements, the use of calibrated and certified gas flow calibration systems is recommended.

#### **Product gas composition**

Different physical principles and analytical devices exist for analysis of the product gas composition. The suitable device is chosen dependent on the gas species of interest (see Table 6), the necessary accuracy and the desired detection range. The most common analytical devices are listed below

- Gas chromatograph (GC)
- Mass spectrometer (MS)
- Non-dispersive Infrared sensor (NDIR)
- Electrochemical sensors
- Thermal conductivity analyzers

The devices differ in the components they are able to detect, the response time and their measurement range. The following table gives an overview of the most common components that are of interest when operating solar receiver-reactors and the analytical devices that can be used to detect them.

*Table 6: Suitability of different physical principles for the detection of various gases*

	H <sub>2</sub>	O <sub>2</sub>	CO	CO <sub>2</sub>	CH <sub>4</sub>
Gas chromatograph	x	x	x	x	x
Mass spectrometer	x	x	x	x	x
NDIR			x	x	x
Electrochemical O <sub>2</sub> sensor (lambda sensor)		x			
Thermal conductivity sensor	x				

The analytical devices listed above are only an overview of the most common devices used in combination with solar receiver-reactors, but of course the list is not exhaustive.

The detailed description of the working principle of the listed analytical devices can be found in concise text books on the topic as well as in the respective manuals. In the following, general comments and considerations are given for the individual devices.

### **Temperature of reactants**

In case of homogeneous gaseous reactions often the gas temperature is of interest for the investigator. To measure the temperature of a gas stream, usually shielded thermocouples are applied. Note that the use of shielded thermocouples is essential, because otherwise the measurements are falsified through direct solar irradiation or irradiation of the surroundings.

In case of heterogeneous catalytic or gas-solid reactions, the temperature of the solid reactive structure is usually measured. In this case thermocouples are introduced into the structure and attached to the surface. Here again attention must be paid that the thermocouple is well attached to the solid surface and does not receive direct irradiation from the solar concentrating system.

### **Pressure of receiver-reactor**

For pressure measurements inside the receiver-reactor, commercially available pressure sensors can be applied.

## ***Specification for the equipment to be used for measuring product gas composition***

### **Gas chromatograph**

A gas chromatograph (GC) is equipped with one or several detectors. The detectors determine the components that can be analyzed, because a detector is only sensitive to specific components. The specific configuration of a GC can be determined by the customer together with the manufacturer. Typically, a GC is equipped with two or more detectors allowing a wide range of detectable components, such as H<sub>2</sub>, O<sub>2</sub>, CO, CO<sub>2</sub>, CH<sub>4</sub>, N<sub>2</sub> and Ar. To allow accurate quantitative measurements, the components of interest have to be calibrated. The most accurate way is to use gas standards with predefined gas concentration ratios that are commercially available. In order to obtain high accuracy, the selected gas concentrations must cover the expected measurement range. The calibrations have to be repeated in certain time intervals specified by the manufacturer. In any case, before connecting a GC to a receiver-reactor system, signal stability should be checked by the user. If the calibration is done accurately, the GC can be considered as one of the most accurate and stable measurement

devices.

A drawback of a GC is that due to the measurement principle, no continuous measurements are possible. A GC takes batches of product gas and analyzes them successively. The sample rate and the retention time are dependent on the detector and the analyzed components and usually lie in the range of several minutes. Therefore a GC is only suitable for steady processes with unchanging or slowly changing product gas composition. It is not suitable for unsteady processes, where fast changes in the product gas composition have to be tracked. In such cases other measurement devices with faster response times must be used.

### **Mass spectrometry**

Like gas chromatographs, mass spectrometers (MS) are available in different configurations and for different applications. For analysis of product gases a gas phase mass spectrometer must be chosen. Due to its measurement principle, a mass spectrometer is capable of measuring a wide range of components, such as  $H_2$ ,  $O_2$ ,  $CO$ ,  $CO_2$ ,  $CH_4$ ,  $N_2$  and  $Ar$ . But attention must be drawn here to the present components in the product gas of a receiver-reactor. Because of cross-sensitivities, certain combination of components might not be distinguishable. This must be checked before a mass spectrometer is used.

For quantitative measurements, the components of interest have to be calibrated. Similar to calibration of a GC, calibration of a MS can be done by using predefined gas standards and have to be repeated in certain time intervals.

In contrast to the GC, continuous measurements are possible with a MS. Usually the sample rate lies within a few seconds. Therefore also unsteady processes, with changing gas composition over time can be monitored with an MS.

### **Non-dispersive infrared sensors**

Non-dispersive infrared sensors (NDIR sensors) are able to detect IR active components like  $CO_2$ ,  $CO$ ,  $CH_4$ . Usually multiple-component devices are available that can detect several components. The specific components and the measurement ranges can be determined by the customer together with the manufacturer. Note that the accuracy of the measurement decreases, when the actual gas concentration lies outside the specified measurement range. NDIR sensors can be used for continuous online measurements with response times usually less than a second. The devices run usually very stable. Still accuracy of the measurements should be checked in repeated time intervals by the user.

### **Other sensors**

Especially for the measurement of  $O_2$ , electrochemical sensors or lambda sensors are an interesting option. They are small, which enables easy integration for example into the product gas line of a receiver-reactor. Furthermore they are available for wide measurement ranges and have a fast response time. Especially when it comes to the detection of very small amounts of oxygen of less than 100 ppm, electrochemical  $O_2$  sensors can be applied.

For the measurement of  $H_2$ , thermal conductivity sensors can be used. Note that those devices are limited in their minimum detection range. For the detection of trace amounts of  $H_2$ , other analytical devices, such as GC or MS are better suited.

## *Recommendations*

Measurement concepts for gas composition are to be adapted to the individual requirements of every measurement application with respect to gases and detection ranges. For quantitative measurements, the instruments have to be calibrated using predefined gas standards for the components of interest. In order monitor and assess measurement accuracy calibrations need to be repeated in regular intervals. The instruments have to be calibrated using Calibration detection range

## *Literature*

*J. H. Gross (2004): Mass Spectrometry – A Textbook Springer Verlag, Heidelberg (Germany).*

*R. L. Grob and E. F. Barry (2004): Modern Practice of Gas Chromatography, John Wiley and Sons (USA).*

*H. Güzler, H.-U. Gremlich (2002): IR Spectroscopy – An Introduction, WILEY-VCH Verlag, Weinheim (Germany).*

*B.H. Stuart (2004): Infrared Spectroscopy: Fundamentals and Applications (Analytical Techniques in the Sciences), WILEY-VCH Verlag, Weinheim (Germany).*